Final Report

PROPELLANT COMBUSTION PHENOMENA DURING RAPID DEPRESSURIZATION

Prepared for:

CHIEF, SOLID PROPULSION TECHNOLOGY
NATIONAL AERONAUTICS AND SPACE ADMINISTRATION
WASHINGTON, D.C. 20546
ATTN: CODE RPS

STANFORD RESEARCH INSTITUTE

MENLO PARK, CALIFORNIA

STANFORD RESEARCH INSTITUTE
MENLO PARK, CALIFORNIA

31 October 1967

Final Report

PROPELLANT COMBUSTION PHENOMENA DURING RAPID DEPRESSURIZATION

Prepared for:

CHIEF, SOLID PROPULSION TECHNOLOGY
NATIONAL AERONAUTICS AND SPACE ADMINISTRATION
WASHINGTON, D.C. 20546
ATTN: CODE RPS

By: C. E. WOOLDRIDGE, G. A. MARXMAN, E. L. CAPENER

SRI Project PGU-5577

Approved: MARJORIE W. EVANS, DIRECTOR
POULTER LABORATORY FOR HIGH PRESSURE RESEARCH

Copy No. 15

FOREWORD

The theoretical and experimental studies described in this report were performed principally by G. A. Marxman (theory), C. E. Wooldridge (theory and experiments), and E. L. Capener (experiments). The overall program, which was initially under the direction of L. A. Dickinson, has been under the direction of G. A. Marxman since March 1967.

The program was under the management of the Chief, Solid Propulsion Technology, Code RPS, OART, NASA, Washington, D.C. (R. W. Ziem), with technical management by High Temperature Materials Branch, Langley Research Center (A. R. Saunders). Administration of the program was under the direction of NASA-Western Operations Office (E. F. Wyszpolski).

The activation energy measurements which are reported in the experimental studies section of this report were instigated and carried out solely by Norman A. Kirshen. The major contributions of R. J. Kier and A. J. Amaro to the program are also gratefully acknowledged.

ABSTRACT

The theoretical studies carried out during this program were concerned with the analysis of an idealized combustion model in which, in addition to surface pyrolysis and gas-phase chemical reactions, exothermic or endothermic reactions are permitted at or very near the solid-gas interface and are therefore coupled with the thermal response of the solid. These surface-coupled reactions are assumed to occur in a zone of negligible thickness, relative to the penetration depth of the thermal profile, so that the associated heat release can be treated as a boundary condition on the solid phase. The results of the analysis of the model show that a relatively small proportion of surface-coupled heat release (e.g., 10 percent) has a profound effect on the burning rate response to environmental pressure changes.

Differential thermal analysis measurements have shown that ammonium perchlorate composite propellants have a much greater surface-coupled heat release than do potassium perchlorate propellants. Lower deflagration limit studies have shown that the p_{DL} is much higher for potassium perchlorate propellants than for ammonium perchlorate propellants, reflecting one consequence of the lower surface-coupled heat release.

Adiabatic self-heating measurements, which establish the overall activation energy of the surface processes, have shown that the oxidizer size distribution and the inclusion of additives such as aluminum have a strong effect on the activation energy. This result implies an ultimate effect on the proportion of surface-coupled heat release which may be highly significant.

Fiber-optic studies of the combustion zone microstructure clearly indicate the existence of important heat-release phenomena in the vicinity of the surface. Aluminum particles were observed to ignite and partially burn in the low temperature region at the surface, implying that the ignition must be induced by intermediate products of the perchlorate decomposition process.

The depressurization studies carried out during the program indicated that extinction could be obtained at pressures an order of magnitude above the lower deflagration limit for a sufficiently large depressurization rate. However, little information about the transient burning rate response could be obtained from the pressure-time history of the depressurization event. For this reason, pressurization experiments in a small-volume burner were initiated to provide a check on the nonlinear predictions of the combustion model. This work is being continued under a follow-on contract.

CONTENTS

ILLUSTRATIONS

Figure

TABLES

NOMENCLATURE

a	frequency factor in Arrhenius law
A_b	burning surface area
A_t	nozzle throat area
C	constant
c_p	specific heat capacity of gas at constant pressure
c_s	specific heat capacity of solid
E	activation energy for pyrolysis at interface
E_D	activation energy for pressure-insensitive surface-coupled reactions
E_f	activation energy for gas-phase reaction
E_H	activation energy for pressure-sensitive surface-coupled reactions
E_w	activation energy for pyrolysis at interface
h	enthalpy
h^*	nondimensional rate of external enthalpy addition by pulser
h_{g_w}	energy carried into gas phase with vaporizing propellant per unit mass
h_{s_w}	energy carried by convection from unreacted solid phase per unit mass
H_D	heat release (positive) per unit mass propellant in pressure-insensitive surface-coupled reactions
H_e	enthalpy per unit mass of externally supplied gases
H_H	heat release (positive) per unit mass propellant (at a reference temperature and pressure) in pressure-sensitive surface-coupled reactions
k	thermal conductivity of solid
L	heat of vaporization per unit mass of propellant

L^* characteristic length of rocket motor chamber

m order of heterogeneous reaction; mass flux from wall

m^* nondimensional rate of external mass addition by pulser

$\dot{m}_e$ external mass addition rate

n order of gas-phase reaction

p chamber pressure

Q_D heat of reaction per unit mass of reactant in pressure-insensitive surface-coupled reaction

Q_D^* nondimensional heat of reaction per unit mass of reactant in pressure-insensitive surface-coupled reaction

Q_H heat of reaction per unit mass of reactant in pressure-sensitive surface-coupled reaction

Q_H^* nondimensional heat of reaction per unit mass of reactant in pressure-sensitive surface-coupled reaction

Q_r heat of reaction per unit mass of reactant in gas-phase reaction

Q_T total heat of combustion

R gas constant

r burning rate

T temperature

t time

V chamber volume

x distance into propellant from surface

y transformed distance

Greek letters

γ specific heat ratio, c_p/c_v

ϵ_r mass fraction of reactant at propellant surface (nearly unity)

ζ_D fraction of steady-state total heat of combustion, Q_T, associated with pressure-insensitive surface-coupled reactions

ζ_H fraction of steady-state total heat of combustion, Q_T, associated with pressure-sensitive surface-coupled reactions

K thermal diffusivity of solid = $k/\rho_s c_s$

ρ_s density of solid propellant

X number of sites that undergo surface-coupled reactions per unit mass of solid propellant

Subscripts

c chamber

f gas-phase flame

g gas phase

i initial value at t = 0

o conditions at $x \rightarrow \infty$

s solid phase

w conditions at wall (gas-solid interface)

Superscripts

* nondimensional quantity normalized to steady-state value; e.g., $r^* = r/r_i$, $T_f^* = T_f/T_{f_i}$. Note one exception: $T_o^* = T_o/\bar{T}_w$. Also, $t^* = r_i^2\, t/K$ and $x^* = r_i x/K$

INTRODUCTION

In recent years, numerous studies have been conducted on solid propellant combustion termination by rapid depressurization of the combustion chamber.[1,2] Most of these studies have been based on an empirical approach, and a major effort has been directed toward correlating extinction behavior with a single critical parameter (such as dp/dt). Such correlations generally have completely neglected real gas-dynamical processes in the chamber; moreover, it has been customary to characterize propellants in terms of a single parameter, usually the burning rate.

Investigations at Stanford Research Institute as well as at other laboratories,[3,4,5] however, have demonstrated that the chemical and physical composition of the propellant is an extremely important factor in the response of the combustion mechanism to pressure disturbances. For example, two propellants with the same burning rate but differing compositions usually respond quite differently to a pressure perturbation. The response is strongly influenced by the relative magnitudes of the various relaxation times that characterize thermal and chemical processes comprising the combustion mechanism, and these relaxation times are largely determined by compositional factors. Thus, the purely empirical approach to combustion extinction problems is inherently of limited potential usefulness. A greatly improved understanding of the transient behavior of solid propellant combustion processes is a prerequisite for a fully satisfactory explanation of combustion extinction behavior. It was the objective of the present investigation to obtain information needed to fulfill this prerequisite.

Theoretical studies during this program have been directed toward the development of an adequate model of transient combustion. Parallel experimental studies provided essential insight and guidance for the theoretical effort, as well as tests of the theoretical predictions. Theoretical and experimental developments during the entire program are summarized in this report.

THEORETICAL STUDIES

Several serious shortcomings in the available theoretical treatments of solid propellant combustion extinguishment were revealed by a literature review at the outset of this program. In particular, in these treatments the time required for relaxation of temperature profile in the grain following a sudden change in heat flux was neglected; an empirical, steady-state burning rate law was used to relate burning rate and pressure during transients, and the propellant surface temperature was assumed constant. The consequences of these assumptions were discussed in some detail in an earlier report.[6] It was shown that such assumptions lead to a quasi-steady combustion model that is of questionable value in dealing with the highly transient extinguishment process.

The objective of the theoretical studies performed during the program was to overcome the most critical limitations of earlier treatments by taking a more fundamental approach to the problem. It was recognized that a meaningful theoretical analysis of transient propellant combustion would have to consider surface-coupled reactions as well as relaxation phenomena, both of which were ignored in earlier treatments. The transient combustion model subsequently developed[6,7,8] represents an effort to include these features in a reasonably realistic manner that is still mathematically tractible. A relatively simple mathematical analysis of the model, employing suitable simplifying assumptions, served to emphasize and interpret qualitatively the physical processes that are important during transient modes of combustion.[6,7] Later, a more sophisticated and more rigorous mathematical treatment was presented.[8] This analysis confirmed earlier general conclusions and provided a much more complete description of certain aspects of the transient combustion behavior, especially in relation to the frequency response.

The theoretical investigation performed during the program has established a direct relationship between the combustion extinguishment response and the combustion stability characteristics of a solid propellant. In addition, it has been shown that the transient response of the combustion mechanism is strongly influenced by the distribution of energy release between reactions in the gas phase and those that are thermally coupled effectively to the solid phase. The theory indicates that when even a very small fraction of the total energy release occurs in surface-coupled reactions, the likelihood of unstable combustion and also of difficult extinguishment, possibly accompanied by "chuffing," is greatly enhanced. This theoretical conclusion appears to be consistent with experimental observations.

Theoretical studies performed during this program are summarized in detail in the appendices to this report. The combustion model is developed (Appendix A), and both an approximate perturbation analysis of the model (Appendix B) and a more rigorous treatment (Appendix C) are presented. Together, these analyses show the relationship between extinguishment response and the combustion stability criterion for a propellant. Because of this relationship, some theoretical consideration of combustion instability phenomena became essential during the program, although the chief concern of the investigation was combustion extinguishment. Thus, the treatment in Appendix C serves primarily to define with greater precision the propellant combustion stability characteristics that ultimately influence extinguishment behavior. A modified combustion model, designed for use in nonlinear computer studies, appears in Appendix D.

The Combustion Model

Because the mathematical details of the combustion model formulated during this investigation are presented in Appendix A, this discussion will be confined to a brief consideration of the unique features of this model and of the concepts underlying those features.

As has been mentioned, the most significant difference between the formulation above and other combustion models[1,2] lies in the method of accounting for surface reactions. It has been the usual practice in virtually all other related theories to employ what may be described as a "one-step" description of surface kinetics. Specifically, the quantities Q_H and Q_D, representing the surface-coupled heat release (Eqs. A4 and A5), have been assumed to be proportional to the burning rate, r, alone. If one follows this procedure, the Arrhenius temperature dependence of the last two terms in Eq. A10 vanishes. This general approach has been used at SRI to describe double-base propellants only, by letting $E_H = E_D = 0$ in Eq. A10. Such a treatment leads to results in agreement with double-base experiments.[9] However, it is felt that the more complex "two-step" description of Eq. A10, in which the surface-coupled heat release is proportional to both r and an Arrhenius factor, is necessary for composite propellants; the experimental results tend to confirm this assumption.[9] A physical interpretation of this description of the surface reaction process in composite and double-base propellants, respectively, will clarify the reasoning that led to the kinetics description incorporated in Eq. A10.

For this analysis, surface-coupled reactions are defined as reactions that occur within a narrow zone in the immediate vicinity of the gas-solid interface and tend to follow the surface temperature variations, rather than temperature variations relatively far out in the gas-phase flame, during transient operation. Gas-phase reactions very near the surface, as well as solid-phase reactions, may be thermally coupled to the surface. For composite propellants, the surface reaction zone may be envisioned as encompassing, first, pyrolysis of the propellant (described by Eq. A2), and subsequently, surface-coupled reactions among the pyrolysis products.

It follows that the activation energies E_H and E_D associated with Eqs. A8 and A9 represent an overall description of a complicated sequence of events, which may include mixing between the various macroscopic constituents of the composite propellant, as well as reaction steps.

In contrast, with a double-base propellant there is no reason to distinguish surface-coupled energetic reactions from pyrolysis reactions, because the constituents are intermixed on a molecular scale. Thus, the pyrolysis and other reactions may be considered as a single sequence, with a single activation energy, E, characterizing the rate-controlling step, and with $E_H = E_D = 0$. A possible exception might occur with heterogeneous reactions, which could call for a very small value of E_H associated with molecular mixing between gas-phase constituents and pyrolysis products.

In summary, according to this interpretation, a composite propellant generally corresponds to $E_H > 0$ and/or $E_D > 0$, whereas for a typical double-base propellant, $E_H = E_D = 0$. It follows from the SRI theory[9,10] that exothermic surface-coupled reactions tend to destabilize composite propellants (by increasing the response amplitude), while they tend to stabilize double-base propellants (see Appendix C). This rather remarkable theoretical conclusion may explain the previous experimental observation that the stable burning regimes of composite and double-base propellants are reversed.[11] It is important to recognize that the possibility of a destabilizing effect associated with surface-coupled exotherms does not arise unless there is a departure from the single-step description of the surface kinetics (i.e., $E_H = E_H = 0$). Because earlier treatments have employed only the single-step description, they have not predicted this effect.

It is evident from the foregoing discussion that the method of incorporating surface reactions in the combustion model is a crucial factor; it is important therefore, to find a demanding experimental test of the kinetics treatment. Of all transient combustion phenomena, combustion instability has received the greatest experimental attention. Instability results afford a means of checking the surface kinetics treatment in the combustion model, for to be a valid representation of extinction behavior, the model must be consistent with the data. Accordingly, detailed comparisons were made between the model developed during this study and instability data.

All experimental results obtained in our laboratory[9,11] associate surface exotherms with instability in composite propellants. Earlier analyses based on simpler kinetics descriptions predict the opposite behavior, whereas the present treatment is consistent with the observations. Additional support comes from the following considerations: (1) The resonance amplitudes and frequencies indicated by the theory are in agreement with experimental observations[12] of typical propellants, within the accuracy of experiment or theory; (2) observed shifts in the resonance curves and other striking consequences of composition alterations are also anticipated within the context of the theory; and (3) the analysis suggests a plausible explanation for the rather striking differences in the behavior of composite and double-base propellants. These factors strongly suggest that an approach similar to that employed in the present investigation is necessary for an acceptable representation of the combustion mechanism.

The Role of the Pressure Gradient in Combustion Extinction

In previous investigations of combustion extinction,[1] an effort was made to correlate extinction data in terms of the pressure gradient imposed on the propellant. Essentially identical analyses of the response of a burning solid propellant to a pressure decay, developed independently by G. von Elbe[2] and investigators at Aerojet-General Corporation,[1] provided the theoretical basis for this approach. These analyses led to the following criterion for extinction:

$$\left| \frac{d \ln p}{dt} \right| > \left| \frac{\bar{r}^2}{k} \right| \qquad (1)$$

Although experiments have demonstrated that the pressure gradient has an important effect on combustion extinction, attempts to correlate the data in terms of this criterion met with only limited success.[1]

Owing to this background, one of the first theoretical tasks undertaken during this investigation was a study of the role of the pressure gradient. The objective was to evaluate the significance and define the limitations of criteria such as that of Eq. 1. Toward this

end, the influence of the pressure gradient was examined in terms of the combustion model discussed above and detailed in Appendix A. From the model, the following pressure-gradient criterion, which is derived in Appendix B, was developed:

$$\left| \frac{d \ln p}{dt} \right| > \left| \frac{\bar{r}^2}{\kappa} \lambda \right| \tag{2}$$

where

$$\lambda = \theta_s - \varphi$$

$$\theta_s = \left(\frac{E_H}{R\bar{T}_w} - m \right) \theta_H + \frac{E_D}{R\bar{T}_w} \theta_D$$

$$\theta_H = \frac{H_H}{C_s \bar{T}_w} \left(\frac{\bar{p}}{\bar{T}_w} \right)^m \exp\left(-E_H / R\bar{T}_w\right)$$

$$\theta_D = \frac{H_D}{C_s \bar{T}_w} \exp\left(-E_D / R\bar{T}_w\right)$$

$$\varphi = \frac{C_p}{C_s} \frac{\bar{T}_f}{\bar{T}_w} \frac{E / RT_w}{\left(\frac{n+2}{2} + \frac{E_f}{2RT_f} \right)}$$

This criterion contains a very important parameter, λ, which is missing from the quasi-steady treatments leading to Eq. 1. The parameter λ is a thermochemical constant that characterizes the propellant; it accounts for the role of chemical reactions in extinction, which have been neglected in the earlier purely thermal theories. The physical meaning of Eq. 2 has to be examined carefully to put this criterion in proper perspective within the overall context of the extinction problem as defined in SRI's recent studies.

First, note that Eq. 2 is derived from a linearized analysis, and therefore characterizes a small departure from equilibrium, or quasi-steady combustion. In the case where

$$\left| \frac{d \ln p}{dt} \right| \leq \left| \frac{\bar{r}^2}{K} \lambda \right|$$

the combustion process is quasi-steady; i.e., the burning rate is in equilibrium with the instantaneous pressure. (Therefore, extinction cannot occur at pressures higher than the lower deflagration limit.) This interpretation of Eq. 2 follows directly from the original analysis (Appendix B), where it is recognized that the perturbation can be based on any quasi-steady state and, in this sense, is not restricted to small departures from the initial steady state. This criterion can be understood in physical terms by observing that (d ℓn p/dt) is just the inverse of the time constant associated with an exponential pressure decay in the combustion chamber, whereas $\bar{r}^2 \lambda / K$ is the inverse of the time constant associated with the response of the combustion mechanism. (Note that $K/\bar{r}^2$ is the well-known thermal relaxation time of a regressing solid surface when there are no reactions present.) Thus, the inequality of Eq. 2 can be restated as

$$\frac{\tau_{comb}}{\tau_p} > 1 \qquad (3)$$

where τ_{comb} = characteristic relaxation time of the combustion mechanism.

τ_p = characteristic time constant of the imposed pressure decay in the combustion chamber.

Therefore, the criterion given in Eq. 2 expresses the minimum pressure gradient that has to be imposed to ensure that the combustion mechanism will no longer be able to respond in phase with the pressure decay. When the pressure gradient exceeds this level, extinction may occur at other than the lower deflagration limit.

This interpretation of Eq. 2 allows a clear explanation of the theoretically predicted influence of surface-coupled reactions. It is shown in Appendix A that θ_s, which enters the parameter λ in Eq. 1, is

roughly proportional to the following ratio: heat release in surface-coupled reactions/total heat release in the entire combustion process. The proportionality constant for many propellants is about 10, so that when exothermic surface-coupled reactions are responsible for 10 percent of the total heat release in the system, $\theta_s \sim 1$; for 20 percent, $\theta_s \sim 2$; etc. The quantity φ is on the order of 10 for typical propellants. Therefore, with exothermic surface reactions, $\lambda = \theta_s - \varphi$ is negative, and an increase in θ_s tends to reduce the magnitude of λ. Thus, as θ_s increases, a lower pressure gradient is required to force a departure from quasi-steady burning. This conclusion is consistent with the physical interpretation outlined above; a higher θ_s corresponds to a lower fractional heat release in the gas-phase which response instantly to pressure changes, and to a higher surface-coupled heat release which does not respond instantaneously. Hence, with a higher θ_s, the overall response of the combustion mechanism is slower.

The main conclusions that emerge from the foregoing discussion are that (1) the distribution of energy release in the combustion process, which is reflected in the value of the parameter λ, has an important effect on the transient response of the propellant; and (2), that the criterion of Eq. 2 is a necessary but insufficient condition for extinction above the lower deflagration limit. Of these conclusions, the first is sufficient to explain why attempts to correlate data with Eq. 1 were largely unsuccessful. The second indicates that even the more correct criterion of Eq. 2, which accounts for kinetics effects that influence the distribution of heat research, is not wholly adequate. To properly account for extinction behavior, a nonlinear analysis is necessary, rather than the linear treatments underlying Eqs. 1 and 2.

Before proceeding with a more detailed consideration of the extinction process and outlining an appropriate nonlinear analysis, it will be useful to briefly consider the application of the combustion model to the combustion instability problem. It is intuitively evident that the transient response characteristics of the combustion mechanism to all forms of pressure perturbation are related. Thus, an examination of combustion instability provides further insight into extinction behavior and also affords a means of testing theoretical concepts.

Combustion Instability and Extinction

Several theoretical studies have been conducted on the transient combustion response of solid propellants, which is usually characterized in terms of the "response function" for application to combustion instability problems. Most of these studies, which are comprehensively summarized elsewhere,[13] have been basically similar and have neglected surface-coupled reactions entirely. Notable exceptions are the recent analyses by Friedly and Petersen[14] and by Culick[15] in which energetic surface reactions are considered. There have also been several treatments produced on the effect of surface reactions by Zel'dovich and his colleagues and students in the Soviet Union, recently summarized by Vantoch.[16,17]

All of these theoretical analyses lead to the conclusion that surface reactions tend to have a stabilizing influence on the propellant. However, this conclusion appears to be in direct conflict with our experimental observations on composite propellants.[9] Thus, it seems quite clear that the combustion models underlying these analyses, which differ mainly in mathematical details, do not adequately represent the true combustion mechanism of this class of propellants. The analyses appear to describe double-base propellants much better than composites, for the former are observed to have instability regimes that are essentially the opposite of those associated with composites.[9]

As has been explained, the new combustion model formulated during this investigation differs from earlier ones[1,2] primarily in the kinetics description of the surface reactions.[18,19] In terms of the surface kinetics, the SRI model distinguishes between composite and double-base propellants, unlike other theories. The application of this combustion model to the interpretation of combustion instability observations has been discussed in the open literature[11,19] as well as in other technical reports.[9] An abbreviated outline of this relatively complex analysis and the related conclusions appear in Appendix C to this report.

Comparisons with instability data have shown that the SRI model is consistent with observations of both double-base and composite propellants. Specifically, surface-coupled exotherms are shown to have a destabilizing effect on composite propellants, whereas pressure-sensitive surface exotherms tend to stabilize double-base propellants. This conclusion, which is confirmed by the instability data, has not been obtained with other theories; therefore the combustion instability results strongly support the theoretical concepts underlying the model developed during this study for consideration of extinction behavior.

In Appendix C, the influence of surface-coupled reactions on combustion instability is expressed in terms of the parameter θ_s. It will be recalled that θ_s is also the key parameter in the criterion of Eq. 2. Thus, this investigation has established a clear relationship between the combustion instability characteristics of a propellant and the extinction behavior of that propellant. This relationship has a significant bearing on determining the pressure gradient that should be imposed to make extinction possible; however, whether extinction will then occur is a considerably more complex question.

For example, it has been shown that composite propellants have a greater tendency to burn unstably as θ_s increases. Thus, if Eq. 1 were the only criterion for extinction, propellants with combustion instability problems might be expected to extinguish more readily than others, which is contrary to our observations. This is not a discrepancy, however; Eq. 1 is a necessary but insufficient criterion for extinction above the lower deflagration limit. To arrive at a complete understanding of extinction behavior, other aspects of the transient process have to be considered. The complex interactions that ultimately govern extinction behavior will be considered below in qualitative terms. This discussion will provide necessary background for the subsequent development of a more quantitative analytical approach to extinction.

Combustion Phenomena During Extinction

Before considering in general terms the qualitative nature of the combustion extinction process, it is appropriate to present the foregoing interpretation of the influence of the pressure gradient.

The lower diagram of Fig. 1 depicts schematically a typical pressure decay curve that might be imposed on a rocket chamber to extinguish combustion. Also shown in the corresponding quasi-steady burning rate curve, i.e., the trace the burning rate would follow if the steady-state burning rate law (e.g., $r = bp^n$) were valid throughout the process. The upper diagram shows the time constant for the pressure decay, which increases slightly with elapsed time only because the pressure decay is not truly exponential. The remaining parallel curves represent the relaxation times associated with the combustion mechanisms of two propellants having different percentages of surface-coupled heat release. Because the burning rate decreases with elapsed time, the combustion relaxation time increases sharply ($\tau_{comb} \approx K/\bar{r}^2 \lambda$). More intense surface-coupled heat release also increases the relaxation time.

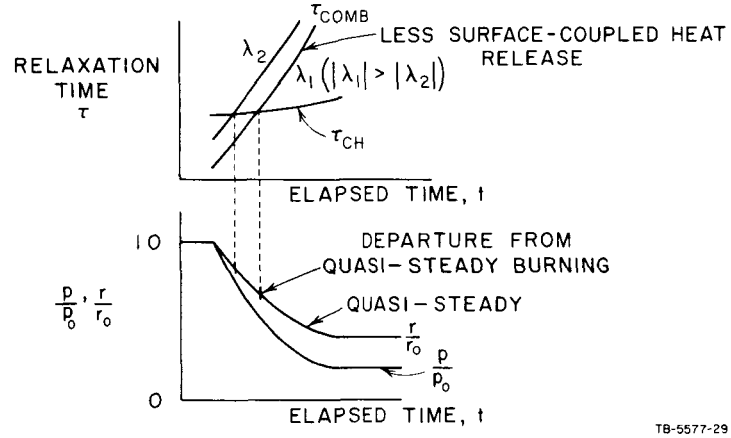

FIG. 1 EXTINCTION CHARACTERISTICS OF CRITICAL COMBUSTION PARAMETERS

As the pressure decay begins, the combustion relaxation time is much less than the time constant of the pressure decay. Therefore, the burning rate follows the quasi-steady curve. Eventually, the two time constants become of the same order, and beyond this crossover (i.e., with greater elapsed time), the inequality criterion of Eq. 2 is satisfied. The crossover point represents the final state of truly quasi-steady burning, and the foregoing interpretation of Eq. 2 assumes the instantaneous burning rate and pressure at this point to be the "initial conditions" ($\bar{p}$, $\bar{r}$) of the perturbation analysis.

Beyond the crossover point, the propellant may continue to burn, but the burning rate no longer follows the quasi-steady curve. If this crossover occurs at a pressure higher than the lower deflagration limit, extinction may (or may not) occur above that limit. If it falls below that limit, extinction will occur when the pressure reaches the lower deflagration limit, and not before. The higher the surface-coupled heat release, the sooner a departure from quasi-steady burning occurs, but to determine whether extinction then results requires consideration of other factors.

When the imposed pressure gradient meets the criterion of Eq. 2, the combustion process may follow one of three courses: (1) there still may be no extinction, unless the deflagration limit is reached; (2) there may be a "transient extinction," i.e., extinction followed by reignition; or (3) there may be true extinction (at a pressure higher than the deflagration limit, in general). The main consideration determining which alternative will occur in any given extinction experiment appears to be the transient heat transfer behavior in the solid grain between the solid and gas phases.

There is always a certain amount of thermal energy stored within the solid propellant, beneath the surface reaction zone, during the burning process. The total energy stored in this manner, $\int_0^\infty Cp\,(T-T_0)\,dx$, can be represented as the area under the temperature profile, as shown in Fig. 2. As the burning rate decreases, the steady-state profile becomes less steep; consequently, more energy is stored within the grain

with lower burning rates, assuming the profile has achieved its steady-state shape.

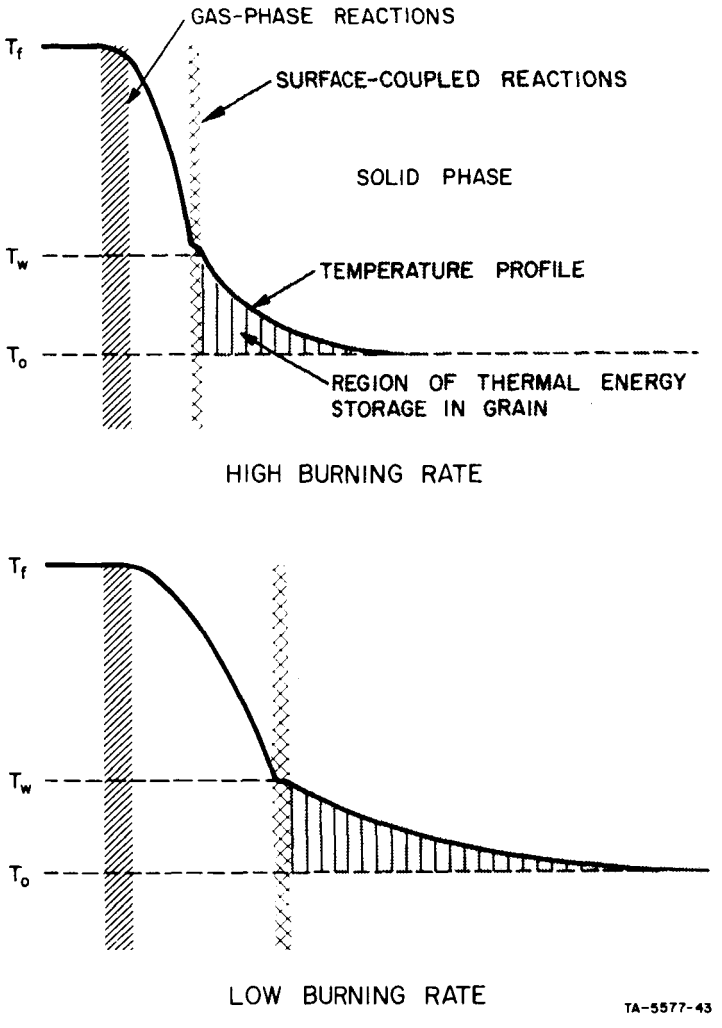

FIG. 2 THERMAL PROFILE AS A FUNCTION OF BURNING RATE

The complex interplay of several mechanisms that dominate extinction behavior can be clarified by following the transient temperature profile during a rapid depressurization and relating it to other transient combustion phenomena. Assume that the imposed pressure decay is sufficient to meet the criterion of Eq. 2 at some pressure level well above the lower deflagration limit. Before this point has been reached, the burning

rate and temperature profile closely correspond to their steady-state values at the instantaneous pressure. After this point (where Eq. 2 is satisfied), the burning rate begins to depart from the steady-state curve, as explained above. This departure occurs because the relaxation time of the combustion mechanism becomes greater than the time constant of the pressure decay (see Fig. 1). It follows that the burning rate tends to become higher than the steady-state value for the instantaneous pressure, because a lag in the combustion response means that the surface-coupled reactions tend to operate with a surface temperature higher than the steady-state value. Thus, the mass evolution from the surface, or the burning rate, is higher too.

During this initial period of departure from quasi-steady combustion, the temperature profile in the grain tends to stay approximately in equilibrium with the instantaneous burning rate, although the latter is not in equilibrium with the pressure. This conclusion is derived by noting that the burning rate is actually changing more slowly than the steady-state curve would indicate (Fig. 1), so that the profile can stay approximately in phase with the burning rate.

It is essential to remember that an operating regime is being considered in which gas-phase reactions always respond essentially instantaneously to the pressure decay. (For typical propellants and burning rates, this regime includes depressurization rates with a time constant of about 10^{-4} sec or greater, i.e., rates of primary practical importance.) Thus, although at lower pressures the surface-coupled reactions tend to proceed faster than they would with quasi-steady burning, causing a correspondingly higher burning rate, the gas-phase reactions do not. They proceed at the steady-state rate corresponding to the instantaneous pressure. Therefore, the relatively high mass evolution from the lagging surface-coupled reactions become more than can be consumed in the gas-phase reactions. As a result, the gas-phase flame becomes diluted, and may eventually be quenched. When the flame becomes diluted, the main source of energy feedback to the propellant surface is eliminated, since surface-coupled reactions typically provide only about 10 percent of the total energy. Consequently,

the temperature at the propellant surface begins to fall, as does the surface-coupled reaction rate and therefore the burning rate.

The sequence just described is illustrated schematically in Fig. 3. The imposed pressure decay and the resulting burning rate behavior are shown as solid curves. The quasi-steady burning rate trace, such as might be given by an empirical law of the type $r = bp^n$, is shown as a dashed curve. Shortly before point 1 on the figure is reached, the criterion of Eq. 2 is satisfied; therefore, at point 1 the burning rate departs from the quasi-steady curve. The resulting relatively high mass efflux begins to swamp the gas-phase flame at point 2, sharply reducing the energy feedback to the propellant. This leads to a rapid decrease in the burning rate. Whether extinction ensues depends on the relative importance and the relative time scales of subsequent interactions.

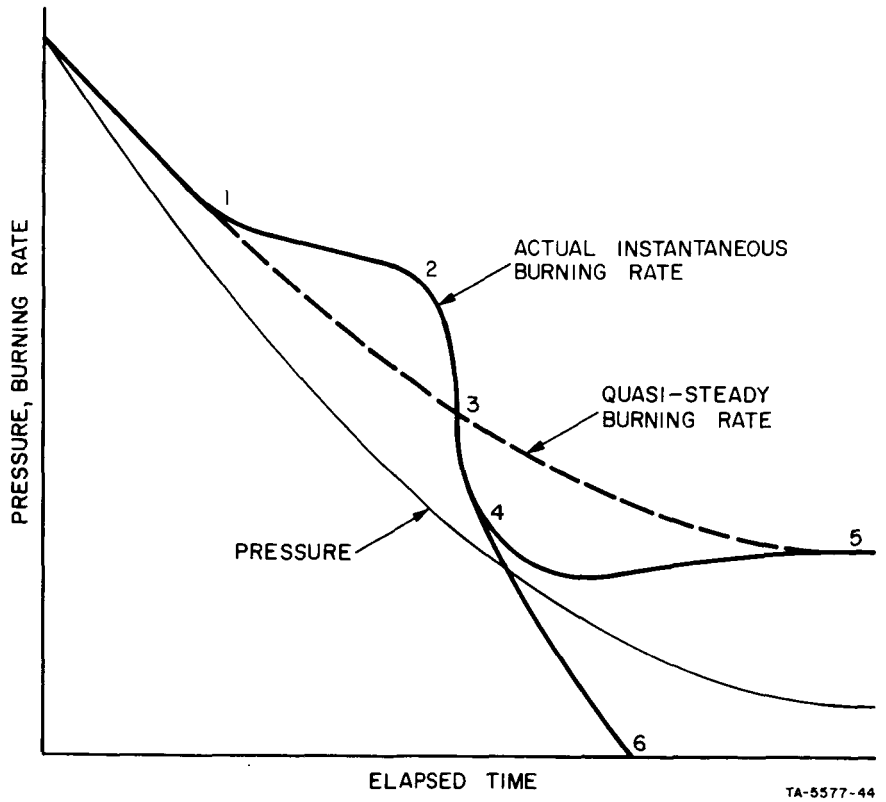

FIG. 3 BURNING RATE BEHAVIOR DURING DEPRESSURIZATION

At point 2, the temperature profile is still roughly the same as the steady-state profile corresponding to the instantaneous burning rate at that point. However, as the burning rate decreases rapidly, a substantial heat flux to the propellant surface is needed to maintain a quasi-steady profile, for more energy is stored in the grain at lower burning rates. (See Fig. 2). In general, the heat flux will be insufficient to maintain a quasi-steady profile, since the gas-phase flame has been effectively quenched at point 2, and the surface temperature will start to drop, enhancing the chance of extinction. However, note that at point 3 the burning rate becomes less than the quasi-steady value. This means that the excessive mass evolution that quenches the gas-phase flame at point 2 no longer exists.

Thus, the presence of hot combustion products may start the gas-phase flame again (e.g., at point 4), with a corresponding increase in heat transfer to the propellant. If this heat flux is sufficient to make up the difference between the energy stored in the grain at point 2 and that at the lower burning rate corresponding to the final chamber pressure (point 5), extinction will not occur. Instead, the burning rate will follow the path to point 5, ultimately achieving its steady-state value at the final pressure. On the other hand, if the heat transfer during this brief period is insufficient to develop the required final temperature profile, extinction will occur as indicated on the branch of the curve labeled 6. Whether branch 5 or 6 is taken depends on how different the profiles at points 2 and 5 are, how much time elapses between points 2 and 4, how great the energy release is after point 4, etc. These factors, in turn, depend on both the propellant and the imposed chamber conditions. For example, the difference between the temperature profiles at points 2 and 5 depends on the initial pressure gradient (which determines how soon point 1, and therefore point 2, is reached), as well as the final chamber pressure, or back pressure (which establishes the burning rate and temperature profile at point 5).

Finally, it should be noted that even when branch 6 of Fig. 3 is applicable, permanent extinction is not assured. After extinction occurs

at point 6, the heat transfer from residual hot combustion products in the chamber may be sufficient to establish a temperature profile and eventually induce surface pyrolysis and further exothermic reactions. In other words, reignition is a distinct possibility. In fact, the results reported in the Experimental Studies Section of this report indicate that reignition of this type, or "transient extinction," is one of the more important problems to be overcome. Owing to the relatively low heat transfer rate and the considerable total energy storage requirement in the grain, this type of reignition phenomenon typically occurs tens of milliseconds after the original extinction at point 6. Whether reignition occurs in a given instance also depends on a number of interrelated factors, including the preceding burning rate history (relative positions of points 2 and 4, etc.). The final chamber pressure, or back pressure, may be especially important, for it determines the total energy storage needed in the grain to re-establish steady burning. A low back pressure corresponds to a low burning rate and a high energy storage under the profile; a high back pressure corresponds to the opposite. Thus, a low back pressure greatly increases the total energy flux to the surface needed to cause reignition. Moreover, a low back pressure reduces gas-phase reaction rates, making it harder for these reactions to re-start. In both respects, then, a high back pressure is conducive to reignition, whereas a low final chamber pressure tends to prevent reignition.

In order to correlate extinction data and predict extinction performance, it is necessary to understand the complex interaction of events described in the foregoing discussion. In addition, the response of the combustion mechanism must be recognized as being closely coupled to the gasdynamics of the chamber. For example, in an actual motor, the pressure does not ordinarily follow a purely exponential decay curve as depicted in Fig. 3. Owing to the nozzle flow characteristics, there is usually a pressure spike shortly after the initial depressurization.[20] This spike can be very important, particularly in determining whether reignition occurs. If it arises soon after the original extinction (point 6), the opportunity for reignition is greatly enhanced

according to the argument presented above. Furthermore, if the spike should happen to coincide with the portion of the curve between points 2 and 4, extinction probably would not occur, or "chuffing" might arise. The position and height of the spike depends on the geometric configuration of the motor which is defined by the value of L^*.

It is clear that any quantitatively useful theory of extinction necessarily encompasses all of the inherently nonlinear phenomena discussed above, and therefore calls for a numerical analysis on the computer. The linearized analysis has demonstrated the general validity of the combustion model, which is the key feature of any further analysis. With this background as the justification and motivation, a more advanced analysis has been developed based on the modified combustion model described in Appendix D.

The Nonlinear Analysis of Transient Solid Propellant Combustion[†]

The nondimensional equations that describe the combustion model are as follows:

$$\frac{p_i V}{A_b R T_i}\frac{r_i}{\rho_s K}\left[\frac{1}{T_c^*}\frac{dp^*}{dt^*} - \frac{p^*}{T_c^{*2}}\frac{dT_c^*}{dt^*}\right] = r^* - \frac{p^* A_t^*}{T_c^{*\frac{1}{2}}} + m^* \qquad (4)$$

(chamber continuity)

$$\frac{p_i V}{A_b R T_i}\frac{r_i}{\gamma \rho_s K}\frac{dp^*}{dt^*} = r^* T_f^* - p^* A_t^* T_c^{*\frac{1}{2}} + h^* \qquad (5)$$

(chamber energy)

[†]Under this contract, programming of the nonlinear equations was begun. These theoretical studies are being completed in a follow-on project (Contract No. NAS1-7349) which started in June 1967.

$$r^* = p^{*n/2} \; T_f^{*1+n/2} \; \exp\left[(E_f/2RT_{f_i})(T_f^* - 1)/T_f^*\right] \tag{6}$$

(gas-phase propellant consumption)

$$r^* = \exp\left[(E_w/RT_{w_i})(T_w^* - 1)/T_w^*\right] \tag{7}$$

(solid-phase pyrolysis)

$$\left.\begin{aligned} &\frac{\partial T^*}{\partial t^*} = r^* \frac{\partial T^*}{\partial x^*} + \frac{\partial^2 T^*}{\partial x^{*2}} \\ &-\left(\frac{\partial T^*}{\partial x^*}\right)_w = r^* \left\{ (\epsilon_r Q_r - L)/c_s T_{w_i} - (c_p/c_s)\left[(T_{f_i}/T_{w_i})T_f^* - T_o^*\right] \right. \\ &\qquad \left. + (T_w^* - T_o^*) + (1 - T_o^*)(\zeta_H Q_H^* + \zeta_D Q_D^*) \right\} \\ &T^* = T_o^* \text{ at } x^* = \infty \end{aligned}\right\} \tag{8}$$

(solid-phase thermal profile behavior)

Q_H^* and Q_D^*, which represent the pressure-sensitive and pressure-insensitive contributions to the surface-coupled heat release, can be expressed in terms of an Arrhenius law by

$$\left.\begin{aligned} Q_H^* &= (p^*/T_w^*)^m \exp\left[(E_H/RT_{w_i})(T_w^* - 1)/T_w^*\right] \\ Q_D^* &= \exp\left[(E_D/RT_{w_i})(T_w^* - 1)/T_w^*\right] \end{aligned}\right\} \tag{9}$$

The parameters ζ_H and ζ_D represent the fractions of steady-state total heat of combustion associated with pressure-sensitive and pressure-insensitive surface-coupled reactions.

For large excursions in the burning rate, the net heat release in the gas-phase flame, $\epsilon_r Q_r - L$, must be treated as a variable in such a way that in the steady-state limit, the dependence of flame temperature on pressure matches that predicted from independent thermochemical calculations (see Appendix D). This concept can be introduced mathematically by writing the first boundary condition of Eq. 8 as

$$-\left(\frac{\partial T^*}{\partial x^*}\right)_w = r^* \left[(c_p/c_s)(T_{f_i}/T_{w_i})(\tilde{T}_f^* - T_f^*) + (T_w^* - T_o^*) + (1 - T_o^*)(\zeta_H Q_H^* + \zeta_D Q_D^*) \right] \tag{10}$$

In this case, $\tilde{T}_f^*$ is a fictitious flame temperature, i.e., the flame temperature that would exist in a fictitious steady-state having a surface-coupled heat release equal to the actual transient surface-coupled heat release. The calculation of $\tilde{T}_F^*$ must account for both the correct burning-rate behavior and the flame temperature behavior in the steady state. (Note that this analysis does not relate Q_r to the instantaneous values of T_w and p, but rather to the instantaneous heat release. It is assumed that in the nonsteady combustion process, the gas-phase heat release will be the same as the steady-state value for the same total heat release in the surface-coupled terms.)

EXPERIMENTAL STUDIES

The experimental studies carried out under this program consisted of measurements of the effect of formulational changes on the lower deflagration limit, differential thermal analysis (DTA) experiments, adiabatic self-heating (ASH) experiments, fiber-optic studies of the combustion zone, depressurization experiments in a variable volume burner, and the beginning of pressurization experiments in a small volume burner.

Lower Deflagration Limit (p_{DL}) Studies

Because of the importance of surface-coupled heat release factors in the transient burning rate regime, an experimental determination of the effect of propellant composition on the lower deflagration pressure limit (p_{DL}) was undertaken. The initial studies on the burning rate were made with a modified Crawford strand burner. While the burning rate was determined by conventional techniques, the lower limit for combustion was monitored using a photocell to detect burning as the pressure was slowly lowered (the depressurization rate was about 0.7 psi/sec).

The initial investigations were concerned with composite propellants based on two different binders, polybutadiene acrylic acid acrylonitrite (PBAN) and polyurethane (PU), and two different oxidizers, ammonium perchlorate (AP) and potassium perchlorate (KP). (The influence of a catalyst, Fe_2O_3, and of aluminum was also studied.) A modified composite propellant, Nitrasol, was also examined. The propellant formulations studied are detailed in Table I.

Burning rate plots for PBAN propellants with variable oxidizer loading are given in Fig. 4. Figure 5 is the plot for propellants containing KP and Nitrasol. It is readily apparent that the classical equation $r = ap^n$ does not satisfactorily represent the burning rate

Table I

PROPELLANT FORMULATIONS

Formulation	Weight Percentages			
	Oxidizer	Al	Binder	Ballistic Modifier
PBAN 103	80 NH_4ClO_4		20	
PBAN 285	80 NH_4ClO_4		19.5	0.5 Fe_2O_3
PBAN 286	80 NH_4ClO_4		19.0	1.0 Fe_2O_3
PBAN 287	80 NH_4ClO_4		18.5	1.5 Fe_2O_3
PBAN 288	80 NH_4ClO_4		18.0	2.0 Fe_2O_3
PBAN 289	72.5 NH_4ClO_4	7.5	20.0	
PBAN 290	70.0 NH_4ClO_4	10.0	20.0	
PBAN 291	67.5 NH_4ClO_4	12.5	20.0	
PBAN 292	65.0 NH_4ClO_4	15.0	20.0	
PBAN 293	84 NH_4ClO_4		16.0	
PBAN 294	86 NH_4ClO_4		14.0	
PBAN 295	88 NH_4ClO_4		12.0	
PBAN 109	80 KP		20	
PU 144	80 KP		20	
NIT 101	35 NH_4ClO_4	15.0	50	
PBAN 244	79 NH_4ClO_4		20	1 LiF
PBAN 284	79.5 NH_4ClO_4		20	0.5 $SrCO_3$

PBAN = Polybutadiene acrylic acid acrylonitrile binder

PU = Polyurethane binder

NIT = Nitrasol double base binder

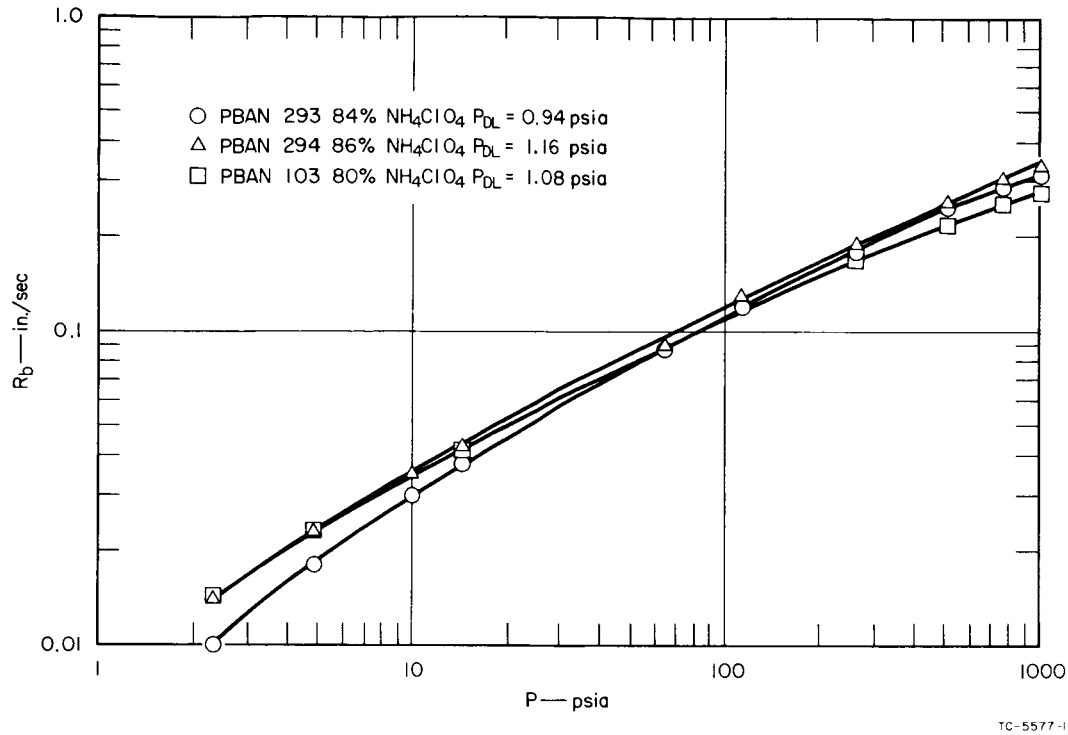

FIG. 4 BURNING RATES FOR OXIDIZER VARIATIONS

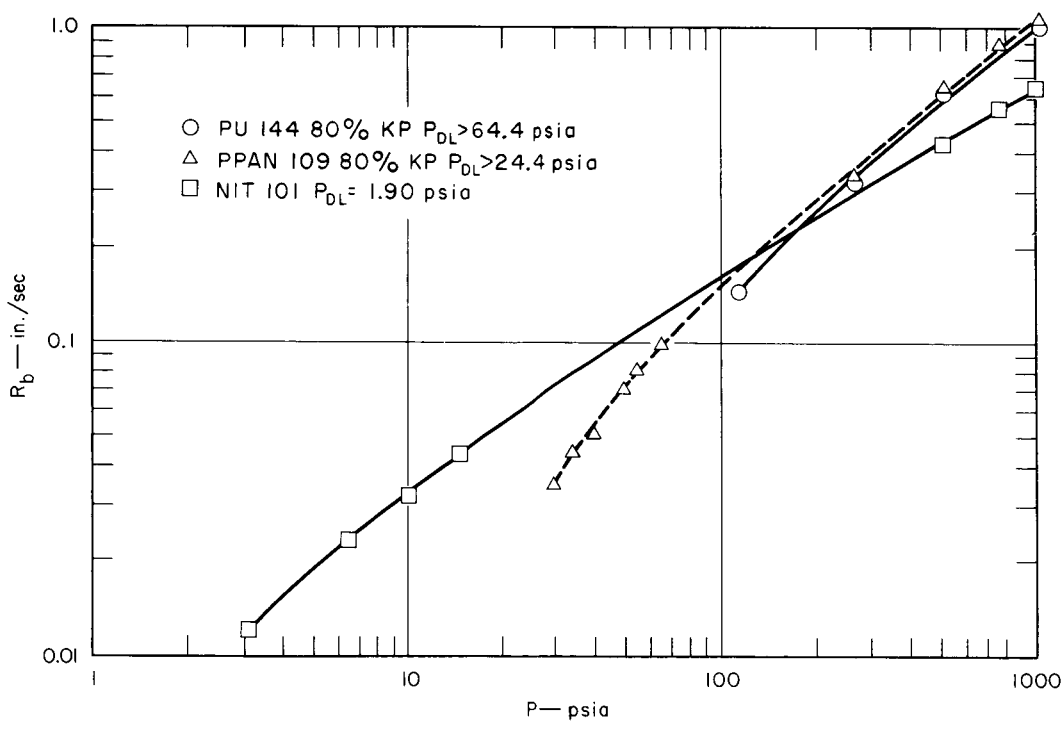

FIG. 5 BURNING RATES FOR POTASSIUM PERCHLORATE PROPELLANTS AND NITRASOL

much below 60 psia. (The deviations appear to be greater with aluminized propellants.) Summerfield[21] has proposed that the equation

$$\frac{1}{r} = \frac{a}{p} + \frac{b}{p^{1/3}}$$

is more applicable from theoretical considerations. He considered the pressure range from 1 kg/cm^2 to 140 kg/cm^2, whereas our study extends the range to 0.08 kg/cm^2. The Summerfield equation can be expressed as

$$\frac{p}{r} = a + bp^{2/3}$$

and a plot of log p/r versus log p should give a straight line. In Fig. 6, the burning rate data for one propellant from each variation study are plotted. The deviations at lower pressures for the aluminum and NH_4ClO_4 variants appear to be about the same as with $r = ap^n$. The burning rate of catalyzed propellants appears to be described better at all pressures by the Summerfield equation.

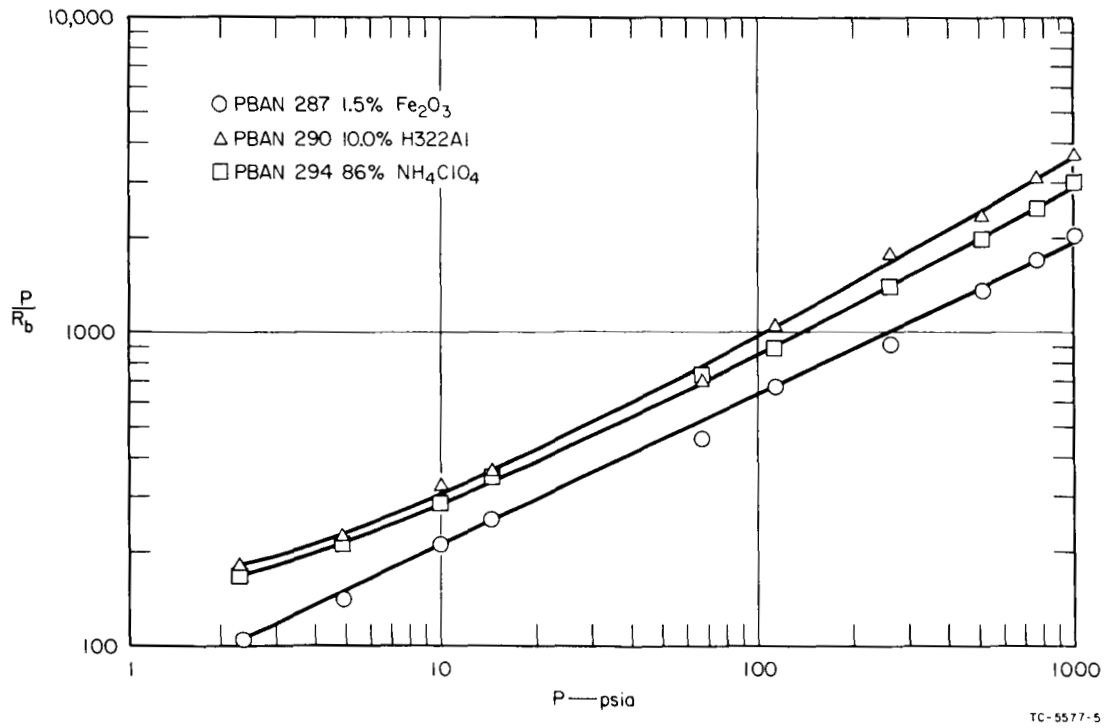

FIG. 6 SUMMERFIELD BURNING RATE

Lower deflagration pressures were measured in the strand bomb using a photocell to detect extinction. The output voltages of the photocell and a pressure transducer were recorded on an oscillograph. The lower deflagration pressure (p_{DL}) was taken as the pressure at which the photocell output became zero during a steady pressure decrease. About 20 seconds were required for the pressure to drop from 14.4 psia to 0.3 psia. Duplicate runs were made with each propellant, and the data obtained are listed in Table II. One of the striking features of these data is the remarkable consistency of the lower deflagration pressure for PBAN propellants containing ammonium perchlorate. Variation of AP from 80% to 86%, aluminum from 0% to 15%, and iron oxide from 0% to 2% did not change the lower deflagration pressure in the range from 0.94 psia to 1.58 psia.

In view of the invariance of NH_4ClO_4 propellants with regard to p_{DL}, other oxidizers and binders were investigated. The use of KP raises p_{DL} to about 24 psia. Surprisingly, a change from PBAN to PU binder with KP oxidizer resulted in a propellant that did not burn below 64 psia; a change to Nitrasol propellant containing both aluminum and AP gave a p_{DL} in the same range as that found for other propellants containing AP.

Another possible method of changing p_{DL} is by catalysis. Numerous investigators have documented the effects of such rate depressants as lithium fluoride and potassium fluoride. Ciepluch[20] reported that potassium fluoride made extinction easier, whereas a binder change from polybutadiene acrylic acid (PBAA) to PU did not influence extinction under his experimental conditions. p_{DL} for propellants catalyzed with lithium fluoride and strontium carbonate differs only slightly from p_{DL} for propellants not containing these ingredients.

A number of materials not usually considered as catalysts were tested in the strand burning bomb to determine their effectiveness in changing the lower deflagration pressures of both PBAN and PU propellant formulations; the only oxidizer used was AP. The related formulations and measured lower deflagration limits are given in Table III.

Table II

LOWER DEFLAGRATION PRESSURES

Formulation	Variable	Pressure, psia
PBAN 103	80% NH_4ClO_4	1.08
PBAN 293	84% NH_4ClO_4	0.94
PBAN 294	86% NH_4ClO_4	1.16
PBAN 295	88% NH_4ClO_4	1.36
PBAN 289	7.5% V.M. H-322 Al	1.58
PBAN 290	10.0% V.M. H-322 Al	1.39
PBAN 291	12.5% V.M. H-322 Al	1.35
PBAN 292	15.0% V.M. H-322 Al	1.41
PBAN 285	0.5% R-5098 Fe_2O_3	1.09
PBAN 286	1.0% R-5098 Fe_2O_3	1.29
PBAN 287	1.5% R-5098 Fe_2O_3	1.25
PBAN 288	2.0% R-5098 Fe_2O_3	1.27
PBAN 109	80% KP/PBAN Binder	>24.4
PU 144	80% KP/PU Binder	>64.4
NIT 101	15% Al/Nitrasol Binder	1.90
PBAN 244	1% LiF	2.10
PBAN 284	0.5% $SrCO_3$	1.40

Table III

PROPELLANT COMBUSTION DATA

Formulation	Catalyst	Oxidizer	P_{DL}
PBAN 296	1% ZnO	AP, 80%, 70/30, UG/11μ	0.77
PBAN 297	1% Cr_2O_3/TiO_2 (100/1)	AP, 80%, 70/30, UG/11μ	0.43
PBAN 298	1% Cr_2O_3/TiO_2 (100/0.5)	AP, 80%, 70/30, UG/11μ	0.89
PBAN 299	1% Cr_2O_3/TiO_2 (100/0.25)	AP, 80%, 70/30, UG/11μ	0.66
PBAN 300	1% NiO/TiO_2 (100/1)	AP, 80%, 70/30, UG/11μ	0.85
PBAN 301	1% $AgClO_4$	AP, 80%, 70/30, UG/11μ	0.43
PBAN 302	1% $CuCl(ClO_4)$	AP, 80%, 70/30, UG/11μ	0.31
PBAN 303	1% TeO_2	AP, 80%, 70/30, UG/11μ	0.62
PBAN 305	2% $Cu(ClO_4)_2$*	AP, 80%, 70/30, UG/11μ	0.83
PBAN 306	2% $CuCl(ClO_4)$*	AP, 80%, 70/30, UG/11μ	1.37
PBAN 308	1% n-Butyryl Ferrocene	AP, 80%, 70/30, UG/11μ	0.54
PU 145	--	AP. 70/30-UG/11μ, 80%	1.69
PU 145m	--	High-purity AP 70/30-UG/11μ, 80%	1.12
PU 148	1% CuO_2O_2P	AP 70/30-UG/11μ, 80%	1.55
PU 149	1% LiF	AP 70/30-UG/11μ, 80%	1.49
PU 146	1.5% Fe_2O_3	AP 70/30-UG/11μ, 78.5%	1.36

*Solution-coated on the 70% unground AP.

Certain of these catalysts were coated on the AP by a fluidized bed technique. The copper perchlorate was prepared by reacting CuO with 70.8% perchloric acid solution and precipitating the copper perchlorate from the saturated solution. Copper chloroperchlorate* was prepared by the reaction of silver perchlorate with anhydrous cupric chloride, as described by Baillie et al.[22] The chromic oxide doped with titanium dioxide was prepared by the method described by Solymosi.[23]

Burning rate data were not obtained for propellants containing 1% TeO_2, 2% $CuCl(ClO_4)$, or 2% $Cu(ClO_4)_2$, since observations during mixing suggested that these formulations were unstable (i.e., the mixtures became highly viscous and changed color). Molar ratios of Cr_2O_3 to TiO_2 were varied from 100/0.25 to 100/1.

It is perhaps significant that $Cu(ClO_4)_2$ and $CuCl(ClO_4)$ at the 2% level appeared to increase p_{DL} for PBAN 305 and PBAN 306. These catalysts were added by coating the 70% unground AP fraction by a solution-coating method employing acetone. The comparison of technical grade and high-purity AP in the polyurethane formulations. PU 145 and PU 145M showed that p_{DL} was lower for the propellant containing high-purity AP.

Differential Thermal Analysis (DTA) of Propellants

The theoretical combustion model that has been developed at SRI predicts a sizeable influence of surface-coupled heat release on the transient burning behavior. The present DTA studies, combined with mass spectrographic analysis of gaseous decomposition products, were used to differentiate between gas-phase reactions and solid-phase reactions that might occur during the decomposition of ammonium perchlorate and potassium perchlorate based propellants. These studies were performed at a series of pressures ranging from 1 to 70 atmospheres.

A DTA cell designed to operate at elevated pressures was fabricated; its detailed construction is shown in Fig. 7. The cell is fitted with safety rupture diaphragms. The gaseous decomposition products can, when

*Copper chloroperchlorate is unique in that it is readily soluble in organic compounds.

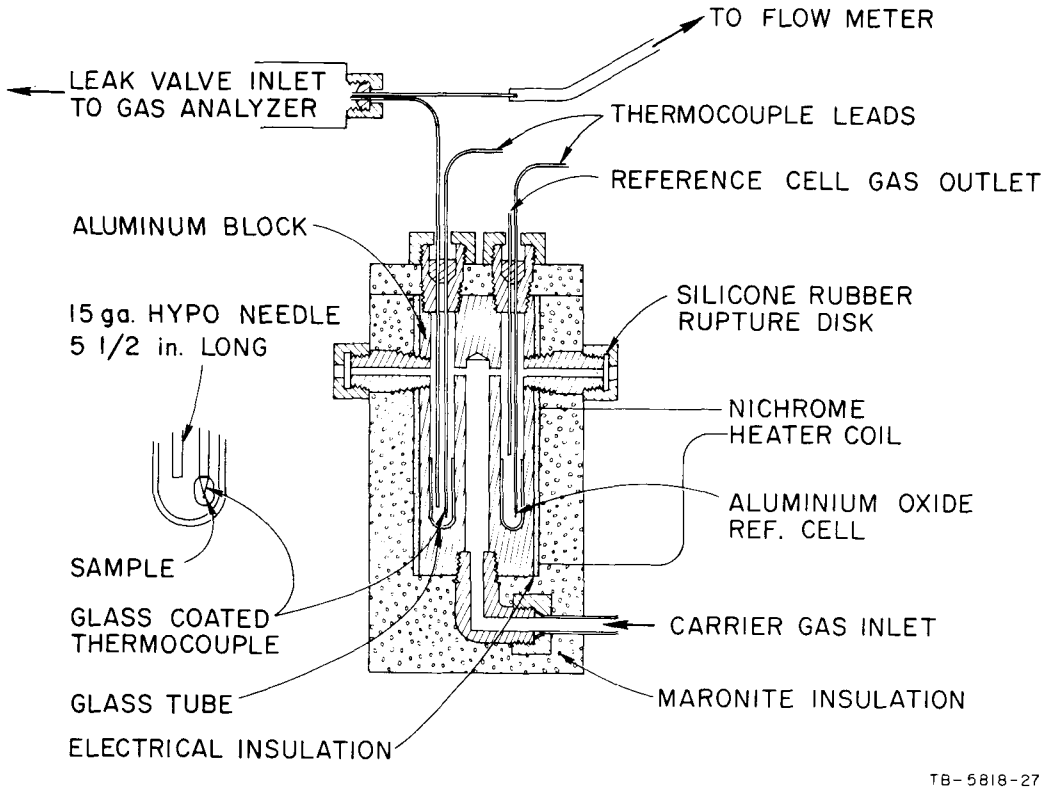

FIG. 7 HIGH-PRESSURE DTA CELL

desired, be ducted to an analytical mass spectrometer. In the studies performed, a quadrupole residual gas analyzer (Electrical Associates Incorporated, Quad 210) was used.

Initial experiments were carried out at atmospheric pressure. The first point to be investigated was the effect of AP purity on the DTA of AP. Figure 8 shows the DTA results on technical-grade and high-purity AP analyzed, as indicated in Table IV. It is seen that technical-grade AP gives an initial decomposition exotherm at 325°C which does not appear on the DTA curve for high-purity AP.

In Fig. 9, the DTA results comparing the behavior of high-purity and technical-grade AP in a polyurethane propellant containing 75% AP are given. The DTA responses are almost identical. It appears that contact with the polyurethane binder caused the exothermic response to

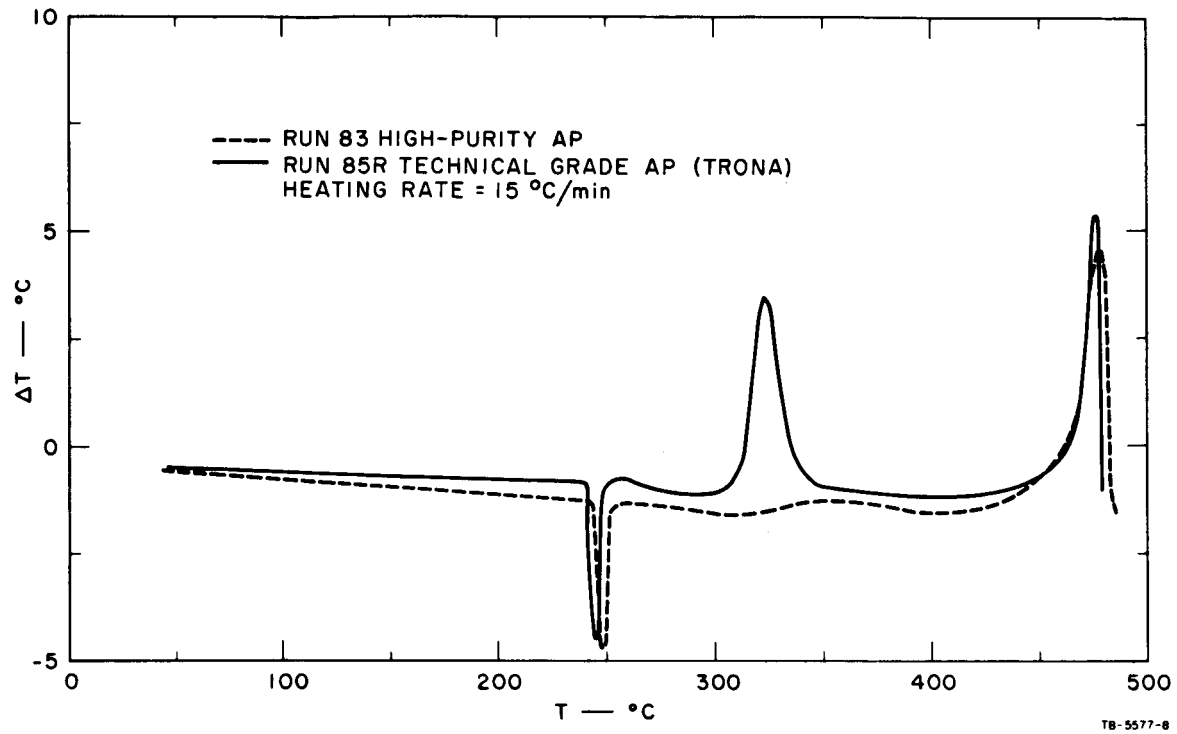

FIG. 8 DIFFERENTIAL THERMAL ANALYSIS OF AMMONIUM PERCHLORATE

Table IV

COMPARISON OF TECHNICAL GRADE
AND HIGH-PURITY AMMONIUM PERCHLORATE

	High-Purity %	Technical-Grade %
NH_4ClO_4	99.8	99.3
NH_4Cl	0.02	0.10
$NaClO_3$	Trace	.007
Sulphated Ash	Trace	0.33
Insoluble	.002	0.109
Total Moisture	0.079	0.048
Metal Oxide (Nonalkali)	0.001	--
pH	5	6
Iron as Fe	--	.0002
Tricresylphosphate	--	0.20
Na	5 ppm	175
K	4 ppm	55

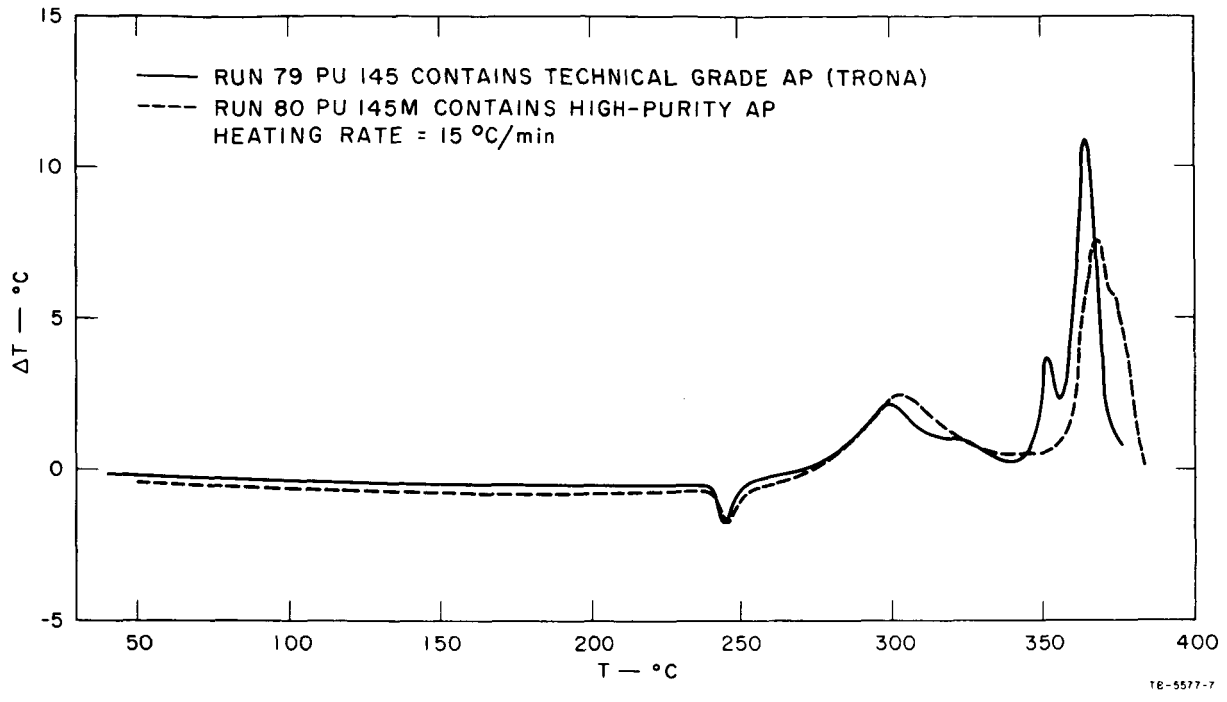

FIG. 9 DIFFERENTIAL THERMAL ANALYSIS OF AMMONIUM PERCHLORATE PROPELLANTS

be the same in both high-purity and technical-grade AP. One possible reason for this is the solubility of AP in the binder and subsequent catalytic effect of binder impurities. Another may be the presence of exothermic surface reactions in the solid phase between the binder and AP.

Figures 10 and 11 show the DTA thermograms for propellants made from technical-grade AP and high-purity AP, the variable being the lack or presence of FeAA as a binder-curing catalyst. The binder is made from a hydroxy-terminated polybutadiene (PBD) cross linked with TDI. The propellant formulation is given in Table V. An equivalence ratio for diol/triol/NCO of 75/25/107 was used in the binder.

The presence of FeAA in the propellant containing technical-grade AP as a curing catalyst clearly causes the predecomposition exotherm and the final exotherm to occur at a lower temperature, perhaps as much as 30°C lower. When high-purity AP is used in the same formulation, the addition of Fe does not appear to be a significant variable.

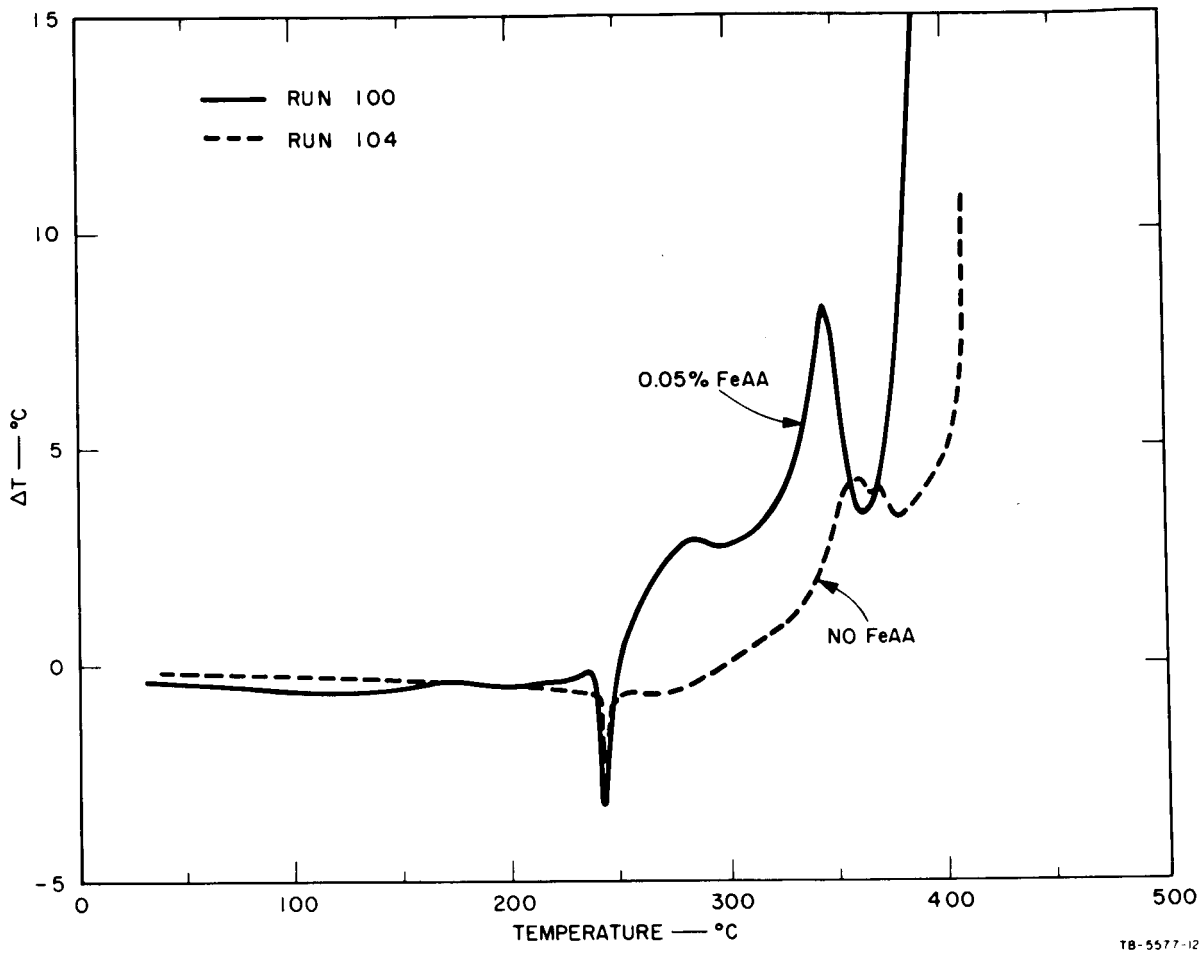

FIG. 10 DTA THERMOGRAMS FOR PBD PROPELLANT WITH TECHNICAL GRADE-AP

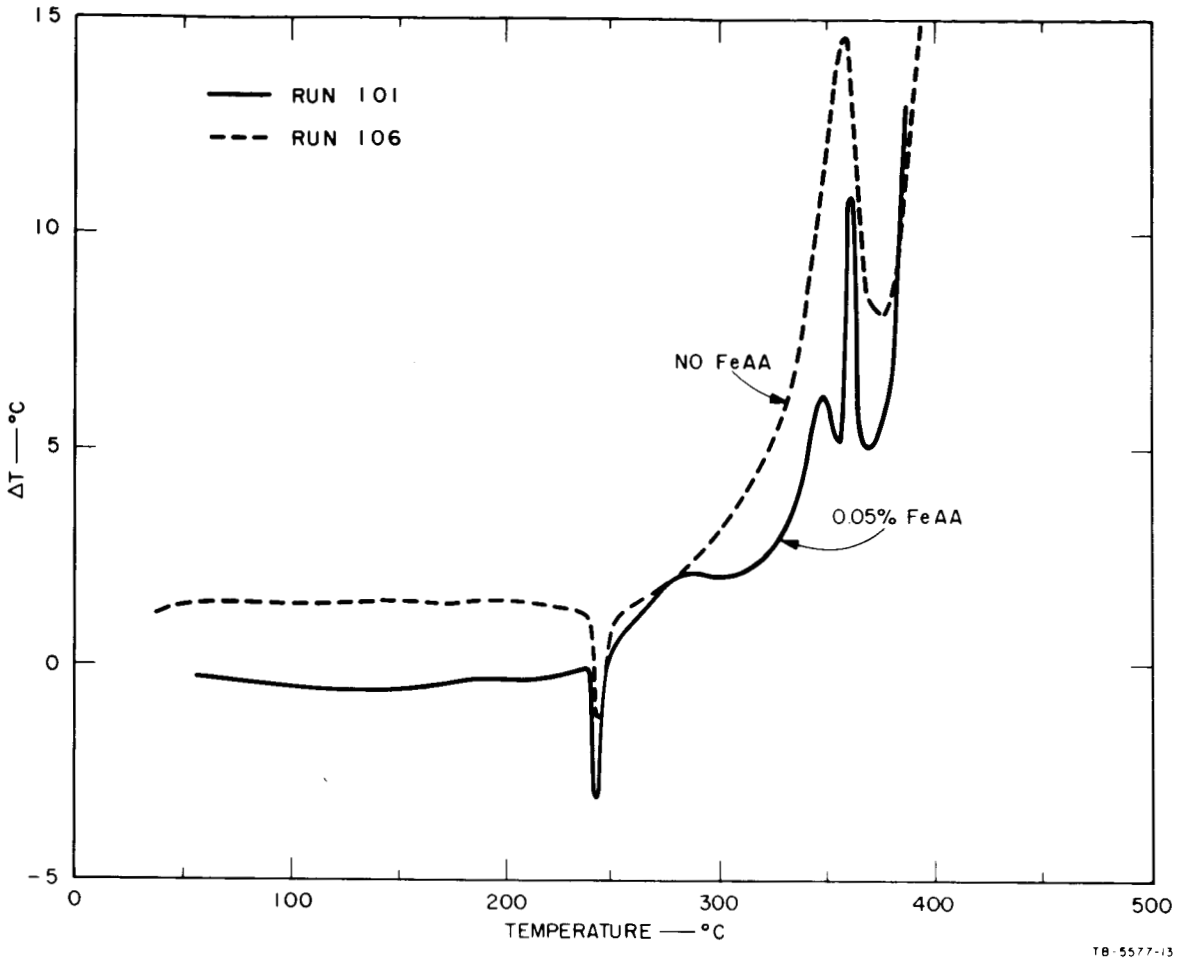

FIG. 11 DTA THERMOGRAMS FOR PBD PROPELLANT WITH HIGH PURITY-AP

Table V

PBD PROPELLANT FORMULATION

Ingredient	Weight %
Ammonium perchlorate, 70/30 UG/11μ	80.00
Sinclair PBD, R45	16.81
LHT 240 (Union Carbide Polyol)	1.23
Tolylene Diisocyanate	1.91
Ferric Acetyl Acetonate (FeAA)	0.05

The DTA thermograms in Fig. 12 show the interaction of technical-grade and high-purity AP with polypropylene glycol (PPG) 2025, the basic ingredient of many polyurethane formulations. Although the predecomposition exotherms are different, both indicate appreciable reaction exotherms before deflagration occurs. On the basis of these data, there is little likelihood that high-purity AP can be used in a formulation containing PPG 2025 (good commercial quality) to eliminate the predecomposition exotherms; however, it appears to significantly decrease the peak temperature of the exotherm (from 380°C to 320°C).

It is desirable to try to delay the exotherm occurring after the crystal change endotherm in AP to as high a temperature as possible. Since all binders seemed to cause the onset of the exotherm at lower temperatures, it appeared that a compatible coating on the oxidizer might give the desired separation to prevent binder/oxidizer interactions. Accordingly, both technical-grade and high-purity AP were coated with 3% by weight of Viton A[24] and 3% of vinylsiloxane.[25] The resulting thermograms are shown in Figs. 13 and 14. Both delayed the predecomposition exotherm of technical-grade AP by only 10°C. Neither caused the early exotherm noted with other binders in contact with high-purity AP, although vinylsiloxane did lower the exotherm to 350°C and Viton A to 395°C from a high of 410°C for the untreated control sample. In propellants, neither treatment was effective on technical-grade AP.

The thermograms for a hydroxy-terminated PBD propellant containing 70% technical-grade AP are shown in Fig. 15. Since the vinyl-siloxane coating was easier to apply and made a more fluid propellant, it was formulated into a PBD propellant containing 70% high-purity AP. The thermograms in Fig. 16 show that the onset of the exotherm appears to be displaced almost 50°C higher than for the sample containing uncoated AP.

In Fig. 17, burning rate curves are shown for the propellants listed in Table VI. Note that propellants containing 2.5% vinylsiloxane were tested with the additive as a coating on the AP and as a free agent.

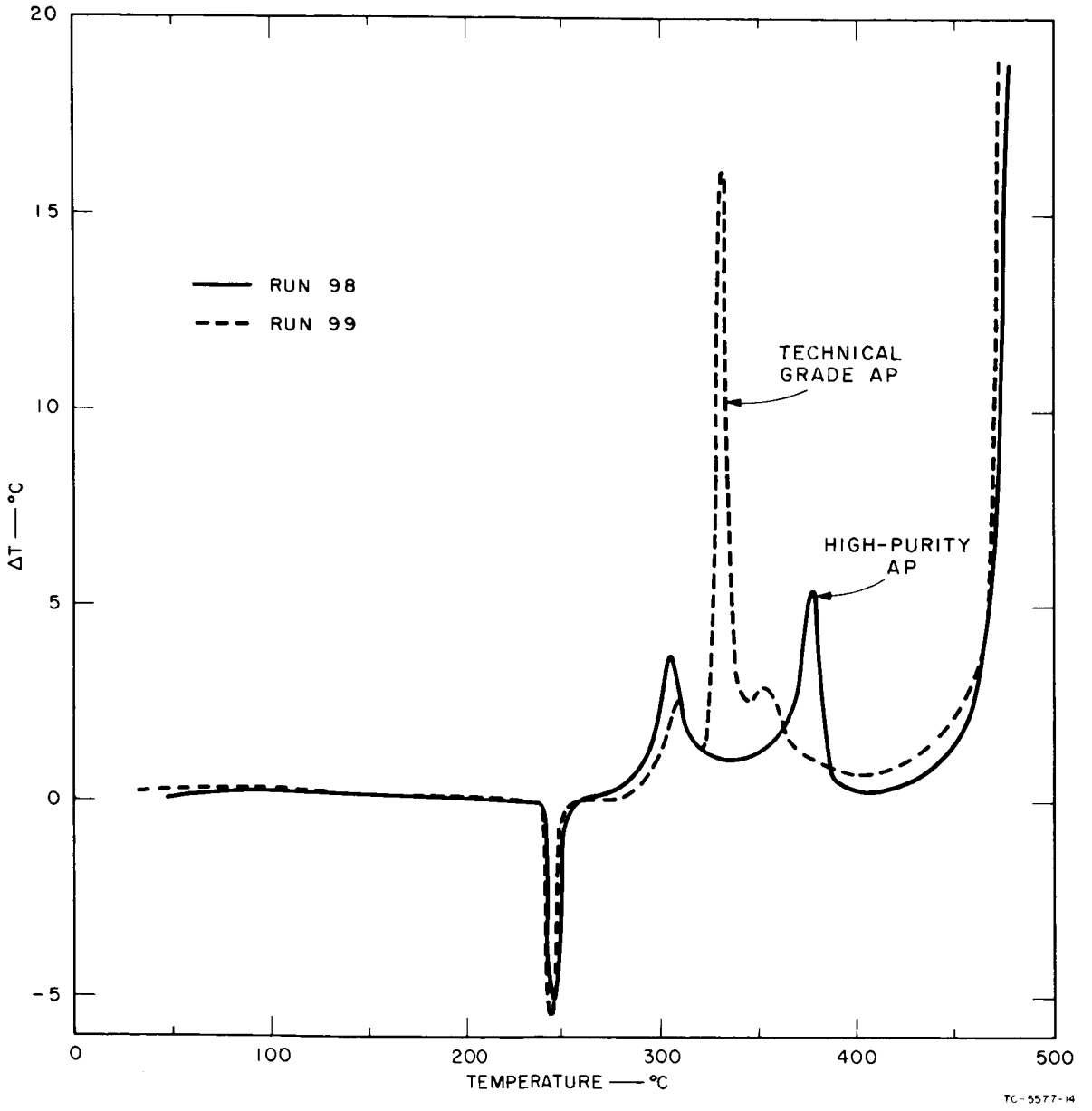

FIG. 12 DTA THERMOGRAMS FOR 80/20 AP/PPG MIXTURES SHOWING EFFECT OF AP PURITY. Heating rate = 15°C/min

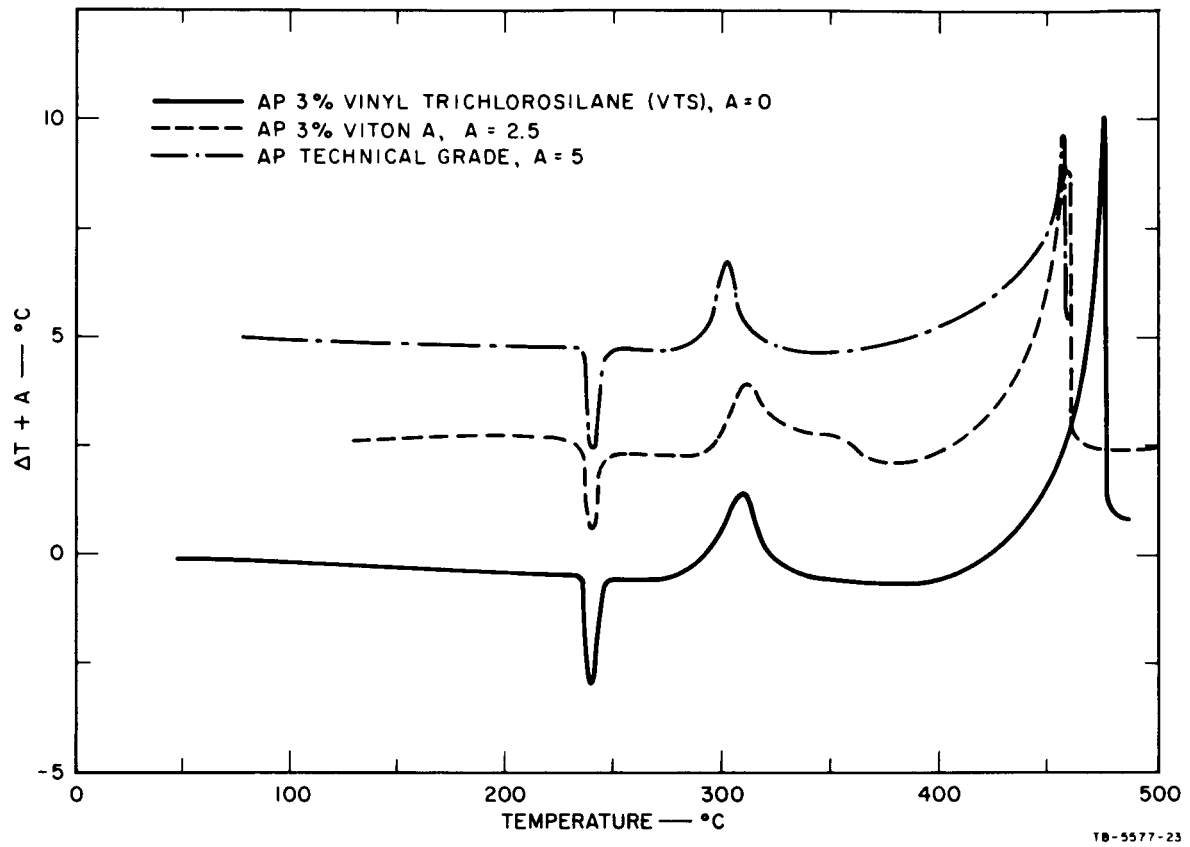

FIG. 13 DTA THERMOGRAMS FOR COATED TECHNICAL-GRADE AMMONIUM PERCHLORATE

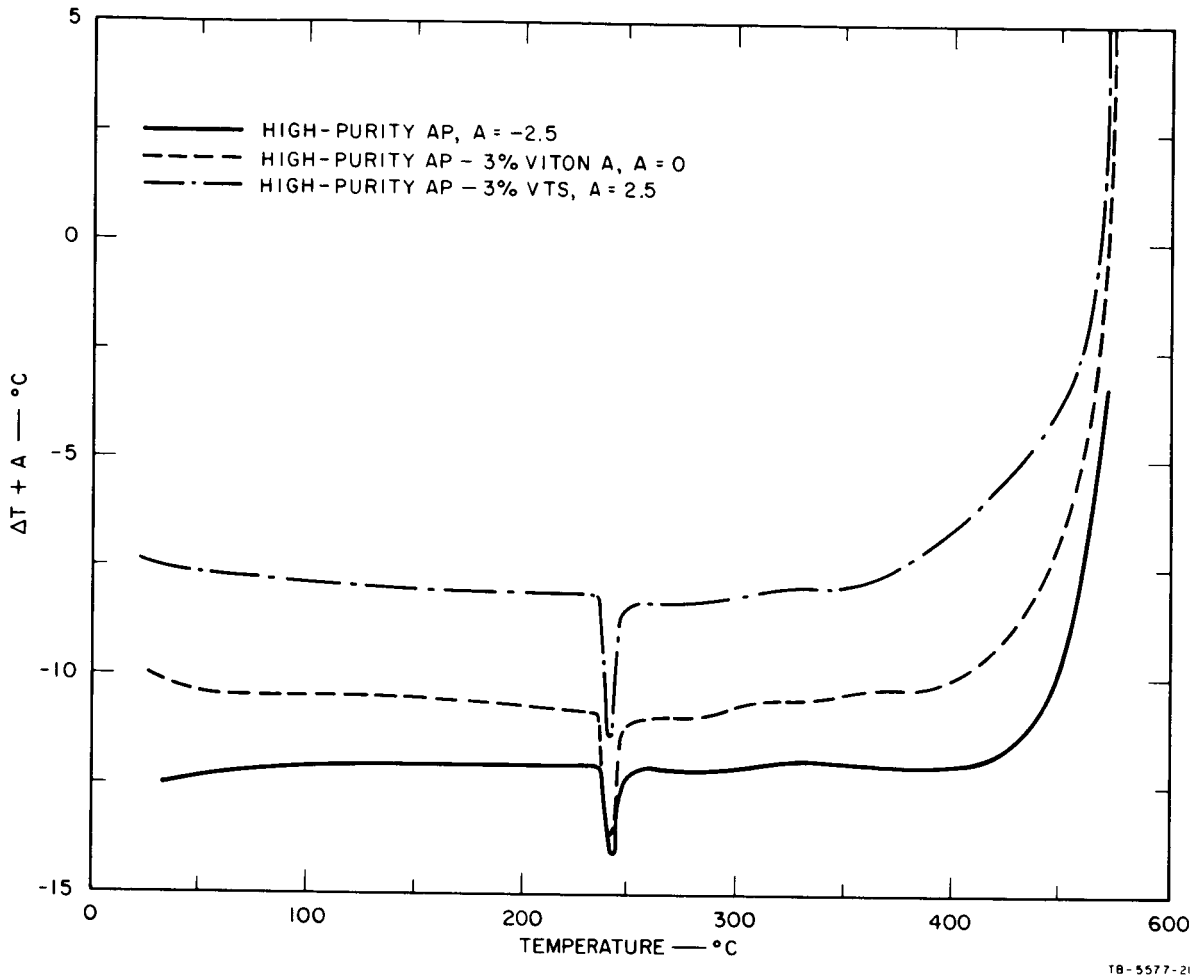

FIG. 14 DTA THERMOGRAMS FOR COATED HI-PURITY AMMONIUM PERCHLORATE

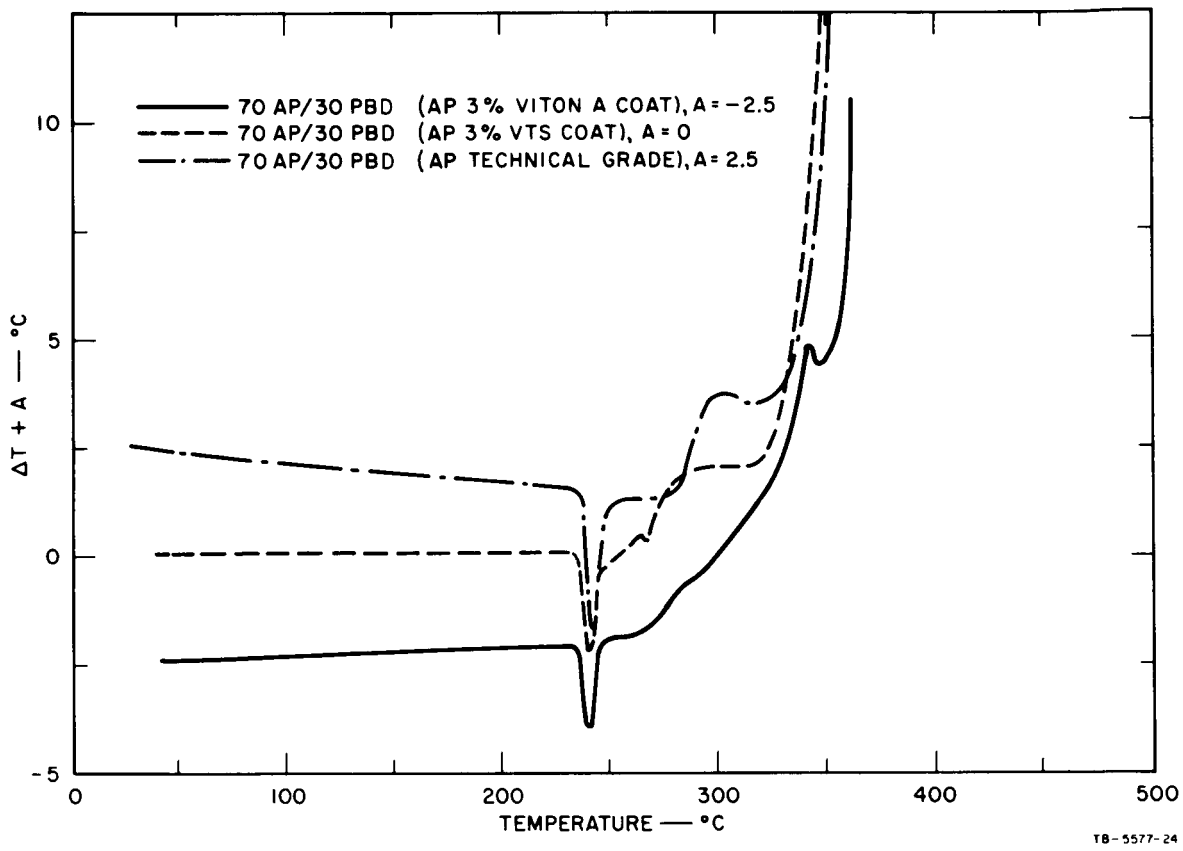

FIG. 15 DTA THERMOGRAMS FOR PROPELLANTS CONTAINING COATED TECHNICAL-GRADE AMMONIUM PERCHLORATE

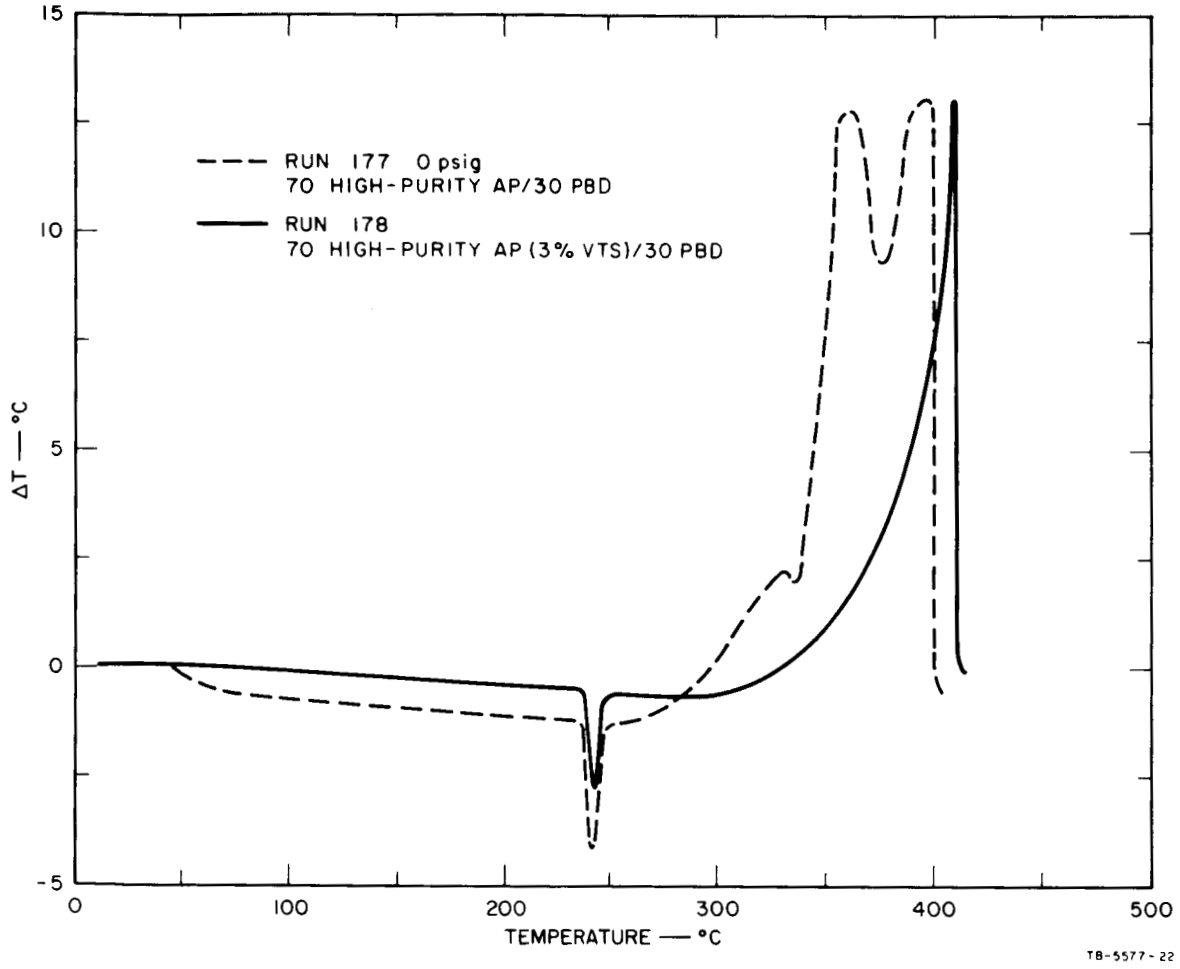

FIG. 16 DTA THERMOGRAMS FOR PROPELLANTS CONTAINING COATED HIGH-PURITY AMMONIUM PERCHLORATE

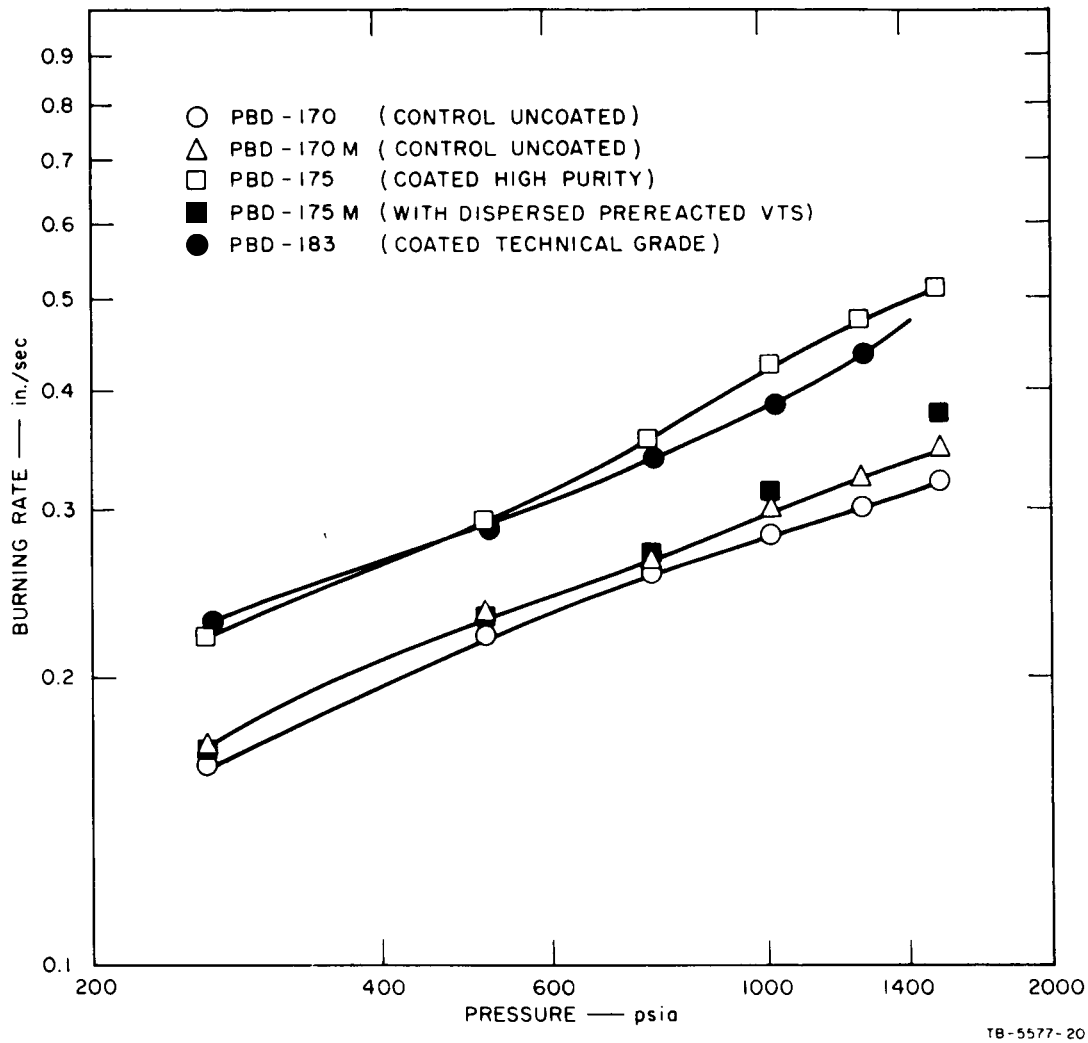

FIG. 17 BURNING RATE FOR PROPELLANTS CONTAINING COATED AND NONCOATED OXIDIZERS

Table VI

PROPELLANT COMPOSITIONS FOR COATED OXIDIZER STUDY

Formulation	Oxidizer[a]	Binder	Ballistic Modifier
PBD 170	80 HPAP[b]	20	
PBD 170M	80 AP	20	
PBD 175	80 HPAP	17.5	2.5 vinylsiloxane[c]
PBD 175M	80 HPAP	17.5	2.5 vinylsiloxane (not coated)
PBD 183	80 AP	17.5	2.5 vinylsiloxane[c]

[a] 70% as received, 30% 11μ ground.

[b] HPAP = high-purity ammonium perchlorate.

[c] solution coated on all AP.

Since the coated AP propellant exhibits the higher burning rate, it is possible that the energy release and temperature profiles have been modified by the suppression of interfacial heterogeneous reactions. These changes may be reflected in the higher burning rate, since the vinylsiloxane did not function as a catalyst when dispersed in the conventional manner.

With the background data established for ammonium perchlorate at atmospheric pressure, the influence of pressure on DTA thermograms was next studied for a specially prepared propellant. This propellant contained 70% by weight of the highly purified ammonium perchlorate and 30% by weight of a specially purified hydroxy-terminated PBD-based binder prepared from a PBD polymer (PBD R-45, Sinclair Petrochemicals) and toluene diisocyanate. (The choice of highly purified ingredients is critical for the clean separation of the observed exotherms.)

This special propellant was studied in the DTA cell at pressures up to 70 atmospheres (1000 psia), and the data obtained are shown in Fig. 18. At pressures up to 25 atmospheres (350 psia), two or more exotherm peaks occur; the first, from 350°C to 360°C, is unaffected by

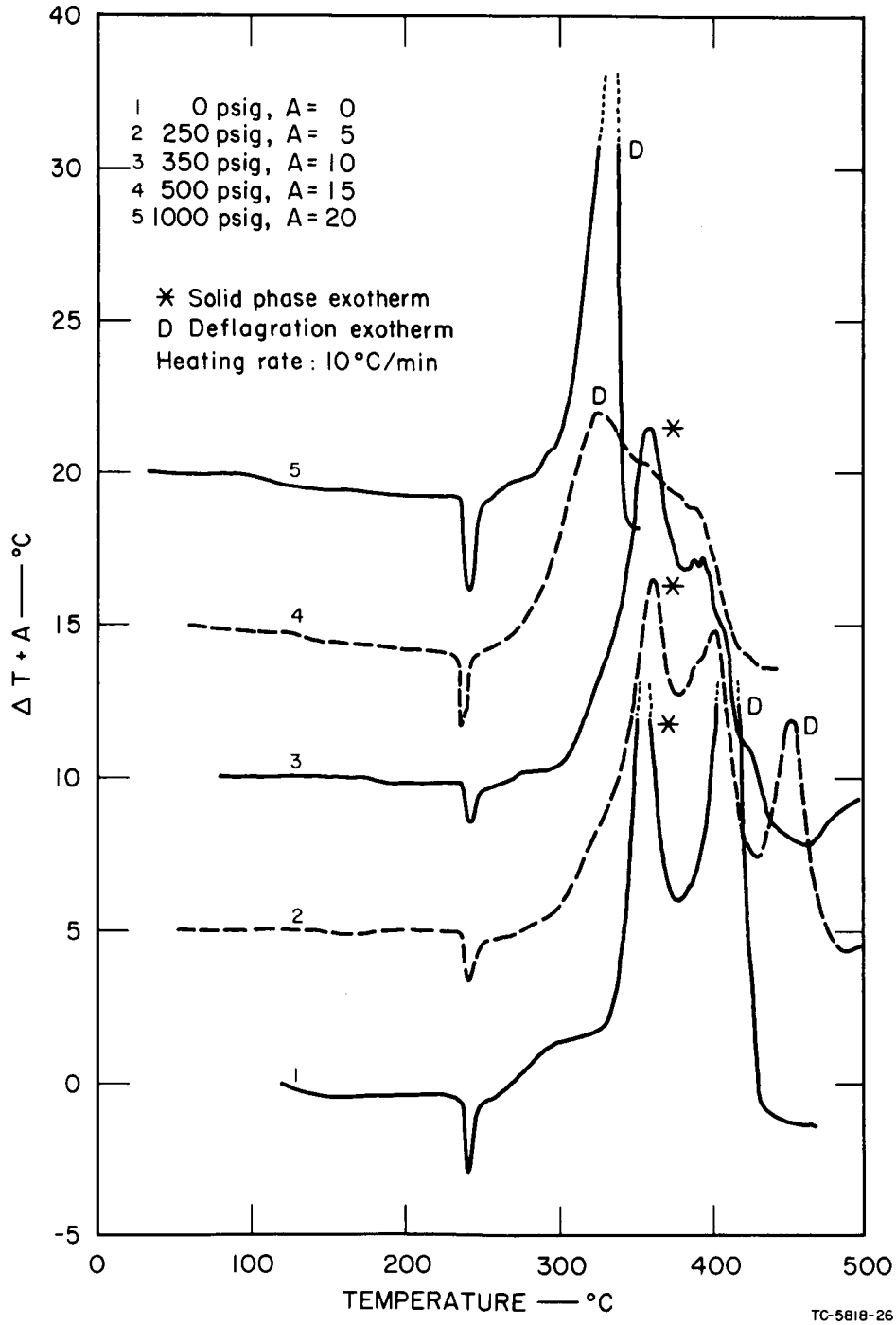

FIG. 18 THERMOGRAMS FOR PURIFIED PROPELLANTS AT AMBIENT AND ELEVATED PRESSURES

pressure change, but as the pressure is increased above 25 atmospheres, the exotherms appear at successively lower temperatures until at 34 atmospheres (500 psia), only one deflagration exotherm is recorded.

To gain additional information that would help explain observed phenomena, the DTA sample capillary was swept with a carrier gas (nitrogen) which was sampled continuously through the quadrupole residual gas analyser. This instrument uses a quadrupole and rf electric field for mass analysis, and provides a rapid response of about 10 milliseconds when scanning the mass range 0-50. All tests were done at atmospheric pressure in order to obtain maximum separation of the exotherms. Any gaseous decomposition products were continuously monitored as the sample temperature increases. The gas transit time through the hot sampling capillary was approximately one second, whereas the duration of a typical exotherm was on the order of four minutes; thus for all practical purposes, sample analysis was instantaneous. Gas sampling data for the production-grade AP (which did not contain an anticaking agent) are given in Table VII. Little gas evolution occurred until the deflagration exotherm commenced above 400°C. A very slight amount of oxygen (less than 10^{-6} moles/100 grams sample) came off during the pre-decomposition exotherm. It can be concluded, therefore, that this is primarily a solid-phase exotherm resulting from decomposition or reaction of trace contaminants; sodium chlorate is a likely candidate,

$$NaClO_3 \longrightarrow NaClO_4 + \tfrac{1}{2}O_2$$

Other unidentified organic contaminants introduced during preparation of ammonium perchlorate may also contribute to this pre-deflagration exotherm.

Relating the data on the first exotherm to the observed trends in behavior shown for the propellant in Fig. 18, it is surmised that, over the interval of 15 psia to 350 psia, pressure sensitivity causes the trailing exotherms to move to lower temperatures until at 500 psia, the gas-phase reactions predominate.

Table VII

MASS SPECTROGRAPHIC
GAS ANALYSIS OF PRODUCTION GRADE

Species Detected		Mass to Charge Ratio m/e
at 310°C	at 460°C	
Trace O_2	H_2O^+	18
	N_2^+	28
	NO^+	30
	O_2^+	32
	HCl^+	36
	N_2O^+	44

By using the known endotherm of 2.3 kcal/mole for the ammonium perchlorate crystal change[26] (identified as the DTA endotherm at 240°C), it is feasible to estimate the percentage of total heat release contributed by the solid-phase exotherm. Since neither the endotherm nor exotherm is associated with the generation of any gases (which would result in mass changes and heat transport), it is considered permissible to relate the areas beneath the endotherm and exotherm of the DTA thermogram to the amounts of heat released or absorbed.[27] Thus, the thermogram at atmospheric pressure indicates that the condensed-phase reaction heat release for the propellant studied is 0.172 kcal/g. This is approximately 18% of the total heat release during explosion, 0.94 kcal/g, as measured in a calorimeter.

The experimental results for the special KP propellant are shown in Fig. 19, and the related gas analysis data are given in Table VIII. The data for the first exotherm at between 360°C and 368°C established that hardly any gas evolved, other than trace amounts of water and carbon dioxide. Thus, the first exotherm is apparently a condensed-phase reaction little affected by pressure. Significant gas evolution is associated with the other exotherms.

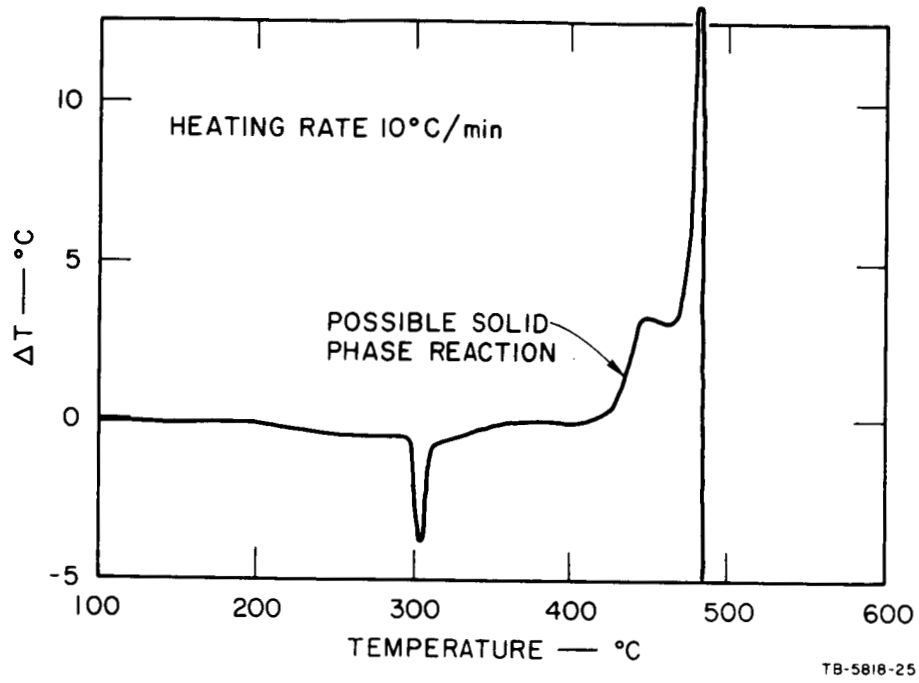

FIG. 19 THERMOGRAM FOR POTASSIUM-PERCHLORATE-BASED PROPELLANT

Table VIII

MASS SPECTROGRAPHIC GAS ANALYSIS OF
70/30 HIGH-PURITY AP/PBD PROPELLANT

Species Detected		Mass to Charge Ratio m/e
at 360°C	at 410°C	
	H_2^+	2
	C^+	12
	NH^+, CH_3^+	15
Trace H_2O^+	H_2O^+	18
	C_2	24
	CN^+	26
	HCN^+	27
	NO^+, CH_2O^+	30
	O_2^+	32
	HCL^+, C_3^+	36
Trace CO_2^+	CO_2^+	44

It is of significance that DTA thermograms for potassium perchlorate and potassium perchlorate propellants showed only a deflagration exotherm. Even a liberal estimate of the heat release associated with solid-phase reactions in the propellant would not be above 5% of the total heat of explosion.

Activation Energy Determination by the Adiabatic Self-Heating (ASH) Technique

The effect of formulational variables on the activation energies for exothermic solid-phase heat release from solid propellants has been investigated by the adiabatic self-heating (ASH) technique.[38] In this method, a propellant sample of approximately one gram is heated rapidly in an aluminum block to the temperature at which self-heating begins. The environmental temperature is then continuously changed to follow the temperature of the self-heating sample. Under these conditions, the rate of reaction is directly proportional to the rate of temperature change. Assuming that the rate of reaction is given by an Arrhenius expression, then

$$\frac{dT}{dt} = Be^{-E_H/RT} \qquad (11)$$

A graph of ln dT/dt versus 1/T will be linear with a slope equal to E_H/R. Examples of data treated in this manner are shown in Figs. 20, 21, and 22. The formulational variable in this case was the binder species. PBD and PU binders differ primarily in the degree of unsaturation in the backbone polymer. These binders are chemically pure, in that inhibitors and metallic catalysts were not used and by-product chemicals left over from manufacturing are at a minumum. The PBAN binder is relatively impure, in that it contains such chemicals as sulfur, phenyl-b-naphthylamine (antioxidant), acetyl-dimethyl-benzyl ammonium chloride (emulsifier), and unreacted acrylonitrile.

With PBD and PU binders, the reaction rate fits the Arrhenius form from self-heating rates of 2°C per minute through 30°C per minute, at which rate the reaction proceeded faster than the external temperature could

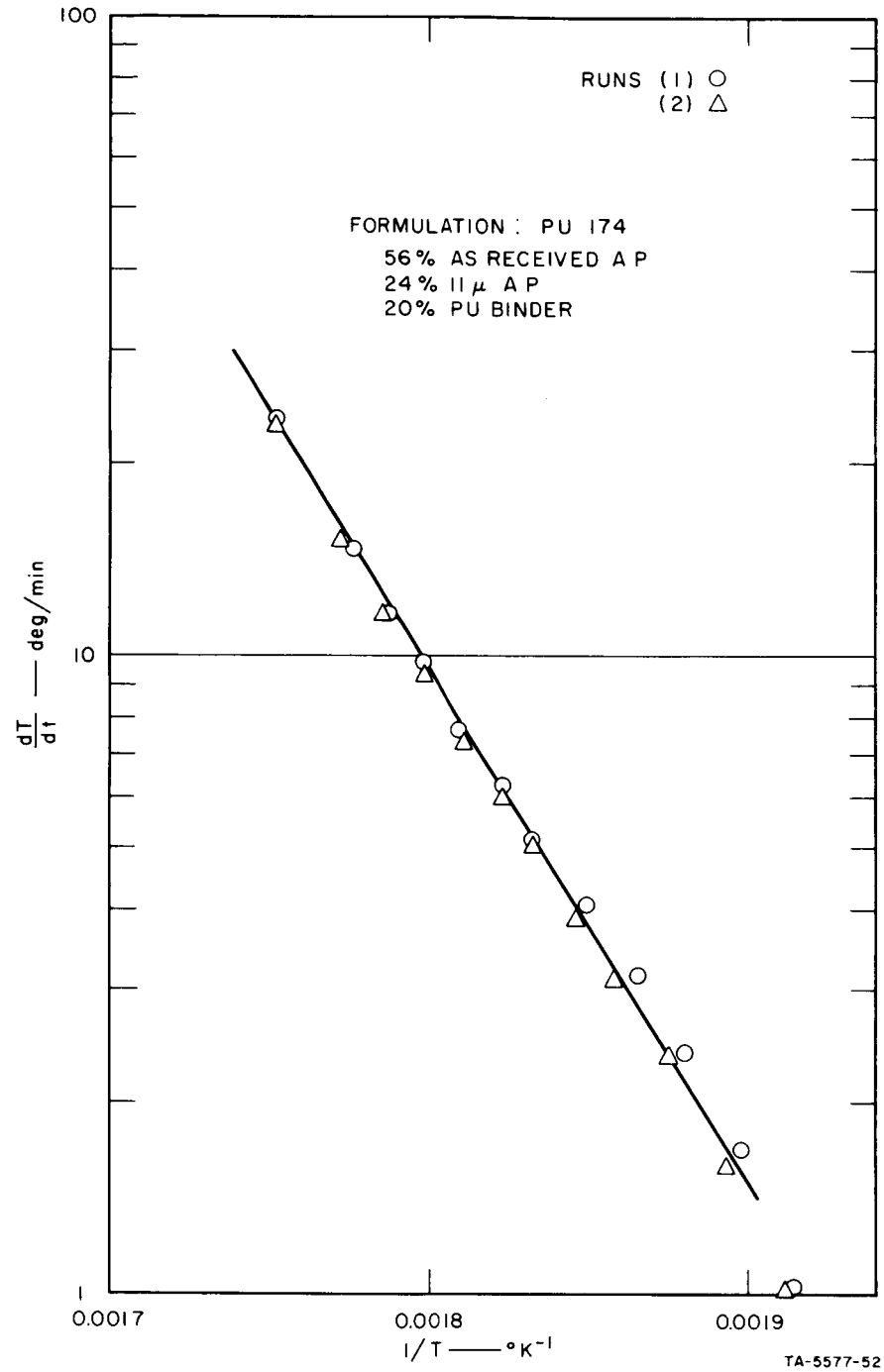

FIG. 20 ARRHENIUS PLOT FOR ADIABATIC SELF-HEATING OF POLYURETHANE PROPELLANT

be maintained. With the PBAN binder, the data deviate from the straight-line relationship at dT/dt values below 10° per minute. Similar behavior with ammonium perchlorate decomposition data is attributed by Inami et al.[29] to the reaction being autocatalytic in nature, and appropriate kinetic equations were developed to compensate for this fact. Such a correction

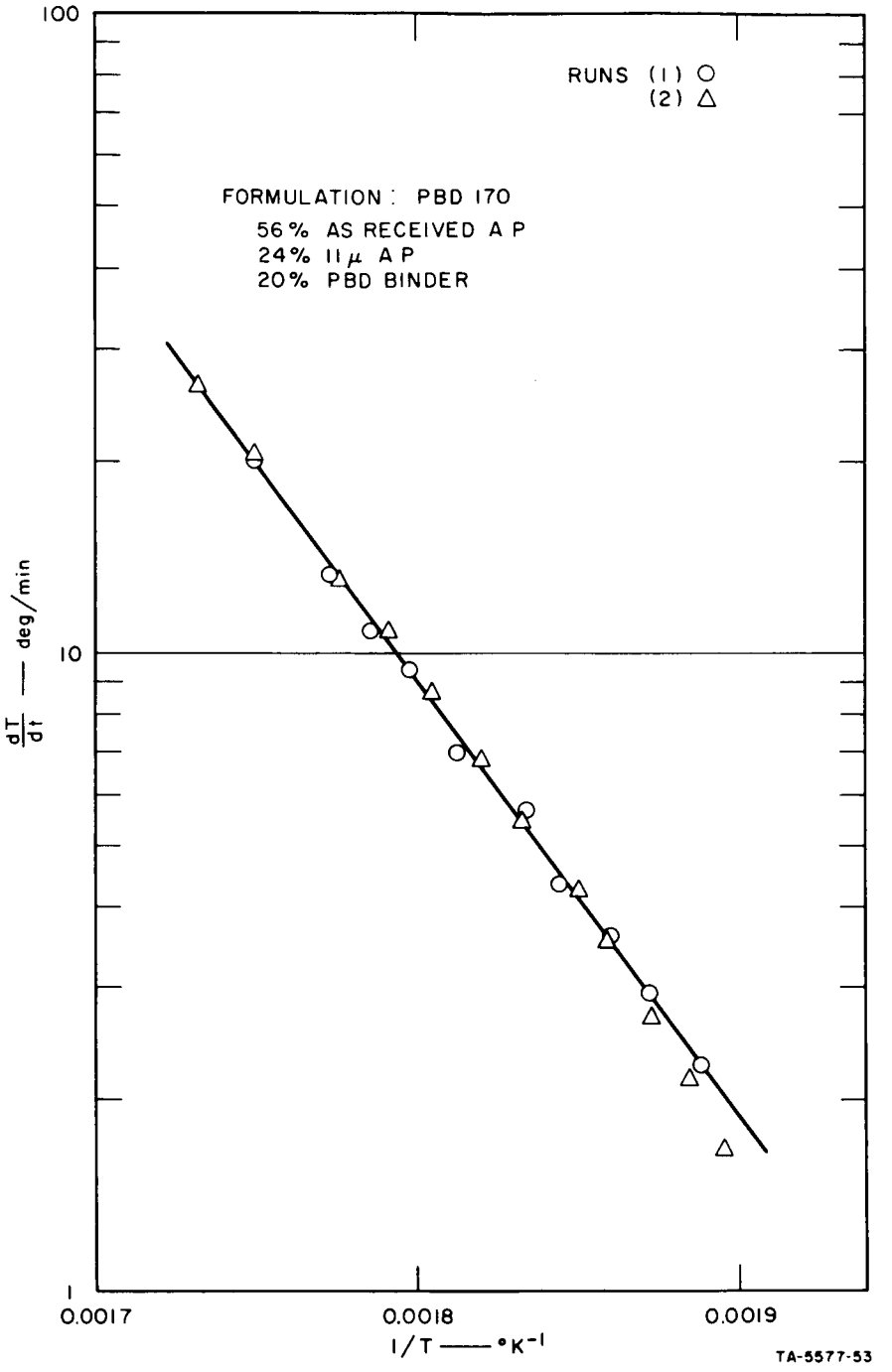

FIG. 21 ARRHENIUS PLOT FOR ADIABATIC SELF-HEATING OF PBD PROPELLANT

lowers the apparent activation energies for propellants exhibiting autocatalytic behavior as opposed to the value obtained when the heating rate is high enough for the reaction rate to be fitted by an Arrhenius equation. It is felt that this more precise determination of activation energies for the PBAN binder propellants will not change the conclusions

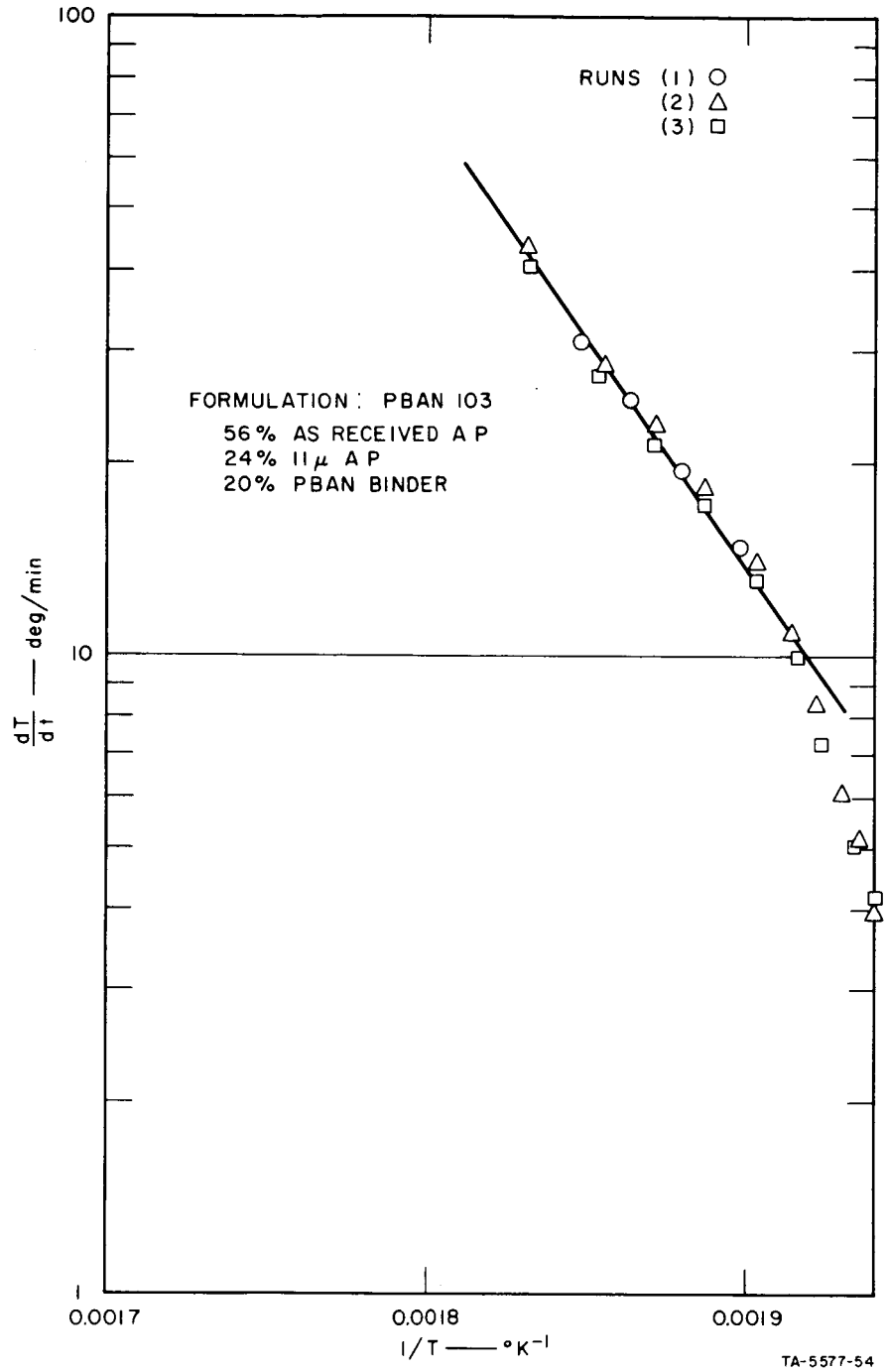

FIG. 22 ARRHENIUS PLOT FOR ADIABATIC SELF-HEATING OF PBAN PROPELLANT

to be made concerning the effect of the formulation variables studies. Consequently, the data presented were all derived from Eq. 11.

Propellant samples were heated very rapidly to an initial self-heating temperature which was predetermined by heating slowly until an exothermic reaction occurred. This temperature was observed to be

different for each binder. PBAN binders started to exotherm at 235°C, whereas PU and PBD binders started at 245°C and 279°C respectively. A summary of the activation energies determined from the ASH experiments is given in Table IX.

There are a number of formulation variables that cause a significant lowering of the activation energy for the initiation of surface-coupled reactions. Binder chemical composition and purity appear to cause a major reduction in activation energy. Another surprising change was noted when different particle distributions of ultrapure ammonium perchlorate were used. In PBD binder, the activation energy was lowered from 30.9 Kcal/mole to 19.1 Kcal/mole, when the oxidizer grind distribution was changed from a bimodal blend containing material ground to 11 microns to either a distribution containing only as-received material with an average particle diameter of 150 microns or to a unimodal distribution with an average particle diameter of 50 microns. The reason for this is not readily apparent. The same effect was observed for production-grade ammonium perchlorate in the polyurethane binder but not in the PBAN binder. Another variable of significance was the addition of aluminum which reduced the activation energy in a PU binder from 35.5 Kcal/mole to 28.3 Kcal/mole.

Formulation changes which produced little or no change in the activation energy for solid phase reactions with PBD and PU binders were the addition of lithium fluoride or the use of ultrapure ammonium perchlorate versus the production grade. Both of these variables did change slightly the activation energy in PBAN binders.

Fiber-Optic Studies of the Solid Propellant Combustion Zone

The use of fiber optics in conjunction with high-speed photography provides a tool for the study of the microstructure in the combustion zone just above the burning propellant surface. The test motor used in this study is shown in Fig. 23. The upper half of the motor contains a single viewing port which is used when self-illumination from the flame zone is being photographed. The lower half of the motor contains

Table IX

SUMMARY OF ASH EXPERIMENTAL RESULTS

A. Effect of Binder on Activation Energy

Binder Composition	E_H (Kcal/mole)
PBD	33.7
PU	35.5
PBAN	25.2

Formulation: 56% AP (~ 150 μ AR*)
24% AP (ground to 11 μ)
20% Binder

B. Effect of Particle Size on Activation Energy

PBD Propellants

AP Particle Size Distribution	E_H (Kcal/mole)
56% Ampot Ultrapure (~ 150 μ) 24% Ultrapure (ground to 11 μ)	30.9
80% Ultrapure (~ 150 μ)	19.1
80% Ultrapure (ground to 75 μ)	23.3

PU and PBAN Propellants

AP Particle Size Distribution	E_H (Kcal/mole)	
	PU	PBAN
56% (~ 150 μ AR) 24% (ground to 11 μ)	35.4	25.2
80% (~ 150 μ AR)	29.6	25.0
80% (ground to 50μ)	30.5	24.2

C. Effect of Aluminum on Activation Energy

Formulation	E_H (Kcal/mole)
56% AR 24% 11μ 20% PU Binder	35.5
49% AR 21% 11μ 10% RE 1-131 Al, 6μ 20% PU Binder	28.3

*AR = production-grade ammonium perchlorate, as received.

D. Effect of Binder Loading on Activation Energy

AP Particle Size Distribution	E_H (Kcal/mole)
56% Ultrapure 24% 11μ 20% Binder	30.9
42% Ultra pure 18% 11μ 40% Binder	28.3

E. Effect of Lithium Fluoride (LF) on Activation Energy

AP Particle Size Distribution	E_H (Kcal/mole)	
	PU	PBAN
56% AR 24% 11μ	35.5	25.2
56% AR 24% 11μ 1% LF	35.0	29.2

F. Effect of AP Purity on Activation Energy

AP Content, Size, and Purity	E_H (Kcal/mole)	
	PU	PBAN
80%-50%, Ultrapure	28.0	29.0
80%-50%, Production Grade	30.4	24.1

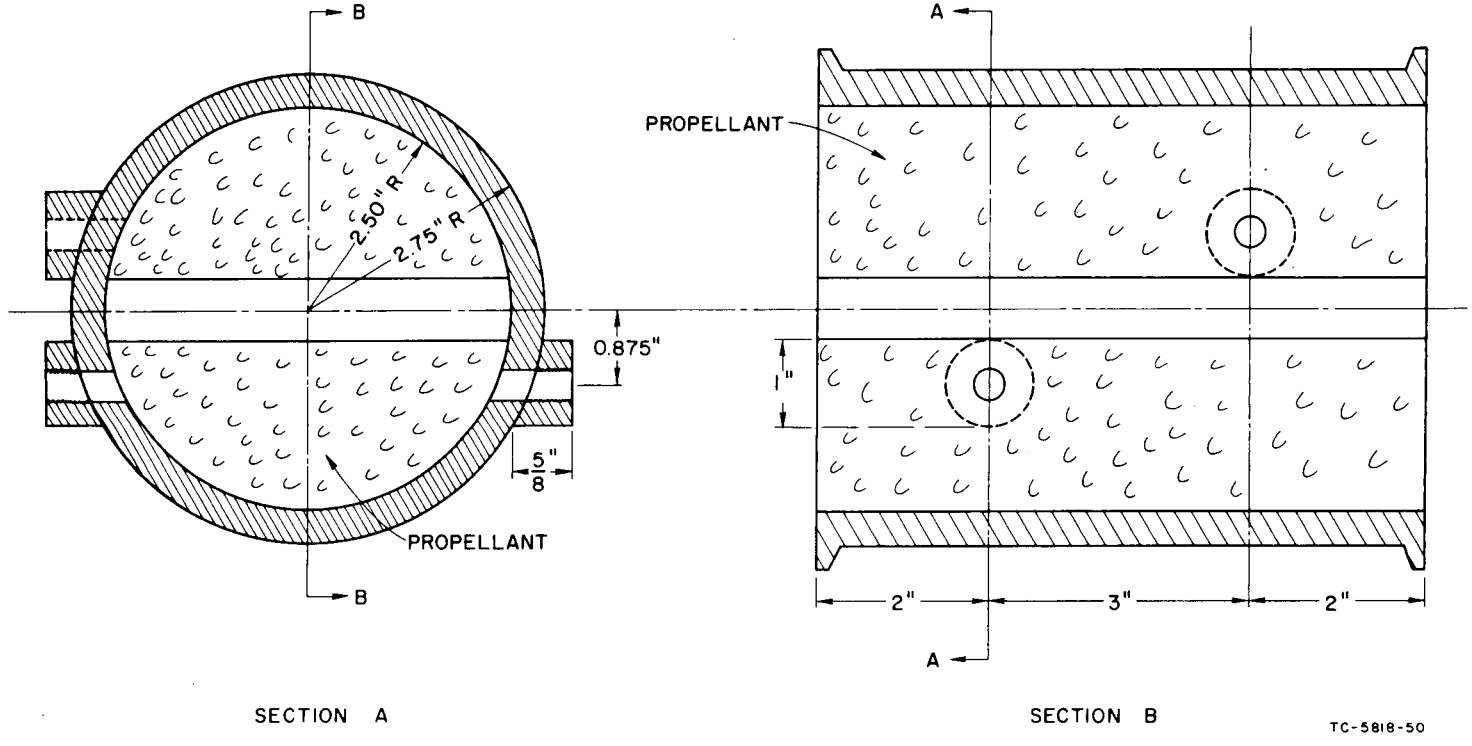

FIG. 23 TEST MOTOR USED TO OBTAIN FIBER-OPTIC PHOTOGRAPHS

two opposed viewing ports which are used when backlighting is required; e.g., for schlieren or shadow photography. Pyrex fiber optics which are 1/8 in. in diameter are screwed into the viewing ports; a high-speed camera is used to view the burning surface as it recedes past the fiber optic.

The transient extinction analysis predicts that surface-coupled reactions (i.e., heat release at or near the surface) have a profound effect upon the transient behavior. The existence of important heat release phenomena in the vicinity of the surface is clearly shown experimentally by the series of photographs presented in the following pages.

Figure 24 is a shadowgraph of a propellant containing 80% ammonium perchlorate and 20% polyurethene. The chamber pressure for this test was 185 psia, and the backlighting was provided by a mercury arc lamp. The sequence of pictures shown is taken from a movie film shot at 8500 frames per second; the first four frames represent events 0.235 msec apart in time and the last frame follows the fourth by 0.118 msec. Frame (a) shows the emergence of an AP crystal above the burning surface. In frame (b), ignition is clearly seen to occur on two faces of the crystal; combustion then continues until ultimately, in frame (e), a final burning bit is seen to leave the surface. This particular crystal is somewhat atypical, as its diameter is about 400 microns, but smaller crystals which are more difficult to observe should behave in a similar manner.

Figures 25 and 26 show the ignition and subsequent partial combustion of aluminum particles at the burning surface. This particular propellant contained 5% aluminum by mass. The framing rate was 8500 per second, giving 0.118 msec between frames; these pictures were obtained without backlighting. Frame (a) of both figures shows a glowing aluminum particle, about 50 microns in diameter, in place on the propellant surface. Ignition occurs in frame (b), and in frame (c), the burning particle is seen to leave the surface.

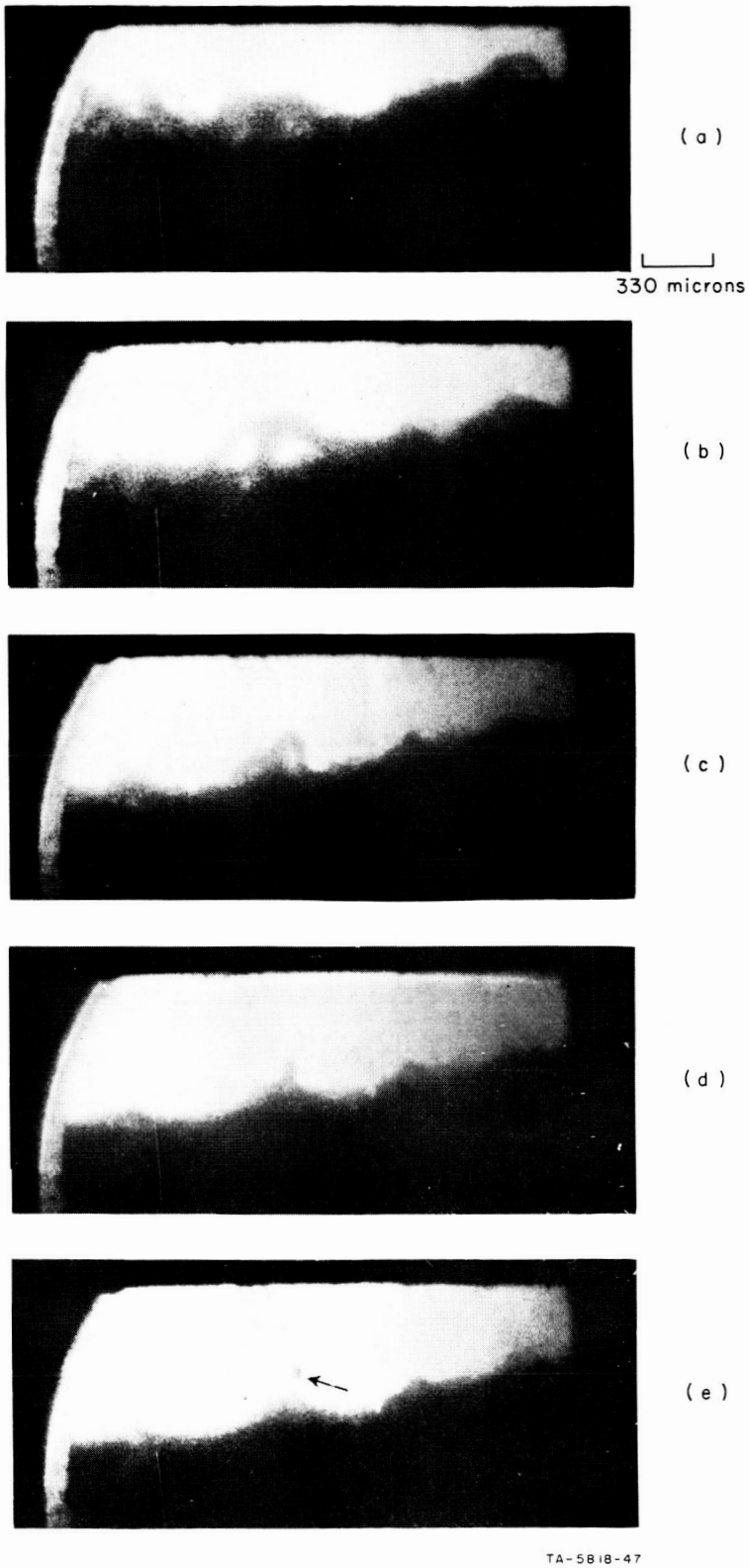

FIG. 24 FIBER-OPTIC SHADOWGRAPH SHOWING THE DEFLAGRATION OF AMMONIUM PERCHLORATE AT THE SURFACE OF A BURNING SOLID PROPELLANT

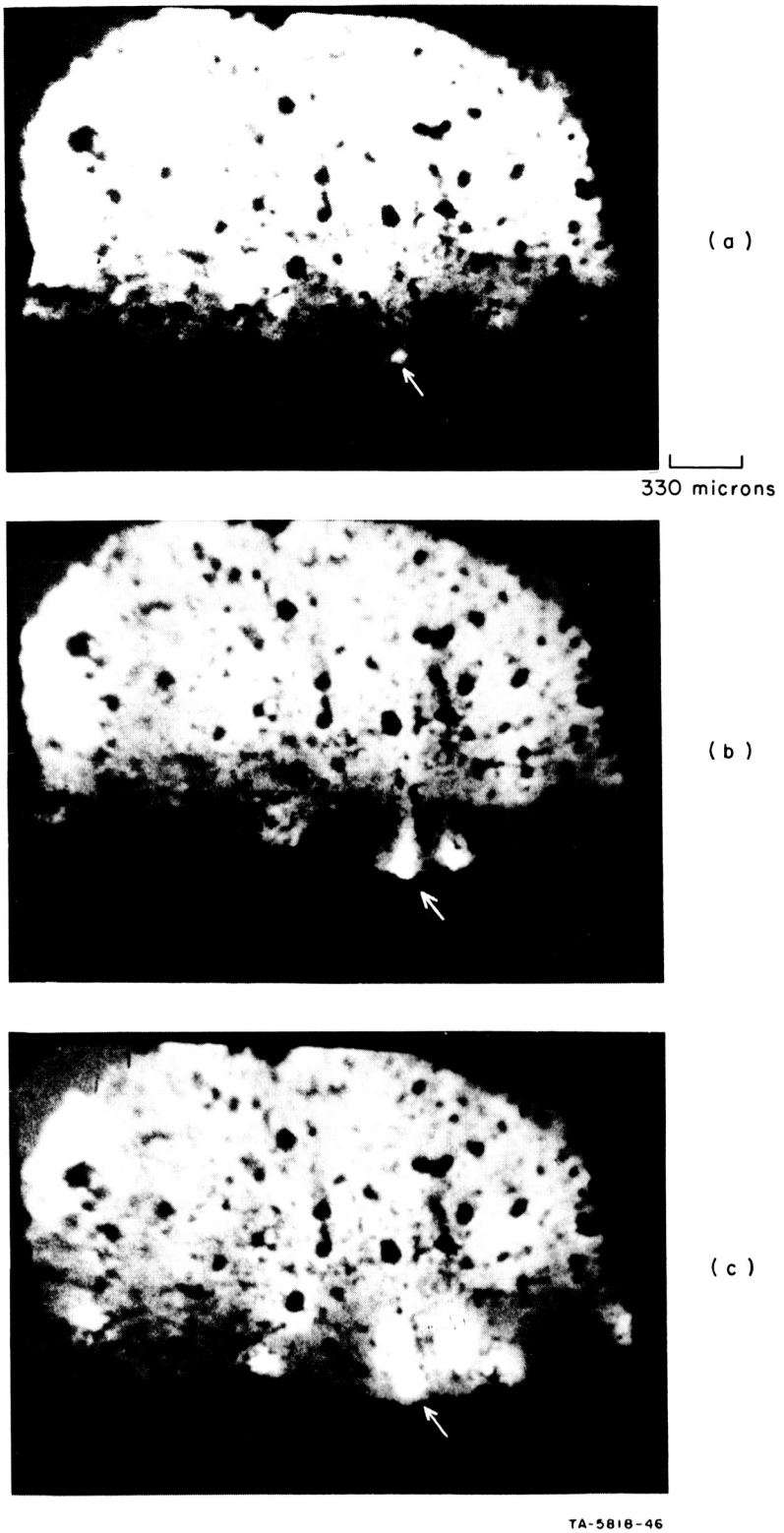

FIG. 25 FIBER-OPTIC VIEW OF THE IGNITION OF ALUMINUM PARTICLES AT THE SURFACE OF A BURNING SOLID PROPELLANT

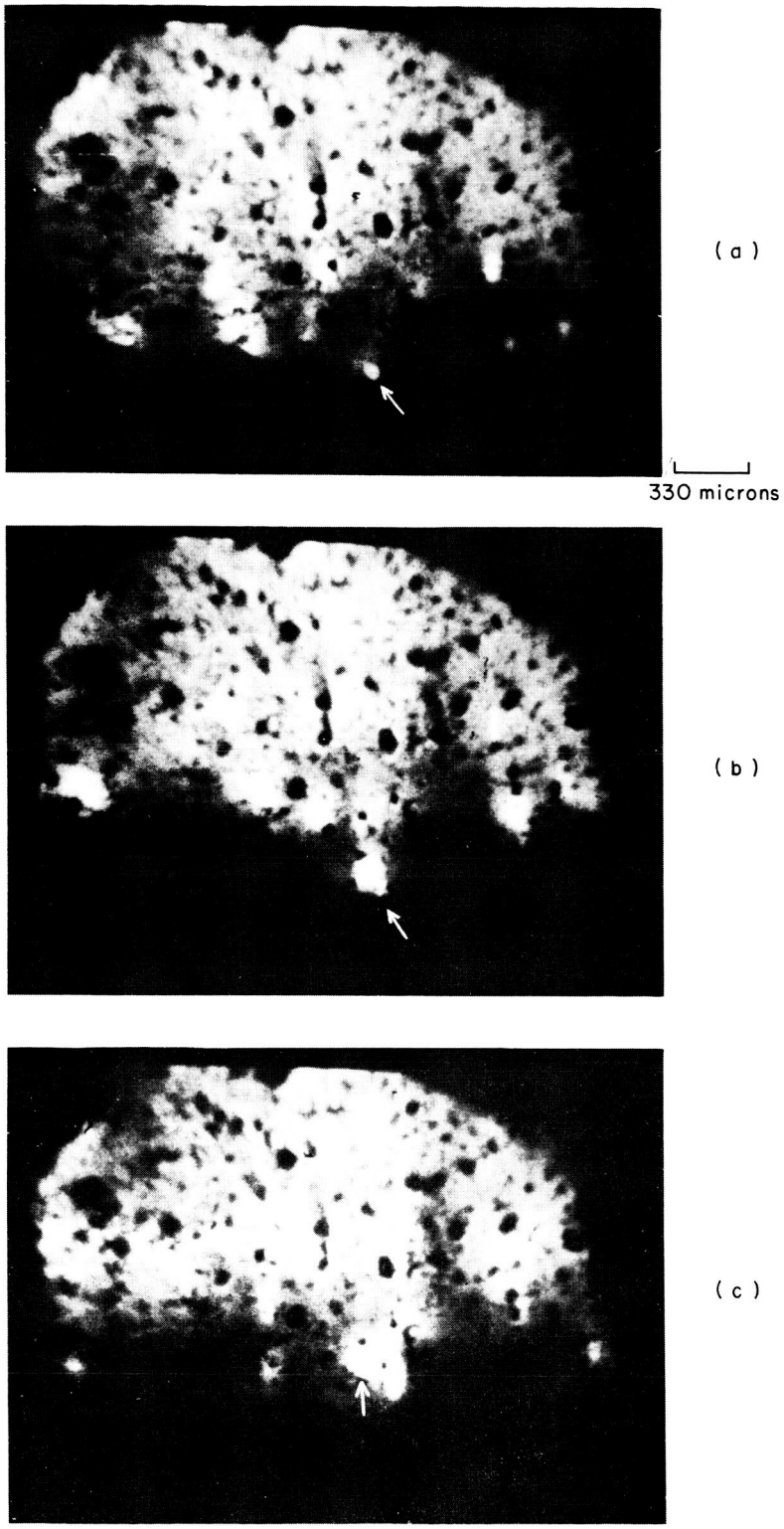

FIG. 26 FIBER-OPTIC VIEW OF THE IGNITION OF ALUMINUM PARTICLES AT THE SURFACE OF A BURNING SOLID PROPELLANT

The sequences in these two figures are representative of many that are observed during a typical test. The fact that aluminum ignition occurs at the surface is very interesting, because the temperature of approximately 1000°K in this region is far below the 2300°K ignition point of aluminum in oxygen. Thus, ignition must be induced by intermediate products of the perchlorate decomposition process.

For the pictures in this series, the burning aluminum provided its own illumination. The particle diameter was estimated from both its image size at the propellant surface upon ignition and from particles that condensed upon the fiber optic at or before their ignition. At 515 psia chamber pressure, most particles were observed to ignite at the surface of the propellant. The projected images of the particle traces were measured as indicated in Fig. 27. After ignition, a jet was formed above the surface, composed of the aluminum combustion products. After combustion has proceeded for a long enough time to reduce the mass of the particle to the point where its weight is equal to the aerodynamic drag force exerted on it, the burning particle is observed to fly off

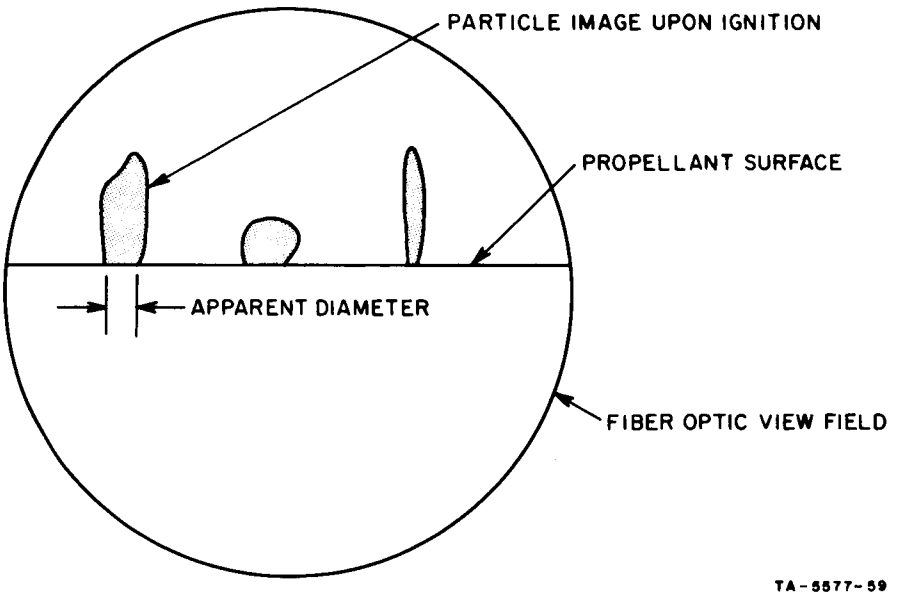

FIG. 27 MEASUREMENT OF ALUMINUM PARTICLE DIAMETER AT IGNITION

the surface. In several instances, large droplets of aluminum in the size range of 40 microns to 60 microns were observed to glow red hot just before igniting.

The picture sequences provided us with a means of estimating the ratio of observed particle diameters before and after ignition. The measured luminous diameters were corrected by this ratio. The resulting particle size distributions are plotted in Fig. 28 as histograms. The data from both methods of analysis indicate that over 75% of the observed surface ignitions occur when the aluminum particle diameter lies in the range from 20 microns to 50 microns.

The size of the particles of aluminum added during processing was 6 microns; the presence of the larger particles observed may be attributable to the aluminum agglomeration phenomenon reported by Crump[30] and other investigators. At the burning propellant surface, the temperature lies in the range of 850°K to 900°K where the small particulate aluminum has just reached its melting point (933°K). Under the influence of the buoyant gas jets from burning AP crystals, molten aluminum particles move about in a random manner, with collisions causing agglomeration, until the preferred diamter of 20 microns to 50 microns is reached. In this size range, the aluminum agglomerate extends upward into a much higher temperature region of the combustion zone.

Experimental measurements[31] by flame pyrometry have indicated that in the surface region, the temperature rises from a surface value of about 850°K to the equilibrium flame temperature of 2200°K within about 100 microns of the surface. With this temperature profile, one would suspect that the preferred agglomerate particle diameter for ignition would be even larger than that measured experimentally, since ignition temperatures for aluminum in oxygen atmospheres have been reported to be above 2000°K. However, the actual gas composition at the propellant surface undoubtedly plays a major role in the ignition process.

Besides oxygen and the conventional combustion products from the burning hydrocarbon binder (CO, CO_2, H_2O), the combustion gases also contain AP decomposition products. These include Cl_2, HCl, $HClO_4$, NH_3,

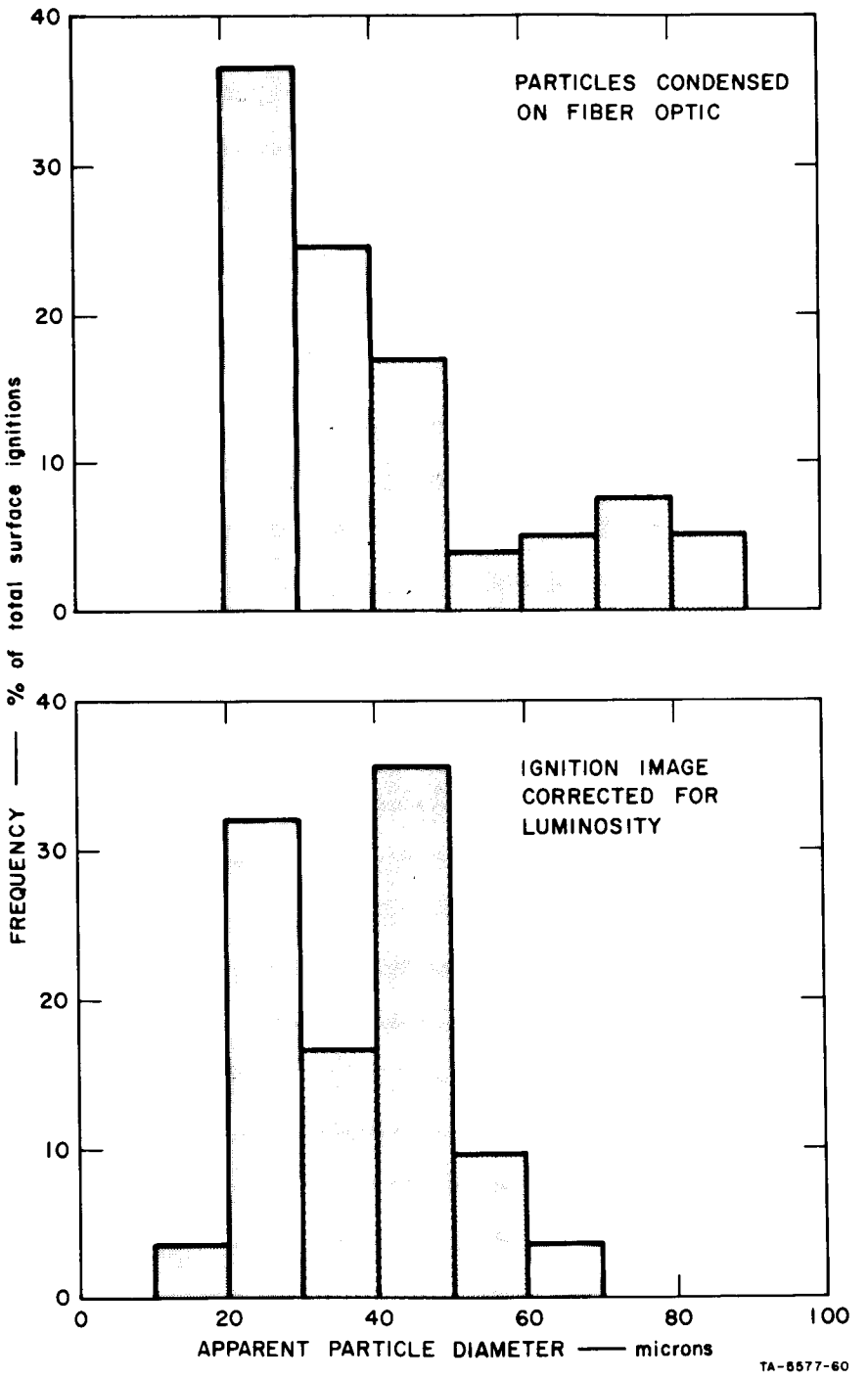

FIG. 28 APPARENT DIAMETER OF ALUMINUM PARTICLES AT IGNITION

and numerous other oxidizing species. It is reasonable to suspect that the ignition temperature of aluminum would be considerably lowered in such a gaseous atmosphere. More recent measurements of the flame thickness by Tourin,[32] Waesche,[33] and Povinelli,[34] using more sophisticated techniques, indicate that the flame thickness is nearer to 1000μ. This makes it even more likely that ignition occurs through chemical attack by species other than oxygen, since the particles are in a region where the temperature is considerably less than 2000°K.

Solid Propellant Response During Depressurization

During the program, two types of depressurization studies were performed in which the characteristic rates differed by two orders of magnitude. The first experimental technique, called the "variable volume" technique, used an end-burning charge associated with a piston-driven expansion process. The second, or "rapid expansion," technique used the same charge, but the piston was replaced by a rupture diaphragm of the same diameter as the charge. In the variable volume expansion experiments dp/dt rates to 20,000 psi/sec were attained by rapidly releasing a piston three inches in diameter which contained the nozzle required for maintaining the chamber pressure. An end-burning charge was used to facilitate high-speed photography (2000 frames per second) of the propellant surface during depressurization. (A sketch of this apparatus is shown in Fig. 29.) The expanded gases were dumped into a vacuum tank which contained a nitrogen atmosphere.

The rapid expansion experiments were done in the same chamber by bursting a diaphragm of the same diameter. (This apparatus is shown in Fig. 30.) Depressurization rates up to one million psi/sec were achieved in this manner. These two types of apparatus allowed depressurization rates varying from those for which the gases were in thermodynamic equilibrium during the expansion to those for which the gases approached pure adiabatic expansion.

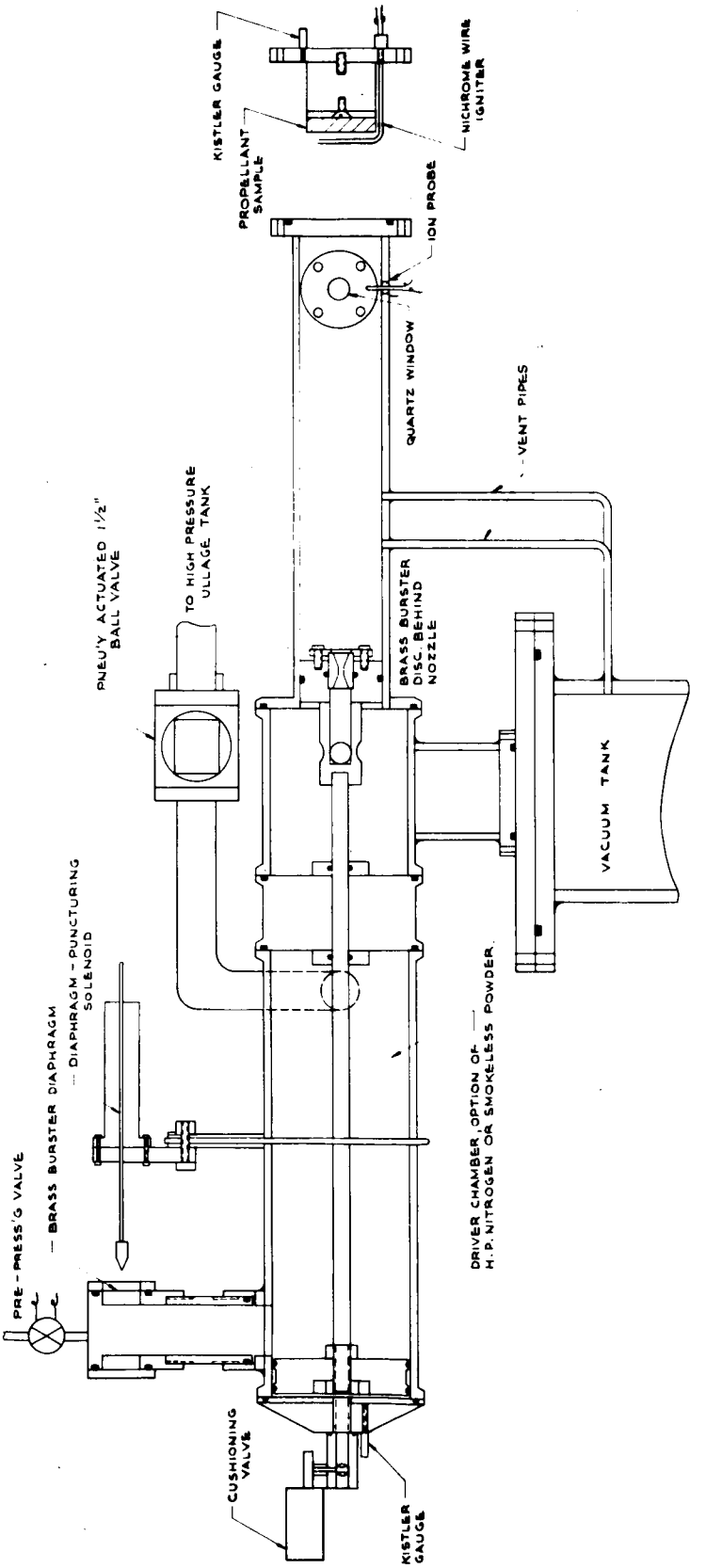

FIG. 29 VARIABLE VOLUME dp/dt BURNER

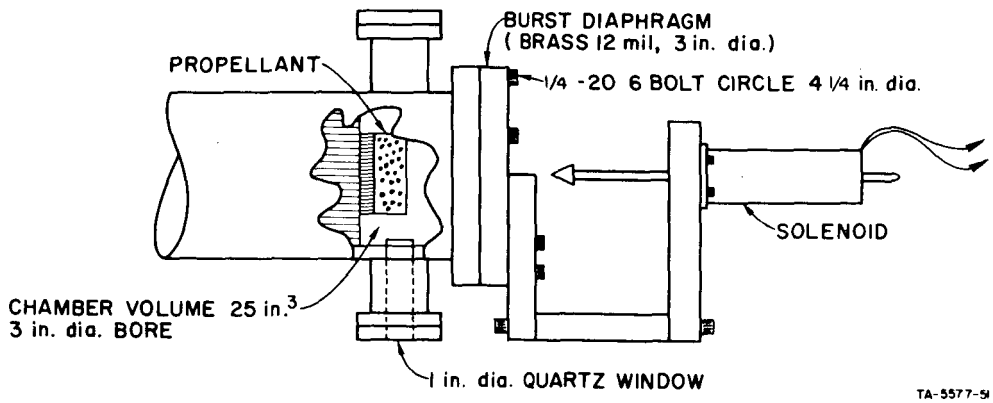

FIG. 30 TEST CHAMBER FOR RAPID EXPANSION

The propellant formulations used in both experiments are listed in Table X. Lower deflagration limits (p_{DL}) were measured by the technique described previously. Strand burning rates over the pressure range from p_{DL} to 1500 psia are shown in Figs. 31-33. PU 185 and PU 193 were formulated to have as near the same burning rate as experimentally feasible. However, in PU 185, a barrier was placed between binder and oxidizer to reduce the percentage of heat release in the solid phase. DTA thermograms show that this barrier causes the first deflagration exotherm of the propellant containing coated perchlorate to be displaced about 50°C higher. It could therefore be expected that PU 185 should be easier to extinguish than PU 193. PU 174, a lower burning rate propellant, was added as a control.

Table X

PROPELLANT FORMULATIONS

Formulation	Ingredients, Wt %			Lower Deflagration Limit, psia
	NH_4ClO_4	Polyurethane Binder	Additive	
PU 185	80 AR	17.5	2.5 Ethyl siloxane	2.8
PU 174	56 AR, 24 (11μ)	20	--	3.3
PU 193	56 AR, 24 (11μ)	18.5	1.5 Fe_2O_3	1.5

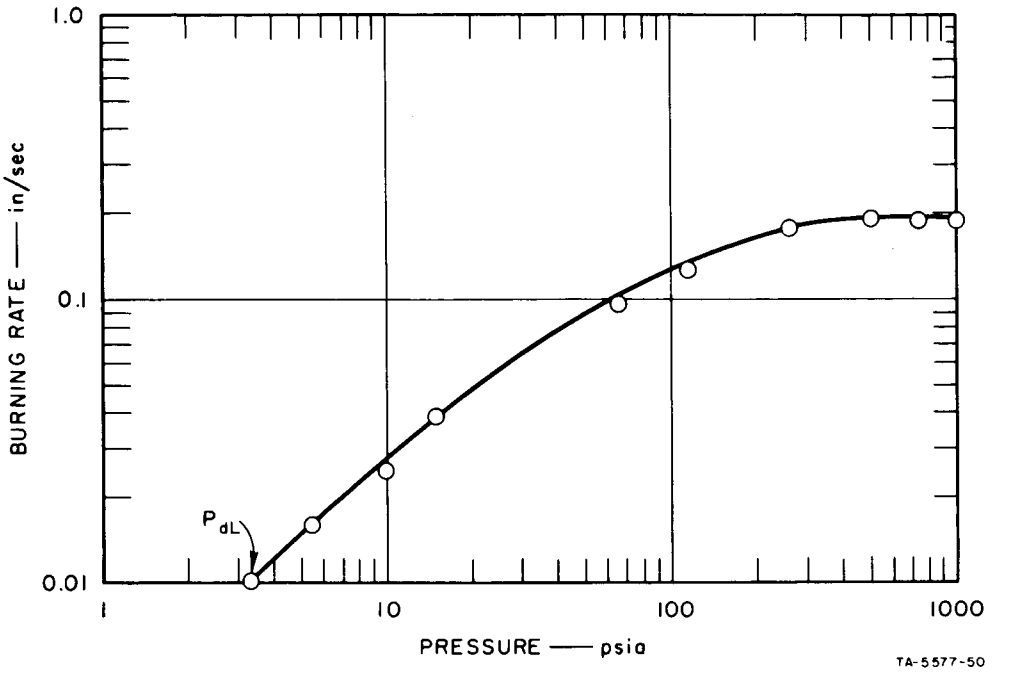

FIG. 31 STRAND BURNING RATE, PU 174

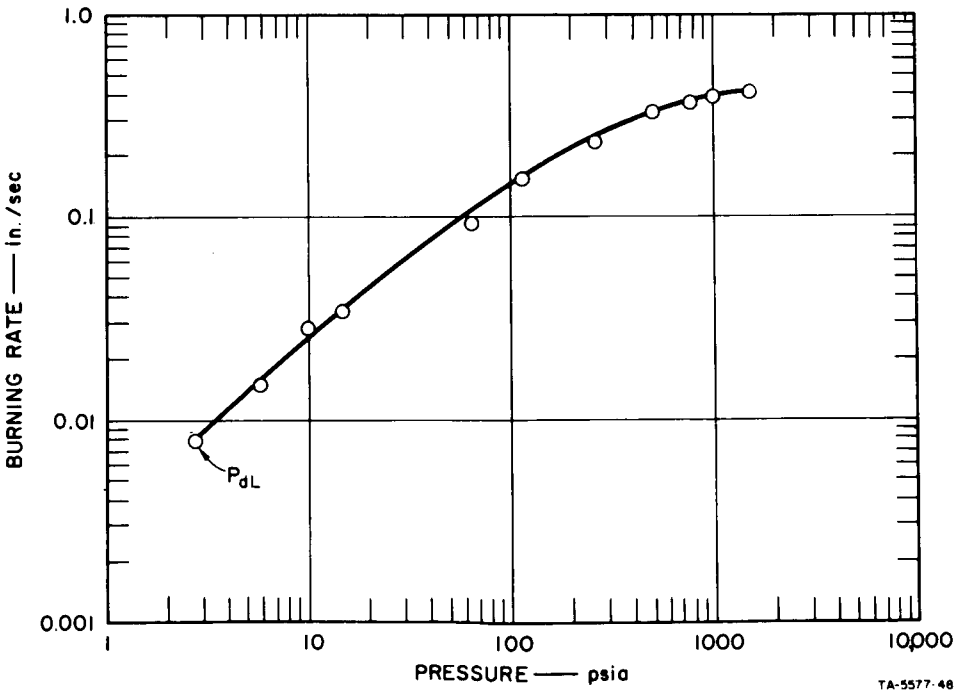

FIG. 32 STRAND BURNING RATE, PU 185

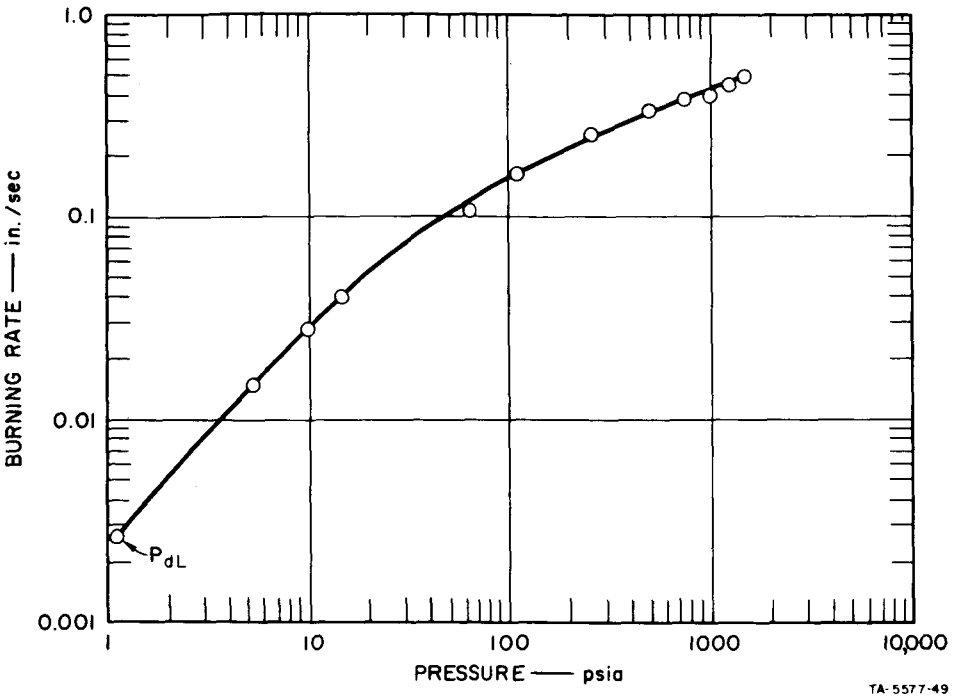

FIG. 33 STRAND BURNING RATE, PU 193

One of the first facts arising from the variable-volume experiments at low dp/dt rates was that extinguishment is more a function of the pressure in the vacuum dump tank than of the rate of depressurization. Since this environmental pressure sink was more easily controlled, a series of "go, no-go" experiments were conducted to determine whether there was a difference in the ease of extinguishability between the formulations being investigated. The results obtained are listed in Table XI. As predicted, both higher burning rate propellants required more stringent conditions to extinguish, i.e., exposure to a lower ambient pressure. This was also indicated by the lower deflagration limits measured for these propellants. The distinction between propellants containing coated AP and those containing noncoated AP with nearly the same burning rates was not apparent from these experiments. Thus, both PU 193 and PU 185 reignited after 10 seconds. The nonextinguishment pressures were 4.9 psia versus 5.2 psia. The most obvious conclusion is that the barrier placed between the binder and oxidizer was ineffective,

Table XI

RESULTS OF EXTINGUISHABILITY TESTS

Test No.	Propellant Type	Chamber Pressure, psia	Vacuum Tank Pressure, psia	Initial dp/dt, psi Sec	Results
20	PU 174	530	9.8	16,500	NE
21	PU 174	600	5.4	20,000	E
22	PU 174	500	7.8	18,000	E
23	PU 174	570	9.3	19,250	TE
24	PU 193	850	0.1	30,000	E
25	PU 193	925	5.9	32,500	TE
26	PU 193	688	3.2	21,900	E
27	PU 193	450	4.4	13,750	E
28	PU 193	465	6.1	16,250	NE
29	PU 193	470	5.2	14,500	TE
31	PU 185	800	5.4	27,500	E
32	PU 185	750	8.3	30,000	NE
33	PU 185	1000	6.1	32,500	TE
34	PU 185	750	4.9	26,900	E
35	PU 185	350	4.9	13,500	TE
36	PU 185	420	6.5	16,000	NE
37	PU 185	445	4.4	15,800	TE*

*Reignited after 10 sec.

E = extinction

TE = transient extinction

NE = no extinction

or that the selected variable (surface heat release) is of minor importance in comparison to burning rate as a variable.

Another factor complicating this experimental technique was reignition, which was also found to be related to the pressure in the vacuum tank and therefore cannot be separated as an independent variable. As the pressure in the vacuum tank was decreased to successively lower values,

the time elapsing until reignition occurs was found to increase, until a vacuum tank pressure was reached in which reignition did not take place.

In an attempt to separate extinguishment and reignition phenomena, further experiments were made to determine by shadowgraph photography the pressure at which extinguishment occurred. To make pictures of this type, the propellant combustion gases must be transparent. PU 174 is such a propellant, and the backlight used was a mercury lamp. Shadowgraphs of the propellant surface were taken during the dp/dt event at 2000 frames/sec. In Figs. 34-36, the pressure-time curves are given for three dp/dt runs at increasingly lower dump tank pressures. Non-extinction was attained with the vacuum tank at atmospheric pressure. The pressures at which gas evolution from the surface ceased, as shown by the shadowgraphs, are noted on the pressure-time curves. The starting chamber pressure was held as close to 500 psia as possible. In each run, the instability that developed somewhat below 100 psia is caused by the driver piston compressing gas at the opposite end of the combustion chamber and bouncing back until the gas is relieved at the vent hole. The effect is amplified in the oscillograms, because a log amplifier is used to give higher resolution at lower pressures.

The shadowgraph data indicate that mass flow from propellant PU 174 burning at 500 psia chamber pressure at depressurization rates under 30,000 psi/sec ceases before the chamber pressure reaches the pressure of the vacuum dump tank. This extinction pressure is appreciably above the lower deflagration limit pressure, i.e., 35 psia versus 3.3 psia. When the dump tank pressure is raised, a back pressure is reached at which extinction no longer occurs. In this region, transient reignition occurs, and this is also dependent upon the pressure in the vacuum dump tank. The shadowgraph taken under these conditions (Fig. 35) indicates that mass addition stopped at 30 psia.

The difference in extinction pressures is not very conclusive, and it may be due to experimental error. One factor that may have influenced the results was that the driver piston impacted on the end of the driver chamber, causing the combustion chamber pressure to oscillate before

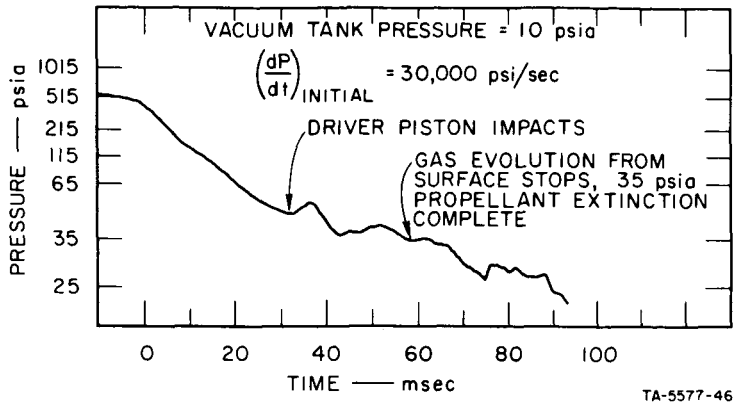

FIG. 34 SHADOWGRAPH EXTINCTION PRESSURE FOR PU 174 IN VARIABLE VOLUME dp/dt BURNER

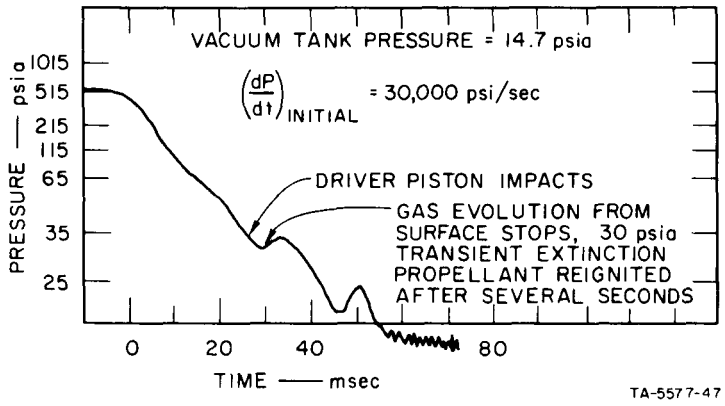

FIG. 35 SHADOWGRAPH EXTINCTION PRESSURE FOR PU 174 IN VARIABLE VOLUME dp/dt BURNER

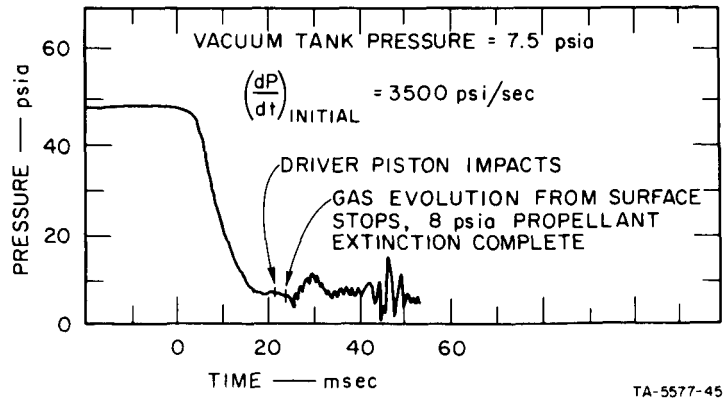

FIG. 36 SHADOWGRAPH EXTINCTION PRESSURE FOR PU 185 VARIABLE VOLUME dp/dt BURNER

extinction occurred. There is also the problem of measuring combustion pressures in the range 500 psia to 0 psia. On a linear scale, sensitivity at the lower pressure end was very poor, and the extinction pressure could not be measured within ± 20 psia. Use of the log amplifier provided improved discrimination at the lower pressure end, but measurements within ± 2 psia were difficult to obtain. Extinction experiments conducted at a lower chamber pressure gave somewhat the same results, as Fig. 36 indicates. PU 185 ceased to give off mass at 8 psia in comparison to the lower deflagration limit of 2.8 psia.

Extinction tests were also carried out utilizing the rapid expansion technique (Fig. 2), during which the escaping gases approached pure adiabatic conditions. In every case, all propellants extinguished at atmospheric pressure. A simple calculation of the cooling effect during an adiabatic expansion of the combustion gases from 500 psia to 10 psia shows that the resultant temperature, 1200°K, is appreciably above the ignition temperature of the propellant. It is therefore improbable that an adiabatic expansion can explain the experimental extinction results. A more likely cause of extinction is the change in enthalpy of the propellant surface and the lag times in readjustment of this temperature profile to fit the equilibrium burning rate associated with each pressure. Thus, at high pressure, the temperature profile within the grain is steeper, and less heat is stored in the propellant surface. As the pressure is rapidly lowered, more heat is required in the surface layer to establish the equilibrium temperature required to maintain the burning rate at the new pressure. Since heat conduction is a relatively slow process, enough heat cannot be accumulated under the conditions of rapid depressurization, and extinction occurs.

The experiments discussed above show that it is very difficult to infer the details of the transient burning rate behavior from the transient pressure behavior during the depressurization process, because the mass addition from the propellant surface during the transient process is small compared to the mass of gas in the chamber. These considerations led to the pressurization experiments described in the following paragraphs.

Solid Propellant Response During Pressurization

To study propellant relaxation phenomena experimentally, it is necessary to induce a rapid pressure change between two pressure levels that correspond to substantially different steady-state burning rates. The transient time of the pressure change must be short in comparison to the characteristic propellant response time, so that the propellant arrives at the new pressure level with a thermal profile corresponding to the original pressure level. The difference in steady-state burning rates at the two pressure levels must be large enough to represent a significant change in the steady-state thermal profile depth. Since the burning rate behavior can only be monitored indirectly by monitoring the chamber pressure, the free volume must be minimized. This will ensure that the propellant mass added during the transient process is an appreciable fraction of the mass present in the volume at the onset of the process. Under these conditions, one can determine the transient burning rate behavior from the record of the transient chamber pressure.

Either a rapid increase or decrease in the pressure level will produce the desired result. An increase in pressure level will lead to a transient overshoot in the pressure, whereas a decrease will lead to an undershoot. To obtain a rapid pressure change while keeping a minimal free volume, an increase in pressure level is the easier to apply experimentally. Combustion is initially established at low pressure, followed by the imposition of a rapid pressure increase.

At the beginning of this experimental phase of the program, it was decided to impose the pressure increase by closing the (small) volume and allowing the propellant to pressurize itself to the desired new level. A burner shown in Fig. 37 was fabricated with two nozzles. The two nozzles together were designed to establish the initial low-pressure operating point. The smaller nozzle was designed to provide the pressure level desired after pressurization. The sequence of experimental events was:

1. With both nozzles open, the propellant was ignited by a hot wire igniter.

2. After ignition was established on the entire surface of the propellant and steady-state operation is attained, the molybdenum probe was explosively actuated to close the large nozzle.

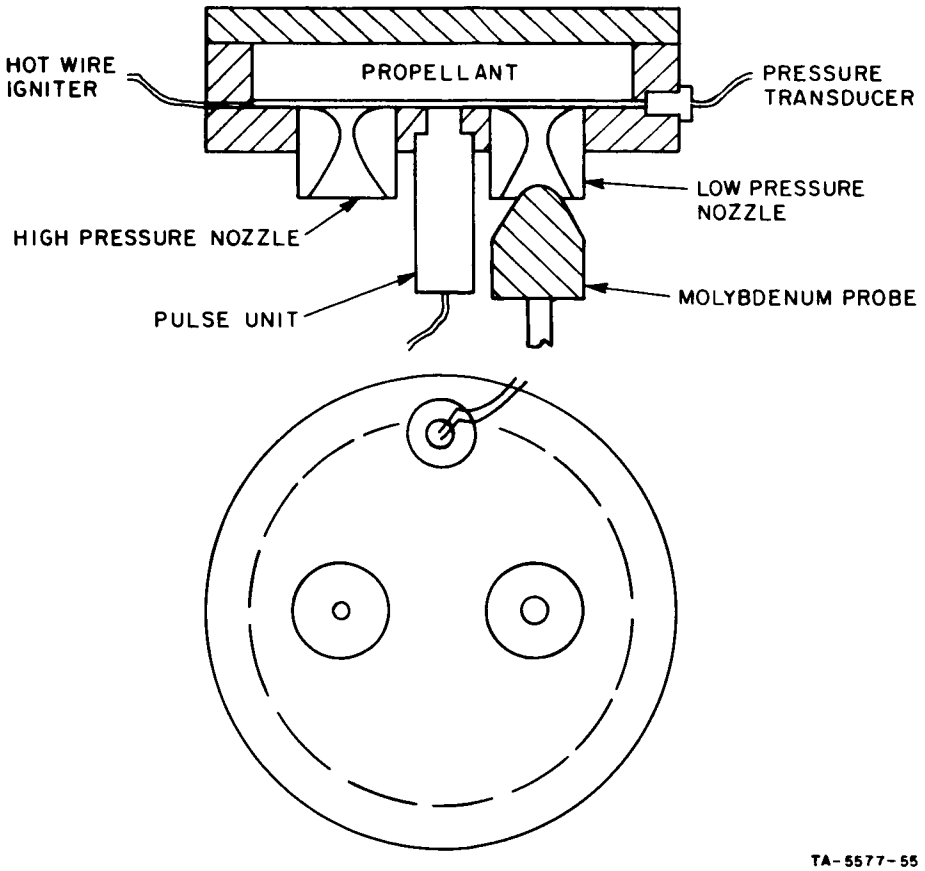

FIG. 37 BURNER FOR STUDYING PROPELLANT RESPONSE TO A RISING PRESSURE TRANSIENT

Experimental evaluation of the burner began with the determination of the minimum possible free volume while maintaining stable ignition and combustion. For this burner, the minimum free volume was determined to be 7 cc, giving a surface-to-volume ratio of 19. Once these initial conditions had been established, an experimental determination of the rise time was undertaken. Even though the surface-to-volume ratio was relatively large, the gas evolution rate corresponding to the low

pressure (typically about 100 psia) was so low that the pressure rise time was about 30 msec for a typical propellant, as shown in the upper pressure trace of Fig. 38. The response time of the propellant is on the order of K/r^2, where K is the thermal diffusivity of the solid and r is the burning rate. Using typical values of $K = 2.5 \times 10^{-4}$ in.^{2}/sec and r = 0.2 in./sec, the propellant response time is seen to be on the order of 6 msec, which is much shorter than the 30 msec rise time noted above. For this reason, there is no observable overshoot in the pressure; the propellant burning rate simply follows the pressure rise in a quasi-steady way.

To overcome this problem, it was decided to increase the rate of pressure rise by augmenting the propellant source with an external gas generator in the form of a powder charge. A squib-initiated double-base powder, having combustion products that are similar to those of the main propellant charge, was selected because of its short response time. The charge was initiated in a small cavity isolated from the main chamber by a brass diaphragm (see Fig. 37). The diaphragm ruptured and allowed the gases to flow into the main chamber. (A schematic of the control instrumentation is shown in Fig. 39.) Care was taken to baffle the gases and destroy the shock wave created by the diaphragm rupturing. The rise time of the pulse was measured to be 0.5 msec. The amplitude and the duration of the pulse were dependent upon charge weight, differential pressure across the diaphragm, combustion chamber free volume, initial pressure, and high pressure nozzle size. The pulse amplitude could be approximately adjusted by varying the charge weight; however, the duration was dependent primarily upon the small nozzle size which was determined by the steady-state propellant burning rate at the final pressure.

Tests were conducted on PU-174 propellant using variations in the pulse amplitude. The results of these tests are shown in the lower two traces of Fig. 38. The response characteristics appear to be relatively independent of pulse amplitude. Note that the initial pressure rise is rapid enough to induce a definite transient burning rate response which manifests itself as an overshoot in the pressure trace.*

*These experimental studies are being continued under the follow-on program, Contract No. NAS 1-7349.

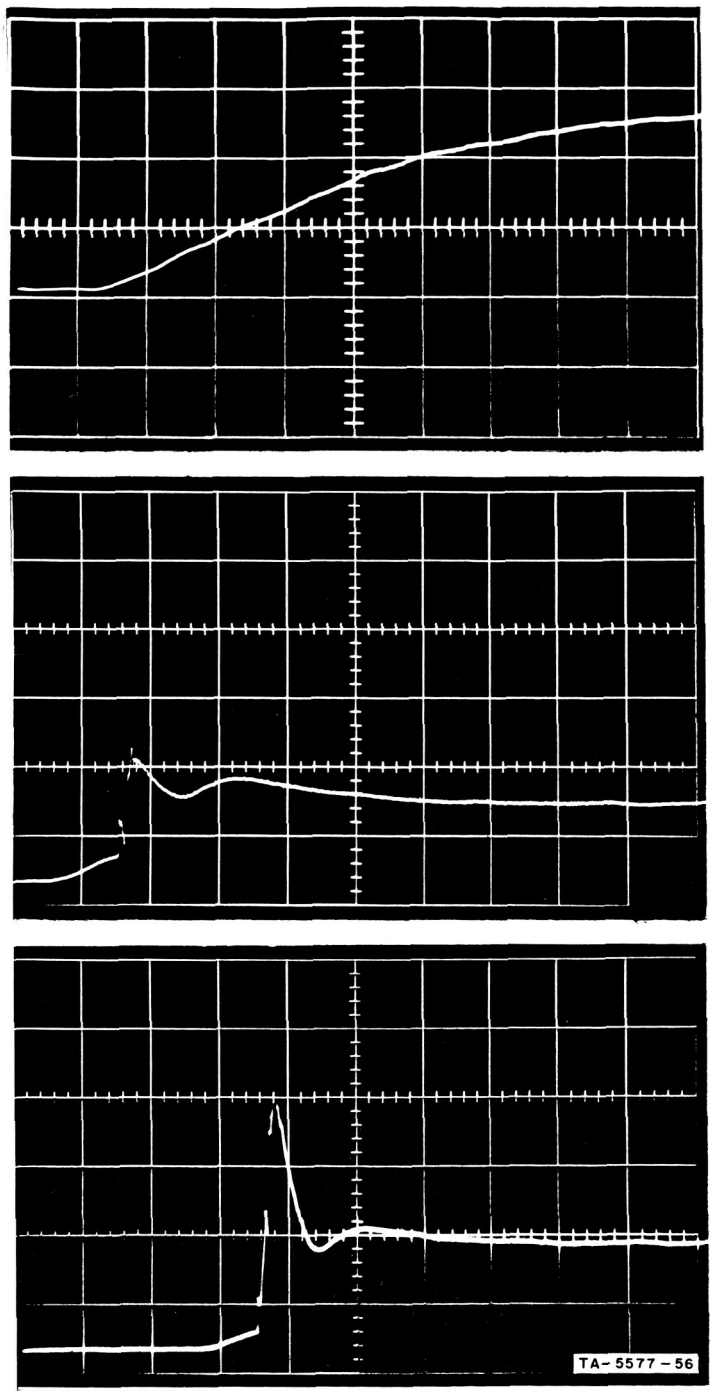

FIG. 38 CHAMBER PRESSURE RESPONSE WITH AND WITHOUT AN EXTERNAL PULSE

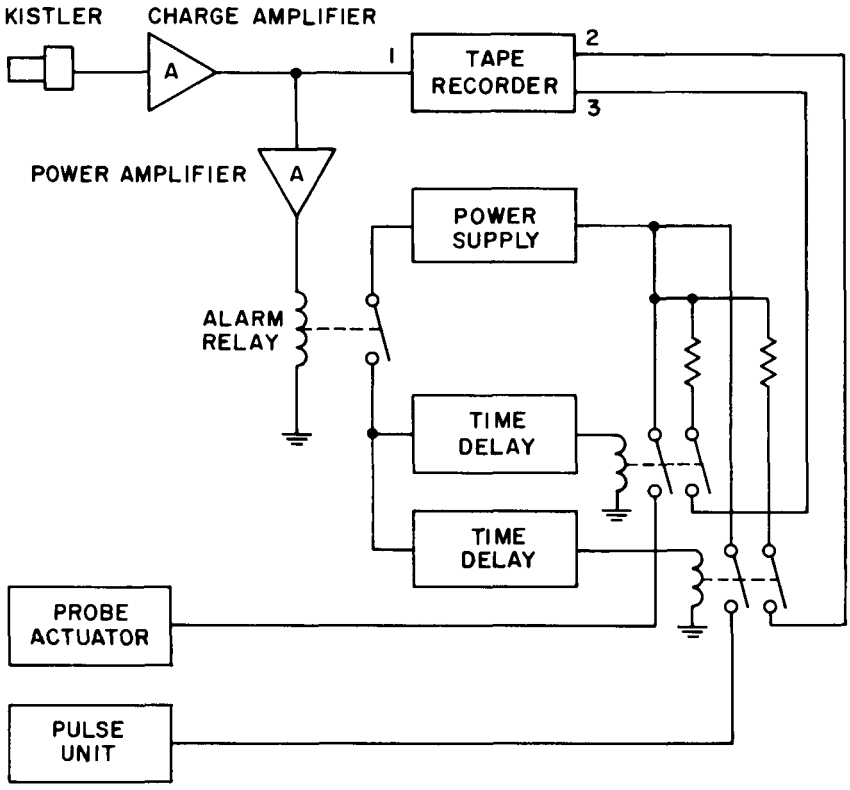

FIG. 39 SCHEMATIC OF BURNER INSTRUMENTATION AND CONTROL SYSTEM

CONCLUSION

The differential thermal analysis measurements carried out under this program leave little doubt that significant chemical reactions, apart from pyrolysis, occur in the gas-solid interfacial zone of burning solid propellants. It is also reasonably certain that the relative importance of these surface-coupled reactions differ with propellant composition, and in particular with the choice of oxidizer. For example, ammonium perchlorate propellants exhibit about three times the proportion of surface-coupled heat release as potassium perchlorate propellants.

An analysis of the combustion model, which has been specifically developed to account for surface-coupled exothermic or endothermic reactions, shows that a relatively small proportion of surface-coupled heat release has a profound effect on the amplitude of the pressure-coupled response. Combustion instability studies, carried out under another contract,[9] have shown ammonium perchlorate propellants to be much less stable than potassium perchlorate propellants, a fact that is attributed to the greater surface-coupled heat release of the former. Thus, the differential thermal analysis measurements, the instability measurements, and the theoretical analysis all support one another; in fact, the linearized stability analysis is able to predict such parameters as the frequency of a traveling wave instability.[9]

Depressurization leading to extinction is, by its very nature, a highly nonlinear phenomena. Depressurization studies carried out during this program showed the difficulty involved in assessing the effects of such propellant parameters as the proportion of surface-coupled heat release from pressure-time records of the event. In lieu of this assessment, one must rely upon the predictions of the model to classify the extinction characteristics of families of propellants. Before the model can be so used as a working tool, its validity in nonlinear regimes of pressure change must be established by a suitable nonlinear experiment. Therefore, the nonlinear pressurization experiments described

above were undertaken. When a solid foundation has been laid for the validity of the combustion model in the nonlinear regime, an important tool will be available for the study of the many subtleties inherent in the extinction process.

APPENDIX A

THEORETICAL COMBUSTION MODEL FOR TRANSIENT BURNING OF A SOLID PROPELLANT

The mathematical formulation of the SRI combustion model, as it has been presented earlier,[2,6,19] is summarized below.

The chief assumptions made in the analysis are the following: (a) the gas-phase reactions can be represented in terms of a single reaction of arbitrary order that obeys Arrhenius kinetics and responds instantaneously to pressure and temperature disturbances (i.e., time-dependent terms are omitted in the gas-phase equations); (b) the Lewis number is unity in the gas phase; (c) surface pyrolysis and surface-coupled exothermic or endothermic reactions follow Arrhenius laws; and (d) the solid phase is essentially homogeneous with temperature-independent transport properties. For typical propellants, assumption (a) is valid for chamber oscillations at frequencies of a few thousand cps or less. Most of the acoustic instability problems of greatest interest fall within this regime.

As (b) implies, the pyrolysis and surface-coupled reactions are assumed to occur in a surface layer of negligible thickness relative to the penetration depth of the temperature profile. It is difficult to evaluate the quantitative effect of assumptions (b), (c), and (d). However, it is important to remember that all analyses of this kind unavoidably rely on a highly simplified picture of the complex combustion process. Within this context, these assumptions are fully justified and even necessary, because they permit a simplified mathematical formulation that is consistent with the underlying concepts.

The formulation begins with the equation governing heat conduction in the solid phase beyond the surface reaction zone:

$$\frac{\partial T}{\partial t} = r(t)\,\frac{\partial T}{\partial x} + K\,\frac{\partial^2 T}{\partial x^2} \tag{A1}$$

The propellant pyrolysis at the wall is assumed to follow an Arrhenius law, so that the burning rate is related to wall temperature as follows:

$$r = a\, e^{-E/RT_w} \tag{A2}$$

The following boundary condition is imposed upon the temperature:

$$x \to \infty; \quad T \to T_o \tag{A3}$$

The remaining boundary condition is obtained through an energy-flux balance at the gas-solid interface. The net heat conducted into the unreacted solid propellant from the interface at the plane $x = 0$ is

$$-k\left(\frac{\partial T}{\partial x}\right)_w = -k\left(\frac{\partial T}{\partial x}\right)_{g_w} - \rho_s r h_{g_w} + \rho_s r h_{s_w} + Q_H + Q_D \tag{A4}$$

The first term on the right-hand side of the equality sign represents the energy coming from the gas phase; the second, the energy carried into the gas with the vaporizing propellant; the third, the energy carried by convection from the unreacted solid phase into the interface; the fourth, the energy released (positive) in surface-coupled heterogeneous decomposition reactions whose reaction rates depend upon the local gas-phase density; and the last, the energy released in solid-phase surface reactions with rates that are independent of gas-phase conditions. It is possible to rewrite this expression as follows:[35]

$$-k\left(\frac{\partial T}{\partial x}\right)_w = -k\left(\frac{\partial T}{\partial x}\right)_{g_w} + \rho_s r[(c_s - c_p)T_w - L] + Q_H + Q_D \tag{A5}$$

Denison and Baum[35] have obtained a solution to the gas-phase conservation equations by assuming that the complex gaseous reaction process can be represented by a single-step reaction of order n, where in some cases n may not be an integer. The present analysis retains their gas-phase solution, which yields the following expression for the heat flux from the gas phase to the wall:

$$-k\left(\frac{\partial T}{\partial x}\right)_{g_w} = \rho_s r[\epsilon_{r_w} Q_r - c_p(T_f - T_w)] \tag{A6}$$

This solution also relates the instantaneous flow of the reactant into the gaseous reaction zone, $\rho_s r$, to the instantaneous gas-phase reaction rate so that:

$$r = Cp^{n/2} T_f^{(n/2)+1} e^{-E_f/2RT_f} \tag{A7}$$

The above derivation assumes that the surface-coupled reactions occur in a thin zone, so that the surface heat release acts as a boundary condition on the solid phase. To derive a suitable kinetics description, the solid propellant can be thought of as containing possible reaction sites such that

$\rho_s r\chi$ = number of sites which undergo reaction per unit area of reaction zone per unit time

where χ is the number of sites that undergo reaction per unit mass of material. The heterogeneous heat release can now be expressed in terms of the above expression and an Arrhenius law as

$$Q_H = \rho_s r\, H_H \left(\frac{p}{T_w}\right)^m e^{-E_H/RT_w} \tag{A8}$$

for a pressure-sensitive reaction. The parameter χ has been absorbed in H_H, the heat-release per unit mass. Note that H_H may depend upon

the thickness of the surface reaction zone (which is related to $\rho_s r$) and upon the specific character of the pyrolysis process (which is also related ultimately to $\rho_s r$). For example, one might choose to write the above kinetics expression with $(\rho_s r)^y$, instead of $\rho_s r$. Then the exponent y would become an unknown and somewhat indirect measure of the extent of surface reactions relative to gas-phase reactions. However, such a modification does not significantly alter the conclusions drawn from the analysis. Therefore, until there emerges a more detailed understanding of the mechanism, any further complications of this type probably are unwarranted and have not been considered.

Except for their independence of pressure, the other surface reactions follow a similar law:

$$Q_D = \rho_s r H_D \, e^{-E_D/RT_w} \tag{A9}$$

Equations A5, A6, A8, and A9 can be combined to obtain:

$$-k\left(\frac{\partial T}{\partial x}\right)_w = \rho_s r \left[\epsilon_{r_w} Q_r - L - c_p(T_f - T_o) + c_s(T_w - T_o) + H_H \left(\frac{p}{T_w}\right)^m e^{-E_H/RT_w} + H_D \, e^{-E_D/RT_w}\right] \tag{A10}$$

Equations A1, A2, and A7, with the boundary conditions of Eqs. A3 and A10, complete the mathematical representation of the combustion model in terms of the dependent variables T_f, T_w, and r. Owing to the non-linear character of these equations, a closed-form solution cannot generally be obtained.

A linearized analysis may be obtained by assuming that each dependent variable, as well as the pressure, is the sum of a steady and a perturbed component:

$$
\begin{aligned}
p &= \bar{p}(1 + \tilde{p}) \\
T_f &= \bar{T}_f(1 + \tilde{T}_f) \\
T_w &= \bar{T}_w(1 + \tilde{T}_w) \\
r &= \bar{r}(1 + \tilde{r})
\end{aligned}
\qquad \text{(A11)}
$$

where, for example, $\tilde{p}$ is the ratio $[p(t) - \bar{p}]/\bar{p} \ll 1$. By introducing these expressions into Eqs. A1, A2, A3, A7, and A10 and retaining only first-order terms in the perturbed quantities, one can obtain a set of linear equations. The solution to these equations gives the first-order response of the combustion mechanism to a perturbation in the chamber pressure.

APPENDIX B

SIGNIFICANCE OF THE IMPOSED PRESSURE GRADIENT IN COMBUSTION TERMINATION

Termination of the combustion process will ultimately occur if the pressure excursion results in the chamber pressure falling to zero, regardless of the pressure gradient initially introduced. However, the rate at which the extinction occurs, (i.e., the time required for the burning rate to drop to zero) is closely coupled to the transient response of the combustion mechanism and therefore to the pressure gradient. In practice, for solid-propellant combustion to terminate, it is necessary that the minimum possible lag in the response of the burning rate to a chamber pressure decay be achieved. In an actual motor, the chamber pressure initially drops, then rises again as a result of the finite chamber volume and nozzle throat area. If the response of the combustion mechanism is slow, reignition may occur as the pressure starts to rise.

To examine the role of the pressure geadient in combustion extinction, it is instructive to develop an approximate analysis of the combustion model presented in Appendix A. In so doing, the mathematical complexity of the problem can be greatly reduced, facilitating a physical interpretation of the results. With this objective in mind, let us integrate Eq. A1 over x to obtain:

$$\frac{\partial}{\partial t}\int_0^\infty (T - T_0)dx = - r(T_w - T_0) - K\left(\frac{\partial T}{\partial x}\right)_w \qquad (A12)$$

To evaluate the integral, which represents essentially the total energy stored in the grain at any instant, it is convenient to consider a steady-state temperature profile,

$$T - T_0 = (T_w - T_0)e^{-rx/K} \qquad (A13)$$

As rapid changes appear in the heat flux, the temperature profile shape will reflect the corresponding small changes in surface temperature much more readily than it will respond to the much larger simultaneous changes in burning rate. Thus, for purposes of the approximate analysis, dT/dr will be neglected. Then Eq. A12 becomes:

$$\frac{K}{r}\frac{dT_w}{dt} = -r(T_w - T_o) - K\left(\frac{\partial T}{\partial x}\right)_w \tag{A14}$$

It is worth digressing briefly to note that the assumptions leading from Eq. A12 to A14 do not reduce the present analysis to a quasi-steady treatment comparable to earlier analyses by others.[1,2] Here, the surface temperature has been allowed to vary and the primary transient in the temperature profile has been considered. Moreover, the possible shift in relative importance of solid- and gas-phase reactions under transient conditions is accounted for in the present approach, as no empirical burning rate law is used.

Equations A11 may now be substituted into Eqs. A2, A7, A10, and A14, and terms of equal order collected. Terms of the order of $\bar{p}$ (or $\bar{T}_f$, $\bar{T}_w$, $\bar{r}$) comprise the unperturbed equations, while those of the order of $\tilde{p}$ form the linearized mathematical description of the response to pressure perturbations.

Combustion Without Pressure Disturbances

The equations for undisturbed burning of the solid propellant are:

$$\bar{r} = ae^{-E/R\bar{T}_w} \tag{A15}$$

$$\bar{r} = C\bar{p}^{n/2}\bar{T}_f^{n/2+1}e^{-E_f/R\bar{T}_f} \tag{A16}$$

$$\frac{K}{\bar{r}^2}\frac{d\bar{T}_w}{dt} = \frac{\epsilon_{r_w}}{c_s} - \frac{L}{c_s} - \frac{c_p(\bar{T}_f - T_o)}{c_s} + \frac{H_H}{c_s}e^{-E_H/R\bar{T}_w}\left(\frac{\bar{p}}{\bar{T}_w}\right)^m + \frac{H_D}{c_s}e^{-E_D/R\bar{T}_w} \tag{A17}$$

These equations are nonlinear, and in general, expect by numerical methods, no solution to them can be obtained. Such a solution, if obtained, would describe the "normal" behavior of the combustion process, i.e., the behavior in the absence of disturbances caused, for example, by acoustical interactions in the chamber. The steady-state solution ($dT_w/dt = 0$) would correspond, within the limitation of the model, to the behavior usually described in terms of an empirical law such as $r = bp^n$.

The First-Order Response to Pressure Perturbations

The first-order response of the combustion model to pressure transients is obtained by collecting terms of the order of ratios of perturbed to unperturbed quantities, i.e., $\tilde{p}$, $\tilde{r}$, $\tilde{T}_w$, and $\tilde{T}_f$. Coefficients in these equations may be simplified by appropriate substitutions from Eqs. A15, A16, and A17. After considerable algebraic manipulation, one obtains the following set of linear equations:

$$\tilde{r} = \frac{E}{R\bar{T}_w}\tilde{T}_w \tag{A18}$$

$$\tilde{T}_f = \frac{\dfrac{E}{R\bar{T}_w}\tilde{T}_w - \dfrac{n}{2}\tilde{P}}{\Sigma} \tag{A19}$$

where $$\Sigma = \frac{n+2}{2} + \frac{E_f}{2R\bar{T}_f}$$

$$\frac{K}{\bar{r}^2}\frac{\partial \tilde{T}_w}{\partial t} = \left[-\frac{K}{\bar{r}^2}\left(\frac{\partial \bar{T}}{\partial t}\right)_w \frac{1}{\bar{T}_w} + \theta_H\left(\frac{E_H}{R\bar{T}_w} - m\right) + \theta_D \frac{E_D}{R\bar{T}_w}\tilde{T}_w\right]$$

$$+ \frac{2}{\bar{T}_w}\frac{K}{\bar{r}^2}\frac{\partial \bar{T}_w}{\partial t}\tilde{r} - \frac{c_p}{c_s}\frac{\bar{T}_f}{\bar{T}_w}\tilde{T}_f + m\theta_H\tilde{p} \tag{A20}$$

where:

$$\theta_H = \frac{H_H}{c_s \bar{T}_w} e^{-E_H/R\bar{T}_w} \left(\frac{\bar{p}}{\bar{T}_w}\right)^m \quad ; \qquad \theta_D = \frac{H_D}{c_s \bar{T}_w} e^{-E_D/R\bar{T}_w}$$

These equations can be combined to obtain the following differential equation for $\tilde{r}$:

$$\frac{d\tilde{r}}{dt} - C_1 \tilde{r} = C_2 \tilde{p} \tag{A21}$$

where

$$C_1 = \frac{\bar{r}^2}{\kappa} \left[\theta_H \left(\frac{E_H}{R\bar{T}_w} - m \right) + \theta_D \frac{E_D}{R\bar{T}_w} - \frac{c_p}{c_s} \frac{\bar{T}_f}{\bar{T}_w} \frac{E/R\bar{T}_w}{\Sigma} \right.$$

$$\left. + \frac{K}{\bar{T}_w \bar{r}^2} \left(\frac{2E}{R\bar{T}_w} - 1 \right) \left(\frac{\partial \bar{T}}{\partial t} \right)_w \right] \tag{A22}$$

$$C_2 = \frac{\bar{r}^2}{\kappa} \frac{E}{R\bar{T}_w} \left[\theta_H m + \frac{n}{2} \frac{c_p}{c_s} \frac{\bar{T}_f}{\bar{T}_w} \frac{1}{\Sigma} \right]. \tag{A23}$$

The chamber-pressure decay introduced within the port of a solid rocket to terminate combustion typically has the form:

$$\tilde{p} = e^{-\beta t} - 1. \tag{A24}$$

(Note that at $t = 0$, $d\tilde{p}/dt = -\beta$ or $dp/dt = -\beta \bar{p}$.) From Eq. A21, the approximate initial response of the burning rate to this pressure decay is:

$$r = \frac{C_2}{\beta + C_1} \left(e^{C_1 t} - e^{-\beta t} \right) + \frac{C_2}{C_1} \left(1 - e^{C_1 t} \right). \tag{A25}$$

A criterion for minimizing the propellant response lag time when under the fnfluence of a pressure decay is obtained by examining the second derivative of Eq. A25.[1] The more negative this derivative, which may be identified as r'', the faster the burning-rate derivative becomes more negative with increasing time. This characteristic is illustrated schematically in Fig. 40, which shows burning rate versus time, after a pressure decay is imposed, for three cases: $\tilde{r}'' > 0$, $\tilde{r}'' = 0$, and $\tilde{r}'' < 0$. It is clear that propellant extinguishment will be enhanced by making $\tilde{r}''$ as negative as possible.

The second derivative of Eq. A25 is:

$$\frac{d^2\tilde{r}}{dt^2} \equiv \tilde{r}'' = \frac{C_2}{C_1 + \beta}\left(C_1^2 e^{C_1 t} - \beta^2 e^{-\beta t}\right) - C_2 C_1 e^{C_1 t} \qquad \text{(A26)}$$

Note that the second term on the right-hand side is always negative, as desired, but the first term can be either positive or negative. Specifically, at $t = 0$ the first term is negative only if $\beta^2 > C_1^2$. Thus, the maximum negativity in $\tilde{r}''$, and therefore the most favorable condition for combustion extinguishment, is achieved if $\beta > C_1$.

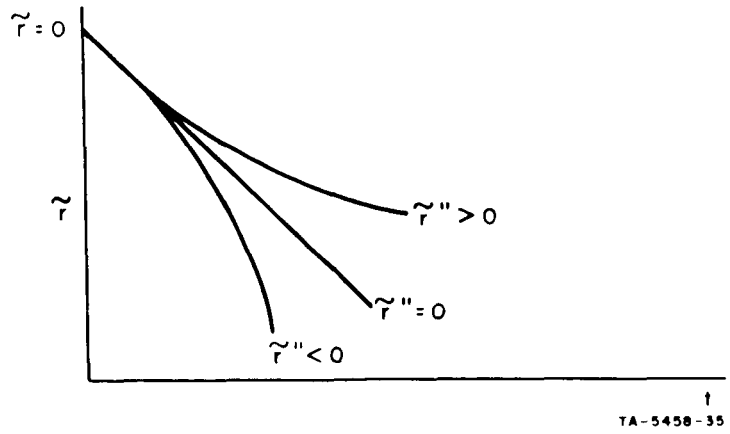

FIG. 40 TIME DEPENDENCE OF BURNING RATE DERIVATIVE

In summary, the approximate analysis of the combustion model defines two criteria for extinction of solid propellant combustion: (1) to prevent unstable combustion as a result of pressure disturbances, it is required that $C_1 < 0$; and (2) to ensure minimum lag in the burning-rate response of the combustion mechanism to an imposed negative pressure pulse, it is required that $\beta > C_1$.

APPENDIX C

COMBUSTION INSTABILITY: AN ANALYTICAL DESCRIPTION OF THE RESPONSE FUNCTION

The role of the solid propellant combustion process in determining the stability of the rocket chamber can be defined in terms of the acoustic admittance of the burning surface, which depends directly on the response function, i.e., the ratio of the burning rate perturbation to the pressure perturbation. Both theoretical and experimental investigations of combustion instability generally characterize the propellant in terms of the response function, and the combustion model developed in Appendix A has been analyzed to determine what it predicts for this response parameter.

This analysis was accomplished by performing a mathematical transformation of an earlier treatment by Denison and Baum[35] to make it applicable to the model of Appendix A. Details of this analysis have appeared in the open literature[10, 19] as well as in reports,[9] so that only a condensed summary will be presented here.

By modifying the parameters α and B defined by Denison and Baum,[35] it is possible to generalize the analysis made by these investigators. Their mathematical solution describes the behavior of the combustion model formulated above when it is expressed in terms of the following transformation:

$$\left.\begin{aligned} \alpha &= \alpha_o - \frac{\theta_s}{A} \\ B &= \frac{\alpha_o B_o + m\theta_H}{\alpha_o - \theta_s/A} \end{aligned}\right\} \qquad \text{(A27)}$$

where:

$$A = A_o = \frac{E_w}{R\bar{T}_w}\left(\frac{\bar{T}_w - T_o}{\bar{T}_w}\right) \qquad \text{(A28)}$$

$$\alpha_o = \frac{c_p \bar{T}_f}{c_s (\bar{T}_w - T_o)} \frac{1}{\left(\frac{n+2}{2} + \frac{E_f}{2R\bar{T}_f}\right)}$$

$$\theta_s = \left(\frac{E_H}{R\bar{T}_w} - m\right) \theta_H + \frac{E_D}{R\bar{T}_w} \theta_D \qquad \text{(A29)}$$

$$\theta_H = \frac{H_H}{c_s \bar{T}_w} \left(\frac{p}{\bar{T}_w}\right)^m \exp\left(-E_H/R\bar{T}_w\right) = \frac{Q_H}{Q_T} \left(\frac{\bar{T}_w - T_o}{\bar{T}_w}\right) \qquad \text{(A30)}$$

$$\theta_D = \frac{H_D}{c_s \bar{T}_w} \exp\left(-E_D/R\bar{T}_w\right) = \frac{Q_D}{Q_T} \left(\frac{\bar{T}_w - T_o}{\bar{T}_w}\right) \qquad \text{(A31)}$$

The subscript zero on α, B, and A denotes the value, as defined by Denison and Baum,[35] for zero surface-coupled heat release. It is also convenient to define an overall, steady-state pressure exponent for the propellant, ν, in terms of the usual empirical burning rate formula, $\bar{r} = cp^{\nu}$. It follows that:

$$\nu = \frac{\alpha_o \frac{n}{2} + m\theta_H T_w/(T_w - T_o)}{\alpha_o - \theta_s/A} \qquad \text{(A32)}$$

Note that when there are no surface-coupled reactions, $\theta_s = \theta_H = 0$, and the analysis reduces to that of Denison and Baum,[35] in which case the pressure exponent $\nu = n/2$ (n being the order of the gas-phase reaction).

It can be shown that the parameter θ_s is roughly proportional to the fraction of the total heat release that occurs in surface-coupled reactions. The relationship between θ_H and the fraction released in

surface reactions with pressure-dependent kinetics (e.g., heterogeneous reactions) is indicated by Eq. A30, and that between θ_D and the pressure-independent surface reactions (e.g., decomposition) appears in Eq. A31.

The transient behavior of the present combustion model is easily obtained from Denison and Baum's solution by using the transformation given in Eq. A27. The following results are obtained.

A given propellant may be characterized in terms of three parameters: A, which relates to the surface decomposition kinetics; α, which relates to the gas-phase kinetics; and θ_s, which relates to the distribution of heat release between surface-coupled and gas-phase reactions. Relative to the behavior with no surface-coupled reactions ($\theta_s = 0$), a negative θ_s extends the range of A and of α for which the propellant is inherently stable in the "self-excited" mode;[35] a positive θ_s reduces this range. As Eq. A29 shows, the sign of θ_s is determined by the relative magnitudes of $E_H/R\bar{T}_w$, m, and $E_D/R\bar{T}_w$, as well as by the signs of θ_H and θ_D (which are positive for exothermic reactions, negative for endothermic reactions).

Of course, all practical propellants must have a stable self-excited mode, although some may be closer to the unstable limit than others, depending on their specific values of A, α, and θ_s. The stable zone is described by the relation:

$$q^2 - q - 2A < 0 \qquad \text{(A33)}$$

where

$$q = 1 + \theta_s + A(1 - \alpha_o)$$

Thus, only values of A, α, and θ_s that satisfy Eq. A33 are of practical importance.

The "steady oscillatory" mode corresponds to the response of a propellant, whose parameters satisfy the inequality of Eq. A33, to pressure perturbations. This response may be represented in terms of

normalized (by the pressure index ν) acoustic response function, $\tilde{m}/\nu\tilde{p}$. The real part of the complex response function is of greater practical significance, because it is the component of the mass perturbation which is in phase with the pressure perturbation that tends to drive the oscillations. The analysis shows that the resonance amplitudes of the real part and of the complex response function are almost equal when the latter is less than about 10. Relative to the case where surface reactions are absent ($\theta_s = 0$), an increase in θ_s (positive θ_s) increases the amplitude of the response function; a decrease (negative θ_s) reduces the amplitude, i.e., tends to stabilize the propellant.

As has been explained in the Theoretical Studies section of this report, a composite propellant generally corresponds $E_H > 0$ and/or $E_D > 0$, whereas for a double-base propellant, $E_H = E_D = 0$ (with the relatively minor exception noted above). When there are exothermic surface-coupled reactions ($\theta_H > 0$, $\theta_D > 0$), for example, it follows from Eq. A29 that $\theta_s > 0$ for composite propellants, whereas $\theta_s < 0$ (unless $E_H/RT_w > m$ owing to molecular mixing) for double-base propellants. It follows that exothermic surface-coupled reactions tend to destabilize composite propellants (by increasing the response amplitude), while they tend to stabilize double-base propellants. This remarkable theoretical conclusion is consistent with the experimental observation[9] that the stable burning regimes of composite and double-base propellants are reversed. The effect of surface-coupled reactions, therefore, may explain this surprising observation.

APPENDIX D

MODIFIED COMBUSTION MODEL

To conduct the nonlinear analysis required to properly examine combustion extinction behavior, a simple but important modification has been introduced into the combustion model described in Appendix A. The following discussion explains the concepts underlying this modification.

Predicted Steady-State Behavior of the Flame Temperature

Unlike many other combustion models,[1,2] the model summarized in Appendix A predicts that the gas-phase flame temperature will increase as the burning rate rises, even in steady-state combustion. This behavior is a consequence of the surface-coupled reaction kinetics employed in the model, as will become evident from a careful examination of Eq. A34. (This equation, which is a boundary condition, is derived in Appendix A and appears there as Eq. A10.)

$$-k\left(\frac{\partial T}{\partial x}\right)_w = \rho_s r \left[\epsilon_{r_w} Q_r - L - c_p(T_f - T_o) + c_s(T_w - T_o) + H_H \left(\frac{p}{T_w}\right)^m e^{-E_H/RT_w} + H_D e^{-E_D/RT_w}\right] \quad \text{(A34)}$$

In steady-state combustion, the net heat flux into the unreacted solid propellant is equal to the energy required to condition the propellant for surface pyrolysis; i.e., $-k(\partial T/\partial x)_w = \rho_s r c_s (T_w - T_o)$. Thus, in the steady-state limit, Eq. A34 becomes a simple expression for the gas-phase flame temperature in terms of the total heat release in the combustion process:

$$c_p(T_f - T_o) = \rho_s r\left[\epsilon_{r_w} Q_r + H_H \left(\frac{p}{T_w}\right)^m e^{-E_H/RT_w} + H_D e^{-E_D/RT_w} - L\right] \quad \text{(A35)}$$

The first term within the brackets of Eq. A35 represents the heat release associated with combustion in the gas-phase flame; the next two terms describe, respectively, pressure-sensitive (heterogeneous) and pressure-insensitive energetic surface-coupled reactions; the last term represents the latent heat of phase change or decomposition near the burning surface. As the burning rate increases, so does T_w (see Eq. A2 of Appendix A). Thus, the magnitude of the surface-coupled heat release increases with the burning rate, and it follows from Eq. A35 that T_f rises as well. For a reasonable choice of parameters such as E_H and E_D, a large change in pressure (and therefore burning rate) may lead to a greater increase in T_f than is normally encountered with actual propellants. (Composite propellants typically exhibit a modest increase in flame temperature with pressure up to about 200 psi, after which T_f is almost constant. Double-base propellants often have a somewhat greater dependence of flame temperature on pressure in steady-state combustion.)

The predicted behavior of T_f suggested that a modification of the model was in order, because the accuracy with which the model predicts the steady-state behavior of all dependent variables could be regarded as a legitimate test of its applicability to nonsteady phenomena. In general, the model, in the form summarized in Appendix A would not yield the exact steady-state behavior of flame temperature versus pressure for a given propellant unless certain restrictions were imposed on the numerical values assigned to kinetics parameters such as E_H and E_D. This situation is not entirely satisfactory, because the flame temperature is actually a purely thermodynamic quantity, determined primarily by the heat of reaction of the propellant; it is quite independent of the reaction kinetics. (Note that T_f is normally obtained from an "adiabatic flame temperature" calculation, in which the propellant composition and heats of reaction appear but not the kinetics parameters.[38]

To idenfiy the source of this apparent anomaly in the combustion model, it is worthwhile to re-examine the theoretical description of gas-phase and surface-coupled heat release in the combustion process. A brief study of the steady-state combustion mechanism will reveal the

minor but potentially important correction that was introduced into the model to overcome the difficulty described above, and it will also clarify the physical basis for the surface kinetics treatment that earlier[8,9,10,19] was shown to be the most important feature of the model.

Theoretical Description of the Distribution of Heat Release in Solid Propellant Combustion

The solid propellant combustion mechanism is illustrated in Fig. 41. It is convenient to envision the propellant as moving at a negative velocity, equal to the burning rate, toward the surface zone ($x = 0$) where pyrolysis occurs; the pyrolysis products then proceed into the gas phase, where further reactions complete the combustion and the final flame temperature T_f is achieved. During this process, the total heat release per unit area of propellant surface, and per time, is $\rho_s rQ$, where Q is the total heat of combustion of the propellant. Of this total, a portion, $\rho_s rQ$, is released within a relatively narrow pyrolysis region near the surface of the solid; i.e., Q_s is the heat of decomposition of the propellant.

In a typical ammonium perchlorate composite propellant, for example, Q_s would be essentially the heat of decomposition of ammonium perchlorate. The pyrolysis products then initiate a complex sequence of reactions, which occurs in a zone extending from the propellant surface into the gas phase for whatever distance is required to complete combustion. The thickness of the gas-phase flame zone depends on both the total mass flux, $\rho_s r$, and the kinetics of the reactions within this zone. For example, as the pressure increases, the local reactant concentration rises, causing an increase in the local reaction rates. Thus, at higher pressures, the reactions are accomplished more rapidly and the flame zone is thinner.

To express the total heat release in the combustion process in terms of that associated with each of the constituent reactions, it is convenient to define a parameter ϵ, which is essentially a measure of the "completeness" of combustion. Specifically, the concentration of reactants entering any given reaction plane in the flame zone, such

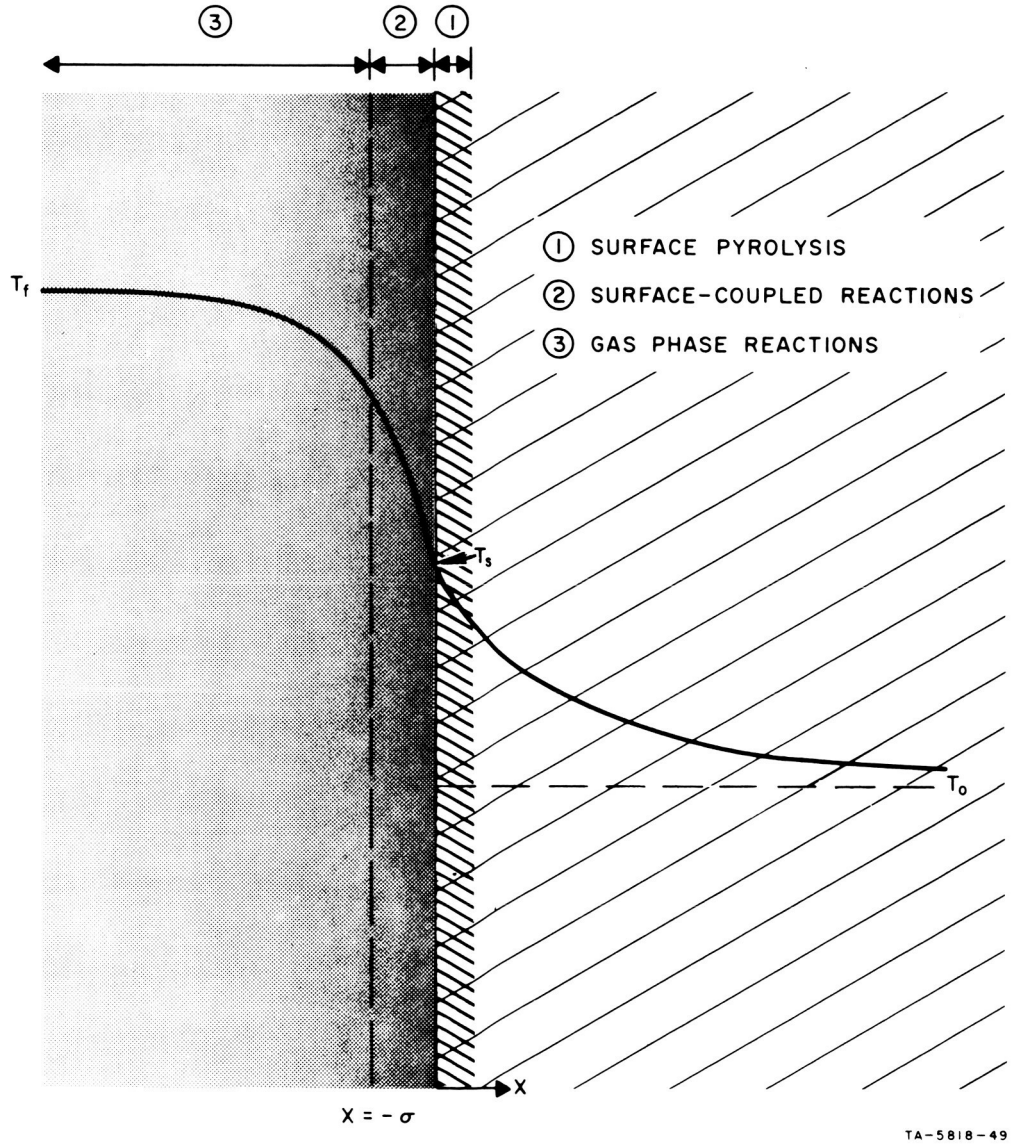

FIG. 41 SIMPLIFIED MODEL OF THE DISTRIBUTION OF HEAT RELEASE IN THE SOLID PROPELLANT COMBUSTION PROCESS

as $x = -x_1$, is $\rho_s r[1 - \epsilon(x_1)]$. At the gas-solid interface, $\epsilon \ll 1$, because the flow at that point consists almost entirely of pyrolysis products that are available for further reactions. As the distance from the propellant surface grows larger, ϵ increases, since more and more combustion products are present and the concentration of potential reactants is less. The position at which $\epsilon = 1$ marks the edge of the flame zone; i.e., when $\epsilon = 1$, there are no more reactants, combustion is complete, and the flame temperature has been achieved.

This visualization of the combustion process leads to the following relatively simple expression for the total heat release per unit time and surface area:

$$\rho_s rQ = \rho_s rQ_s + \rho_s r \int_0^{-\infty} H(x) [1 - \epsilon(x)] e^{-E(x)/RT(x)} dx \quad \text{(A36)}$$

As was noted above, the concentration factor, ϵ, is a function of x, changing from nearly zero at the propellant surface to unity at the edge of the flame zone. In addition, the local heat of reaction, H, the local activation energy, E, and the temperature, T, vary with x. All of these variables depend on the specific sequence of reactions involved in the process; at any given position x_1, the quantities H and E characterize the particular reaction occurring at that point, whereas ϵ and T reflect the history of reactions closer to the surface. To perform the integration of Eq. A36, it would be necessary to assume a specific reaction sequence and solve the conservation equations to determine the concentration and temperature profiles. This would be a formidable task, hardly justifiable or even possible because of the general lack of information available about reactions in the flame zone. Nevertheless, Eq. A36 suggests some interesting and useful concepts for the combustion model.

First, note that Eq. A36 expresses the total heat release in terms of the constituent reactions in either steady or nonsteady combustion. Second, note that as the general temperature level rises, as when the burning rate or pressure increases, the integral is completed over a

shorter distance; i.e., the flame zone is thinner. Alternatively, as the temperature increases, a greater fraction of the total heat release occurs within an arbitrarily narrow zone of thickness, σ (see Fig. 41), near the surface. This observation is important in nonsteady combustion, because those reactions near the surface will be "surface-coupled," or governed primarily by the relatively slow thermal response of the solid, whereas those farther out in the flame zone will follow the much faster thermal response of the gas. It is this aspect that led to the unique kinetics description of surface-coupled reactions employed in the SRI theory[6,10,19] as will be demonstrated below.

Modification of the Combustion Model

In principle, the combustion model described in Appendix A should contain the right-hand side of Eq. A36 in place of the first and the last two terms of Eq. A10 which represents the gas-phase and the surface-coupled heat release, respectively. However, in this form, the combustion model would almost exclude the possibility of reasonable mathematical analysis, as was explained in connection with Eq. A36. Therefore, it was necessary to introduce a major simplification while retaining those features of Eq. A36 that are of major importance in both steady and nonsteady combustion. This simplification was accomplished by dividing the flame zone into two regions: one relatively thin zone adjacent to the propellant surface (e.g., the zone of thickness σ in Fig. 41) and the other occupying the remainder of the flame zone. Reactions in the first zone occur practically at the surface temperature, T_w, and in nonsteady combustion, the temperature profile in this region tends to be in phase with T_w; i.e., it is dominated by the thermal response of the solid phase. This zone of surface-coupled reactions is characterized by the fact that $\epsilon \ll 1$. The other zone encompasses the "true" gas-phase reactions, or those that follow the faster thermal response of the gas phase. With this approach, Eq. A37 takes the following much simpler form:

$$\rho_s r Q = \rho_s r \left\{ Q_s + \int_{x=-\sigma}^{-\infty} H(x)\left[1 - \epsilon(x)\right] e^{-E(x)/RT(x)}\, dx \right\}$$

$$+ \rho_s r H\, e^{-E/RT_w} \qquad \text{(A37)}$$

A comparison of Eq. A37 with Eq. A34 shows that the last term of Eq. A37 represents the surface-coupled heat release; this term has been separated into two parts in the combustion model: one describing pressure-sensitive or heterogeneous reactions, and the other those that are pressure insensitive. The bracketed quantity in Eq. A36 is clearly identified with Q_r in Eq. A34.

This comparison reveals the modification that was introduced into the model for application to nonlinear behavior. In the model, Q_r was treated as a constant, whereas Eq. A37 shows that it may vary. The way it varies for a given propellant is determined by the behavior of the total heat of reaction, Q, which can be determined from thermochemical calculations. (In fact, knowing the dependence of Q on pressure in steady combustion is equivalent to knowing the behavior of the flame temperature, T_f.) If Q is known, then for any value of the last term in Eq. A37, Q_r, which corresponds to the quantity in brackets, is also known. Thus, for large excursions in the pressure or burning rate, Q_r should be treated as a variable such that in the steady-state limit, the dependence of the flame temperature on the pressure is as predicted by thermochemical calculations. Note that this method of ensuring a correct flame temperature behavior in the model involves only the heats of reaction and is completely independent of the kinetics parameters, such as E_H and E_D. In this way, the objection raised earlier in this appendix, concerning the predicted flame temperature behavior is overcome.

It can be shown that the influence of a varying Q_r, relative to a constant Q_r in Eq. A34, is a second-order effect. Therefore, it was possible to simplify the treatment by using the assumption Q_r = constant for linearized analyses such as those in Appendices B and C. However,

for a nonlinear analysis the modified combustion model with the variable Q_r is needed. Inasmuch as the foregoing discussion has centered on steady-state combustion, a brief commentary on the method of modifying the model for a nonsteady analysis follows.

In general, as the burning rate and surface temperature rise, the amount of surface-coupled heat release increases. Normally, the total heat release increases too, but only slightly. Therefore, Q_r must decrease as the surface terms increase, to preserve the correct total heat release, Q_T. The dependence of the surface terms on T_w or on the burning rate (see Eq. A2) is known. The dependence of the adiabatic flame temperature, and therefore of Q_T, on the pressure (or the burning rate or T_w) is known from thermochemical calculations. The difference between Q_T and the surface terms is Q_r, and the thermochemical calculation establishes a unique value of Q_r for every value of T_w and the surface terms.

It appears reasonable to assume that in nonsteady combustion, the heat release in the gas phase, Q_r, will be the same as the steady-state value for the same total heat release in the surface-coupled terms. Note that this assumption does not relate Q_r to the instantaneous value of T_w or p, but to the instantaneous heat release, thereby preserving the thermochemical characteristics of the propellant. In the steady-state limit, this assumption reduces to the correct behavior, as described above.

REFERENCES

1. Landers, L. C., et al., "Development of An extinguishable Solid Propellant," Report No. 0855-81Q-2 (Classified), Aerojet-General Corporation, October 23, 1964.

2. von Elbe, G., "Theory of Solid Propellant Ignition and Response to Pressure Transients," Bulletin of the 18th ICRPG Meeting, 1963, p. 95.

3. Jensen, G. E., "A Stop-Start Study of Solid Propellants," Final Technical Report, United Technology Center, Contract No. NAS 1-6601, November 1967.

4. Price, E. W., et al., "Combustion of Solid Propellants and Low Frequency Combustion Instability," Technical Publication 4244, U. S. Naval Ordnance Test Station, June 1967.

5. Summerfield, M., Krier, H., T'ien, J. S., and Sirignano, W. A., "Non-Steady Burning Phenomena of Solid Propellants: Theory and Experiment," Aerospace and Mechanical Sciences Report, Princeton University, Contract No. AF 49(638)1405, July 1967.

6. Capener, E. L., Dickinson, L. A., and Marxman, G. A.,"Propellant Combustion Phenomena During Rapid Depressurization," Annual Report, Stanford Research Institute, Contract No. NAS7-389, September 1966.

7. Capener, E. L., Dickinson, L. A., and Marxman, G. A., "Propellant Combustion Phenomena During Rapid Depressurization," Quarterly Report No. 2, Stanford Research Institute, Contract No. NAS7-389, January 31, 1966.

8. Capener, E. L., Dickinson, L. A., and Marxman, G. A., "Propellant Combustion Phenomena During Rapid Depressurization," Quarterly Report No. 3, Stanford Research Institute, Contract No. NAS7-389, March 31, 1966.

9. Capener, E. L., et al., "Response of a Burning Propellant Surface to Erosive Transients," Annual Report, Stanford Research Institute, Contract No. AF 49(638)-1507, December 31, 1966.

10. Marxman, G. A., "Theoretical Model of Solid Propellant Response in Combustion Instability and Extinction," presented at 3d ICRPG Combustion Conference, J. F. Kennedy Space Center, Cocoa Beach, Fla., October 1966.

11. Capener, E. L., Dickinson, L. A., and Kier, R. J., "Driving Processes of Finite-Amplitude Axial-Mode Instability in Solid Propellant Rockets," AIAA J. 5, 938-945 (1967).

12. Price, E. W., "Experimental Solid Rocket Combustion Instability," Tenth Symposium (International) on Combustion, The Combustion Institute, Pittsburgh, Pa., 1965, pp. 1067-1082.

13. Hart, R. W., and McClure, F. T., "Theory of Acoustic Instability in Solid Propellant Rocket Combustion," Tenth Symposium (International) on Combustion, The Combustion Institute, Pittsburgh, Pa., 1965, pp. 1047-1065.

14. Friedly, J. C., and Petersen, E. E., "Influence of Combustion Parameters on Instability in Solid Propellant Motors--Part I: Development of Model and Linear Analysis," AIAA J. 4, 1604-1610 (1966); "Part II: Nonlinear Analysis," AIAA J. 4, 1932-1937 (1966).

15. Culick, F.E.C., "Calculation of the Admittance Function for a Burning Surface," present at 3d ICRPG Combustion Conference, J. F. Kennedy Space Center, Cocoa Beach, Fla., October 1966.

16. Vantoch, P., "Combustion Instability in Solid Propellant Rockets," Foreign Sci. Bull. 1, 9, (September 1965).

17. Vantoch, P., "Combustion Instability in Liquid and Solid Propellant Rockets," ATD Report 65-106, Library of Congress, November 22, 1965.

18. Marxman, G. A., and Wooldridge, C. E.,"Propellant Combustion Phenomena During Rapid Depressurization," Quarterly Report No. 7, Stanford Research Institute, Contract No. NAS7-389, July 26, 1967.

19. Marxman, G. A., and Wooldridge, C. E., "The Effect of Surface Reactions on the Solid Propellant Response Function," presented at ICRPG/AIAA 2nd Solid Propulsion Conference, Anaheim, Calif., June 1967 (to be published in AIAA J.).

20. Ciepluch, C. C., "Effect of Composition on Combustion of Solid Propellants During a Rapid Pressure Decrease," NASA TN D-1559, December 1962.

21. Summerfield, M., Sutherland, G. S., Webb, M. J., Tabock, H., and Hall, K. J., American Rocket Society Preprint No. 737, 1958.

22. Baillie, M. J., Brown, D. H., Moss, K. C., and Sharp, D.W.A., "Copper (II) Salts of Very Strong Acids," Chem. Comm. 5, 91 (1965).

23. Solymosi, F., Initiation of Ammonium Perchlorate Ignition by Chronic Oxide-Titanium Dioxide Catalysts, Combustion and Flame, 9, 14 (1965).

24. Developed by Naval Weapons Center, IDP 1080, Propulsion Development Department, China Lake, California.

25. U. S. Patent No. 3,190,776, June 22, 1965.

26. Saurer, S. F., "Propellant Chemistry," New York, Reinhold Publishing Co., 1966, p. 296.

27. Reed, R., Weber, L., and Gottfried, B., "Differential Thermal Analysis and Reaction Kinetics," Ind. Eng. Chem. Fundamentals 4, 1:38 (February 1965).

28. Bross, D., and Amster, A. B., "Thermal Explosions: Adiabatic Self-Heating of Explosives and Propellants," 8th Symposium (International) On Combustion, The Williams & Wilkins Co., Baltimore, Md., 1962.

29. Inami, S. H., Rosser, W. A., and Wise, H., "The Adiabatic Decomposition of Ammonium Perchlorate," Stanford Research Institute Final Report, Contract No. NR 3415(00), August 6, 1965.

30. Crump, J. E., "Aluminum Combustion in Composite Propellants," CPIA Publication No. 105, 2d Combustion Conf., May 1966, Vol. 1, p. 321.

31. Summerfield, M., Sutherland, G. S., Webb, M. J., Taback, H. J., and Hall, K. P., "Burning Mechanism of Ammonium Perchlorate Propellants," Solid Propellant Rocket Research, Progress in Astronautics and Rocketry, Summerfield, M., ed., Vol. I, New York, Academic Press, 1960, p. 141.

32. Tourin, R. H., Penzias, G. J., and Liang, E. T., "Infrared Radiation and Temperature Measurements in Solid Propellant Flames," Report No. TR-800-5, Warner-Swasey Co., Contract NONR 3657(00), October 1962.

33. Waesche, R.H.W., "Spectrographic Studies of Solid Propellant Flames," (Confidential), Report No. S1-11, Rohm & Haas Co., Contract No. DA-01-021AMC11536(2), October 1966.

34. Povinelli, L. A., "Study of Composite S.P. Flame Structure Using A Spectral Radiation Shadowgraph Technique," NASA Report No. TMX-52071, 1964.

35. Denison, M. R., and Baum, E., "A Simplified Model of Unstable Burning in Solid Propellants," ARS J. 31, 1112-1122 (1961).

36. Penner, S. S., Chemistry Problems in Jet Propulsion, New York Pergamon Press, 1957, pp. 136-156.